UNIVERSITY OF CALGARY

The Synthesis and Evaluation of Molybdenum-Based Ultra-Dispersed Hydroprocessing Catalysts

by

John Thompson

A THESIS

SUBMITTED TO THE FACULTY OF GRADUATE STUDIES

IN PARTIAL FULFILMENT OF THE REQUIREMENTS

FOR THE DEGREE OF MASTER OF SCIENCE

DEPARTMENT OF CHEMICAL AND PETROLEUM ENGINEERING

CALGARY, ALBERTA

APRIL, 2008

UNIVERSITY OF CALGARY

FACULTY OF GRADUATE STUDIES

The undersigned certify that they have read, and recommend to the Faculty of Graduate Studies for acceptance, a thesis entitled "The Synthesis and Evaluation of Mo-Based Ultra-Dispersed Hydroprocessing Catalysts" submitted by John Thompson in partial fulfilment of the requirements of the degree of Masters of Science in Chemical Engineering.

Supervisor, Dr. Pedro R. Pereira-Almao,
Department of Chemical and Petroleum Engineering

Dr. Gordon R. Moore,
Department of Chemical and Petroleum Engineering

Dr. Maen Husein,
Department of Chemical and Petroleum Engineering

Dr. Ron Spencer,
Department of Geology and Geophysics

Date

Abstract

More efficient catalysts are required for the upgrading of heavy oil. Ultra-dispersed (UD) catalysts are particularly advantageous in that the catalysts can be dispersed in the reaction medium, there is a larger surface area of active sites, large reactants can reach the active sites, and the catalysts have the potential for recovery. The effect of decomposition temperature on particle size in the synthesis of UD molybdenum-based catalysts from water-in-oil emulsions was studied in a horizontal reactor configuration and in a continuous mode, suitable for online application to conventional hydroprocessing or in-situ upgrading. Characterization results indicate that the particle size increases with increasing decomposition temperature and new active phases are formed during reactivity testing; phases which are confirmed through thermodynamic calculations. The results also suggest that the mechanism of particle size increase is most likely caused by physical agglomeration and not crystal growth. UD catalyst synthesis and reactivity tests in a single continuous unit using a heavy feedstock were also studied in a packed porous media (as a first attempt to simulate reservoir conditions) in order to reveal upgrading efficiency and to profile catalyst and coke deposition.

Acknowledgements

I would first like to acknowledge my mentor, Dr. Pedro Pereira-Almao, without whom this accomplishment would not be possible. His ongoing technical and paternal guidance has enabled me to develop a new-found confidence and pride. His teachings and the positive environment he created within his research group will always be remembered.

I specifically acknowledge Vieman Ali Marcano and Enzo Peluso who had the misfortune of sitting next to me in the office, thus assuming the role of Teaching Assistant. I would also like to recognize all other members of the Catalysis for Bitumen Upgrading and Hydrogen Production Group who served as family during my stay: Alejandro, Behdad, Herbert, Francisco, Carmen, Carlos, Eumir, Lante, Latif, Gustavo, Clementina, Luis, Jorge, Maria-Laura, Redescal, Luis-Alberto, Azfar, Lina, Linda, Carola, Baharan and Manuel 'thanks for nothing' Gonzalez. Their contributions both to my work and to my overall experience at the university are very much appreciated.

The substantial financial support provided by the Alberta Ingenuity Fund via Alberta Ingenuity Centre for In-Situ Energy (AICISE) at the University of Calgary is recognized, as well as my fellow graduate students and faculty members of the Department of Chemical and Petroleum Engineering.

Finally, I would like to acknowledge my 'biggest fans' and source for inspiration – my family. The tremendous financial sacrifices made by my parents and their ability to overlook my failures while praising my achievements will be valued forever.

Table of Contents

List of Tables

List of Figures and Illustrations

List of Symbols, Abbreviations and Nomenclature

Symbol	Definition
AHM	ammonium heptamolybdate
API	American Petroleum Institute
ASTM	American Society for Testing Materials
atm	atmospheres
BPR	back pressure regulator
CCR	Conradson carbon residue
CLG	Chevron Lummus Global
CPU	Ultra-Dispersed Catalyst Preparation Unit
CRU	*Pelletized* Catalyst Reactivity Unit
CVD	chemical vapour deposition
DLS	dynamic light scattering
EBR	ebullated bed reactor
EOR	enhanced oil recovery
FBR	fixed bed reactor
FID	flame ionization detector
GC	gas chromatography
HC	hydrocarbons
HCK	hydrocracking
HDN	hydrodenitrogenation
HDS	hydrodesulfurization
HDT	hydrotreating
HR	horizontal reactor
HRI	Hydrocarbon Research Institute
ICP-AES	inductively coupled plasma atomic emission spectroscopy
Ir	iridium
k	kinetic rate constant
K_i	equilibrium constants
Mo	molybdenum
Ni	nickel
P_i	pressure values
PDI	polydispersivity index
PDF	powder diffraction file
PID	proportional-integral-differential
ppm	parts per million
psi	pounds per square inch
PV	pore volume
r	rate of reaction
Ru	ruthenium
SAGD	steam-assisted gravity drainage
SCCM	standard cubic centimetres per minute
SEM	scanning electron microscope
SPAN 80	sorbitan monooleate
SPRU	Sand-Packed Reactivity Unit

STM	scanning tunnelling microscopy
T	temperature (K)
TBP	true boiling point
TGA	thermogravimetric analysis
TPR	temperature programmed reduction
TWEEN 80	polysorbate 80
UD	ultra-dispersed
V	vanadium
VGO	vacuum gas oil
VR	vertical reactor
WHSV	weight-hourly space velocity
w/o	water-in-oil
XRD	X-ray diffraction
Z-Ave	average particle size

Subscripts

$_T$	thiophene
$_H$	hydrogen
$_i$	component ‘i’
$_S$	hydrogen sulfide

Greek Symbols

λ	wavelength of the X-ray
θ	X-ray scattering angle
μ	viscosity

Chapter One: Introduction

A prudent man foresees the difficulties ahead and prepares for them;
the simpleton goes blindly on and suffers the consequences.
Proverbs 22:3

The world is heading towards a global energy crisis due to a decline in the availability of light conventional oil. Alternative renewable power/fuel research will ultimately be required to sustain our activities, but immediate needs require a greater recovery of the abundant unconventional heavy oil resource. This thesis reviews the latest advances in heavy oil hydrotreating catalysis and aims at unveiling further insight into some of the parameters behind the synthesis and use of dispersed catalysts for this science. The ultimate effort is to enhance the efficiency of production and processing of this vast energy resource.

1.1 Background

Crude oil is the name given to all organic compounds which are fluid under reservoir conditions. At present, world resources of unconventional (bitumen and heavy oil) crude oil are estimated to be 5.6 trillion barrels, compared with the rapidly depleting remaining light conventional crude oil reserves of 1.02 trillion barrels (Hein, 2006). In 2006, the world experienced growth in oil demand of 0.80 million barrels per day, representing a 0.9% growth from the previous year. It is speculated that 2007 will witness an increase of 1.49 million barrels per day in global oil demand, corresponding to a 1.8% increase (Alberta Energy and Utilities Board, 2007). Unconventional oils are therefore starting to play a significant role in the world energy market. These oils are more viscous than conventional oils due to the abundance of large heavy hydrocarbons which impose transportation problems and poor recovery potential. They also contain a significant fraction of heteroatoms, such as sulfur, nitrogen, and metals, which make processing more difficult and limit marketability. Increasingly stringent legislative limits on the sulfur concentration in transportation fuels in many countries has spurred the refining

industry to develop new processes to reduce sulfur content to as low as a few parts per million (Official J. Eur. Union, 2003). The purpose of this effort is to protect catalytic converters while at the same time cutting dramatically gaseous sulfur oxide and particulate emissions. Thus, in order to make heavy crude oil reserves more economically and environmentally viable through sulfur and impurity removal and density and viscosity reduction, more advanced technologies, including more efficient catalysts for hydroprocessing, are required.

Unconventional crude oils can be further classified as being either heavy or extra-heavy (also referred to as bitumen). Since viscosity is extremely sensitive to large variations in temperature, API (American Petroleum Institute) gravity is more commonly used in classifying crude oils, whereby the greater the gravity, the lighter the oil. Viscosity is a parameter which determines how well oil will flow while API gravity typically determines the yield from distillation. Additionally, temperature and paraffin content can have a large effect on viscosity values while API gravity is not affected by these parameters. Heavy oils range from 10° to 20° API, whereas bitumen crude oils have API values under 10° (Kuuskraa et al., 1987). For API gravities greater than 10, the petroleum liquid is lighter than water and floats; if its less than 10, it is heavier and sinks. API gravity is thus a measure of the relative density of a petroleum liquid and the density of water, but it is used to compare the relative densities of petroleum liquids

Of the remaining recoverable reserves of conventional crude oil worldwide, only fifteen per cent are in the Western Hemisphere (*International Petroleum Encyclopedia*, 2000). However, the vast unconventional resources of petroleum remain untapped, and most of these deposits are in the Western Hemisphere. As depicted in Figure 1.1, when petroleum sources are expanded to include heavy hydrocarbons, which includes both heavy crude oil and natural bitumen, the outlook for domestic oil supplies is much improved. In fact, of the heavy oil and bitumen resources, over 80 per cent are in Venezuela, Canada and the U.S.A. The largest oil-sand deposits are in Alberta, Canada, accounting for greater than 70 per cent of world bitumen in place (Hein, 2006).

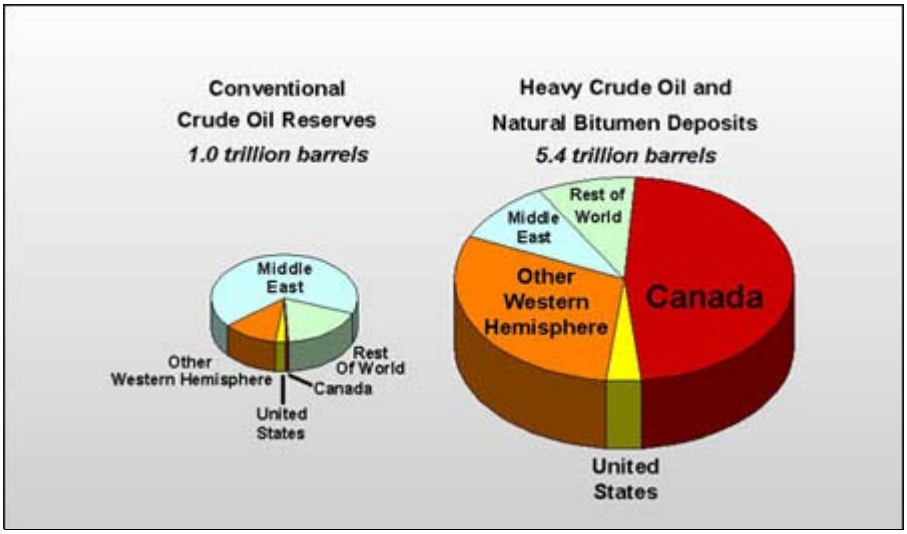

Figure 1.1 – Worldwide distribution of conventional and unconventional crude oil (Herron, 2000)

In Alberta, the total in-situ and mineable remaining proven reserves for bitumen are now 27.5 billion cubic meters or 173 billion barrels. This is represented with respect to all heavy oil bitumen resources in Canada and the United States in Figure 1.2. The ultimate potential recovery of surface-mineable crude bitumen in Alberta has recently been estimated to be 11 billion cubic meters or 69 billion barrels, whereas the ultimate potential recovery of crude bitumen using *in situ* (i.e. in the reservoir) recovery methods is estimated to be 39 billion cubic meters or 245 billion barrels, representing roughly 10 per cent of the resource in place (Alberta Energy and Utilities Board, 2007). This near 2-fold increase in reserve estimation (from proven to potential) is attributed to the potential *in situ* recovery of the resource. At present, most of the in-situ production of heavy oil and bitumen employ some variation of steam injection. Injecting steam into a heavy-hydrocarbon deposit can be effective in two ways. First, the viscosities of all hydrocarbons are greatly reduced as the temperature of the hydrocarbon increases. Therefore, as injected steam raises the temperature of a reservoir, any hydrocarbon liquid within the reservoir will flow more easily. Second, if injected steam heats a reservoir to sufficiently high temperatures, the heavy hydrocarbons within the reservoir will break down (or “convert”) into lighter hydrocarbons. This process is termed ‘in-situ

conversion'. With sufficient *in situ* conversion, the hydrocarbons produced at the surface will have characteristics similar to conventional crude oil (Herron, 2000). It therefore follows that improvements in the technology for *in situ* production, such as catalysis, would serve to aid in increasing the resource recovery factor translating to a greater yield of bitumen to supply the world's energy market.

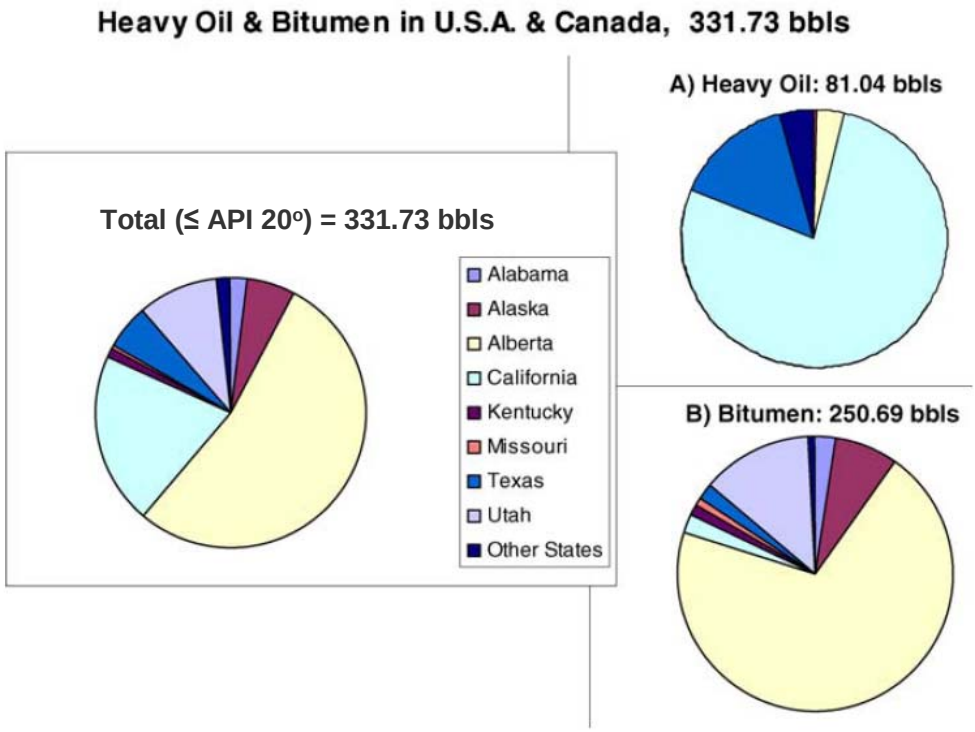

Figure 1.2 – Heavy oil and bitumen reserves in U.S.A. and Canada (Hein, 2006)

1.2 Motivation

Typically, commercial hydroprocessing catalysts are supported on alumina and used in a fixed bed reactor (FBR). In a FBR, the catalyst pellets are held in place and do not move as the liquid reactant travels through the bed. These catalysts are prone to deactivation from heavy feeds because carbonaceous materials (i.e. coke) or metals (mainly V and Ni) deposit near the outer surface of the pellet, causing pore-mouth plugging (Absi-Halabi et al., 1995). Typical catalyst pore sizes are in the 80 to 100 Å

range (Gary and Handwerk, 2001), however Athabasca asphaltene molecules typically present in heavy feeds may be great in size, ranging from 30 to 60 Å (Strausz and Lown, 2003), with a high tendency to aggregate into even larger masses due to the polar nature of the components (Monteagudo et al., 2001). Several attempts have been made to design a catalyst pore structure to facilitate easy access of the large asphaltenic reactants to the interior of the catalyst, but associated losses in surface area are unavoidable (Thakur and Thomas, 1985).

The ebullated bed reactor (EBR) addresses the issues encountered by FBRs when processing heavy feedstocks with high impurity contents. This is accomplished by its built-in on-stream catalyst addition and withdrawal system, which eliminates the need to shut down for catalyst replacement. The low pressure hydrogen recovery system also eliminates the need for high pressure equipment downstream, which is required when using FBRs. The ebullated bed reactor features an internal recirculation of the reactor liquid to fluidize (i.e. ebullate) the catalyst bed. In this way, the catalyst particles are held in suspension by the upward movement of this liquid reactant, in addition to hydrogen flow. Figure 1.3 provides an illustration of an ebullated bed reactor, first commercially featured for heavy oil hydroconversion by the Hydrocarbon Research Institute (HRI) in 1963 (H-Oil process) and later by Chevron Lummus Global (CLG) in 1980 (Ebullating Bed (LC-Fining) process) (Meyers, 2003). Although this technology successfully increases the cycle time by reducing the frequency of shutting down the reactor, it does not remove the issues of catalyst deactivation or facilitate easy access of the large reactants to the active sites.

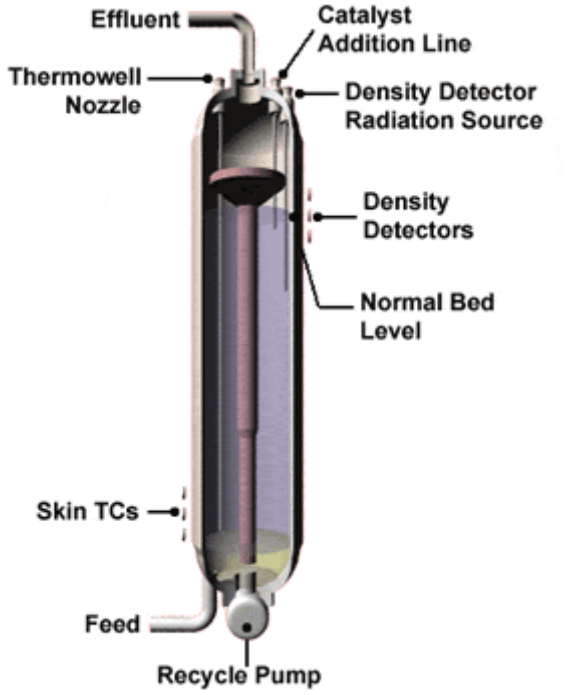

Figure 1.3 – Ebullated Bed Reactor (*Chevron*, 2007)

Trickle bed reactors are also used for hydrodesulfurization, hydrocracking, and hydrotreating of various high-boiling petroleum fractions. The term "trickle bed reactor" is often used to describe a reactor in which a liquid phase and a gas phase flow co-currently downward through a fixed bed of catalyst particles while reaction takes place. At sufficiently low liquid and gas flow rates the liquid trickles over the packing in essentially a laminar film, and the gas flows continuously through the voids in the bed. The direct and capital costs are significantly less for trickle bed operation than for an equivalent hydrodesulfurization unit operating entirely in the vapour phase. The use of this reactor type makes it possible to process feedstocks with such high boiling points that straight vapour phase operation would lead to excessive undesirable side reactions (Hill, 1977).

Several possible ways for improving the activity of the catalyst, including the use of new supports, novel active phases, or optimizing the preparation procedures, have been investigated (Bezverkhyy et al., 2001). Introduction of various additives and

modification of the sulfidation procedure or the promoter distribution by use of complexing agents has also been applied to improve hydrotreating catalysts (Topsoe et al., 1996).

As an alternative to supported catalysts, unsupported catalysts have been developed and, in particular, ultra-dispersed (UD) catalysts are of great interest for the processing of heavy feedstocks (Ren et al., 2004; Yoneyama and Song, 1999). UD catalysts have a number of characteristic advantages over supported catalysts in the upgrading of heavy oil feedstocks, such as minor deactivation, high inhibition of coke formation, ease in re-sulfiding from maximum interaction with oil and hydrogen, and a high degree of catalytic metal utilization due to the absence of diffusion limitations. UD catalysts are highly active due to their greater surface area of accessible active sites leading to an increase in the reactive site-to-mass ratio, thereby allowing large complex molecules (i.e. heavy hydrocarbons) to reach active sites rather than plugging pores as is the case in supported catalysts. Also, it has been discovered that moderate amounts of Ni and V may be deposited on the UD catalyst surface without deactivating the catalyst (Tian et al., 1998). UD hydroprocessing catalysts also have the potential application of upgrading and refining heavy oil *in situ,* as enhanced oil recovery (EOR) production techniques serve to raise the reservoir temperature and pressure conditions to those which favour hydroconversion reactions. From these elevated reservoir conditions, performing these reactions *in situ* would therefore potentially result in significant investment and energy savings.

1.3 Objectives

The main objective of this research is to produce and study molybdenum oxide catalysts synthesized from the decomposition of water-in-oil (w/o) emulsions. The catalysts were prepared in a continuous mode designed for online application to conventional above-ground hydroprocessing facilities or to *in situ* upgrading. For the purposes of establishing simple preparation and characterization procedures, catalysts were prepared in the less active oxide form and were not pre-sulfided before use, as

would be the case for industrial hydrotreating processes due to the favourable poisoning resistance of molybdenum sulfides. The specific objectives are to:

1. study the influence of decomposition temperature on particle size for a horizontal reactor configuration and compare these results to those obtained using a vertical reactor set-up from previous work (Vasquez and Pereira-Almao, 2006).
2. perform reactivity tests using UD particles (in pelletized form) to determine catalyst activity.
3. synthesize and evaluate UD catalysts within a horizontally positioned packed porous media reactor. Evaluation of catalytic performance is based on the upgrading of a heavy feedstock (bitumen and vacuum gas oil mixture).
4. track the profile of molybdenum deposition, if any, within the porous media.

1.4 Organization of Thesis

This thesis is structured as follows: Chapter One has provided some background recognizing the importance of this work and outlines the specific research goals. Chapter Two contains an overview of what has been reported in the literature to date, with direct association to this research. Chapter Three presents the experimental component describing the material, equipment and methodologies applied. Chapter Four presents the results and provides a discussion into their interpretation. Chapter Five summarizes the thesis and offers recommendations for continuing research. This thesis is further divided into three sub-sections. The first focuses solely on the UD Catalyst Preparation Unit. The second explores the reactivity of the particles produced from the preparation unit (after pelletizing). The third presents a preliminary study investigating the synthesis and reactivity of UD Mo-based particles in a continuous mode, using a heavy feedstock in a porous media, revealing the behaviour and activity of these particles in their natural state and in a simulated reservoir environment.

Chapter Two: Literature Review

This chapter introduces certain terminology and processes in the field of hydroprocessing and will provide an overview of previous research available in the open literature related to this topic. The review will then progress to a more detailed look at work performed on ultra-dispersed (UD) catalyst preparation, with specific emphasis on catalysts generated from water-in-oil emulsions with potential application for *in situ* hydroconversion reactions.

There are two possible routes for heavy oil conversion. The first is to remove carbon (in the form of coke) as a product having a low atomic hydrogen/carbon ratio while producing distillate of high atomic hydrogen/carbon ratio, such as C_1-C_4 hydrocarbon gases. These processes include thermal cracking, visbreaking, coking and fluid catalytic cracking (FCC). The second route introduces hydrogen via a hydrocracking/hydrogenolysis mechanism to reduce coke yield in favour of enhanced yields of liquid products and are referred to as hydroprocesses. This thesis focuses on the latter.

2.1 Hydroprocesses

2.1.1 Terminology

The terms hydroprocessing, hydrocracking, hydrogenolysis, hydrogenation, hydrotreating, and hydrodesulfurization are used rather loosely in the industry. This is because cracking and impurity removal reactions occur simultaneously and it is debatable as to which predominates (Gary and Handwerk, 2001). For clarity, these terms will be defined as follows. Hydroprocessing (i.e. hydrotreating and hydrocracking) will be used to refer to all the different processes in which hydrocarbons react with hydrogen. Hydrocracking (HCK) will be used to refer to those hydroprocesses that accomplish a significant conversion of the hydrocarbon feedstock to lower-boiling point products. Hydrotreating (HDT) is a finishing process that will be used to describe those relatively mild hydroprocesses whose primary purpose is to saturate olefins and remove impurities (e.g. S, N, etc.) (and not to change the boiling range) of the hydrocarbon feedstock. When

the hydrotreating process is specifically intended for sulfur removal it is termed hydrodesulfurization (HDS) and for nitrogen removal it is termed hydrodenitrogenation (HDN). Hydrogenolysis is a chemical reaction whereby hydrogen is added over a carbon-carbon or a carbon-heteroatom single bond, effectively causing a "lysis" of the bond. The heteroatom may vary, but usually is oxygen, nitrogen or sulfur. A lower energy requiring reaction is hydrogenation, where hydrogen is added over a carbon-carbon double bond (leading to the ultimate reduction to a single bond).

2.1.2 The Processes: Hydrotreating and Hydrocracking

Both hydrotreating and hydrocracking offer a means to suppress coking but they require significant associated hydrogen costs. Process parameters may require hydrogen pressures of the order of 1500 – 2500 psi (10 – 17 MPa) or even higher at temperatures in the range 643 – 698 K. Hydroprocessing reactions are also often slow thereby requiring residence times of 2 to 4 hours in units requiring thick (10 – 12 inch) walls (Speight, 2004). The operating conditions are adjusted according to the composition of the feedstock. For heavier feeds, the severity of the conditions (i.e. temperature and pressure) is increased. Table 2.1 summarizes the typical operating conditions for hydroprocesses at different severities (Billon and Bigeard, 2001; Heinrich and Kasztelan, 2001; Vasquez, 2007).

Table 2.1 – Hydroprocessing process parameters

Process	Feed	Products	Operating Conditions	Remarks
Hydrorefining Hydrotreating	All cuts	H_2S, NH_3, H_2O and liquids with same MW as feed	0.5 – 16 MPa 533 – 673 K 0.15 – 10 h^{-1}	Hydrogenates the feed with 10% or less hydrocracking. Removes sulfur, nitrogen and metals
Hydrocracking	Medium and heavy cuts	Light gases, naphtha, kerosene, diesel fuel, lube oils, FCC feed	10 – 20 MPa 623 – 703 K 0.2 – 2 h^{-1}	Changes the skeletal structure of the feed, by breaking carbon-carbon bonds
Mild Hydrocracking	Medium and heavy cuts	Kerosene, diesel oils, FCC oils	5 – 8 MPa 623 – 713 K 0.2 – 2 h^{-1}	Same as hydrocracking, but at lower severity. Hydrocracks 40% or less of the feed

To specifically target hydrocracking the world's most difficult, heavy, lower-value hydrocarbon streams (petroleum residuals, heavy oils from tar sands, shale oils, solvent-refined coal extracts, etc.), new reactor systems such as the H-Oil and LC-Fining residual hydroconversion process have been introduced. The Chevron Lummus Global Ebullated Bed Bottom-Of-The-Barrel Hydroconversion (LC-Fining) Process (see Figure 1.3) treats heavy hydrocarbons with hydrogen in the presence of catalyst to produce low sulfur products at conversion levels of 80 per cent and higher, far greater than those possibly obtained from conventional fixed bed reactors (Meyers, 2003).

Figure 2.1 shows a typical schematic of a refinery elucidating the locations for the hydrotreating and hydrocracking stages. It has become clear in recent years that HDT processes are the key to the production of fuels needed for transportation. New emission regulations have been adopted worldwide in an effort to reduce the adverse environmental impact created from the combustion of these fuels. The reductions of sulfur and aromatics have been mandated worldwide, but without sacrificing combustion performance. For light (low molecular weight) petroleum fractions, sulfur will reduce the stability of the product fuels and will poison the platinum based catalysts used for their combustion. For the heavier (higher molecular weight) petroleum fractions that are converted into jet and heating fuels, the motivation to remove sulfur derives from the requirements to reduce SO_x emissions (Zonnevylle and Hoffmann, 1988). Refinery processes for upgrading gasolines also aim at a maximum yield of high octane, nonaromatic components. Isoparaffins and cycloparaffins are desirable compounds since they constitute alternatives to aromatics in increasing octane number in gasoline (American Society for Testing Materials, 1958).

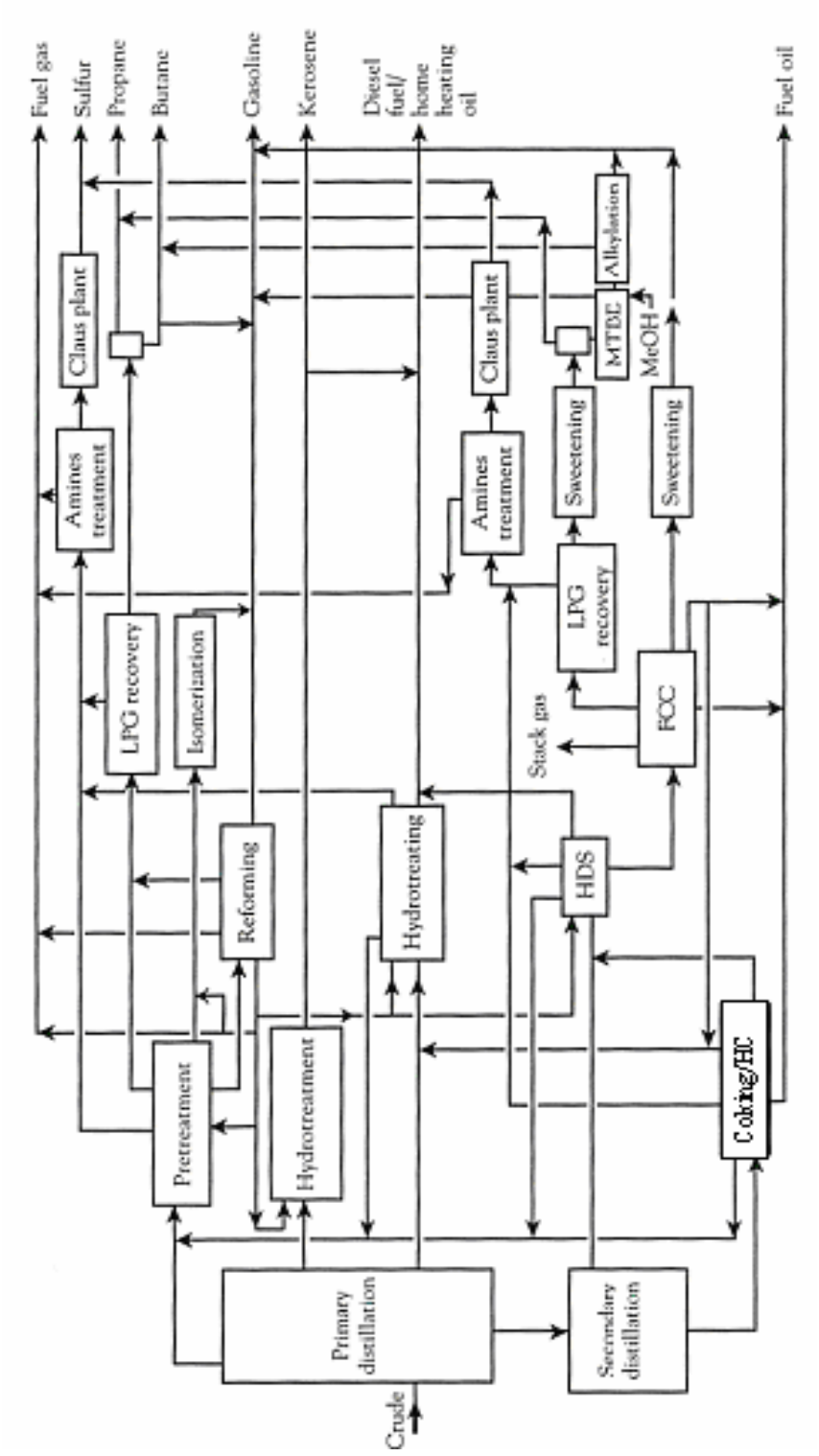

Figure 2.1 – Typical schematic of a refinery (Heinrich, 1995)

2.1.3 Thermodynamics

To illustrate the thermodynamics of hydroprocessing, model molecules have been selected for their hydroconversion and are presented in Table 2.2 for low and high temperature conditions. In order to interpret the calculated results, a brief review of thermodynamic theory is presented.

The equilibrium constant (K), determines if a reaction is feasible (spontaneous) or not thermodynamically. For a given reaction the equilibrium constant provides a relationship among the partial pressures or concentrations;

$$aA + bB \Leftrightarrow cC + dD$$

$$K = \frac{[C]^c [D]^d}{[A]^a [B]^b}$$

The equilibrium constant can be expressed in terms of the change in standard (i.e. relating to conditions of *298 K and 100 kPa*) Gibbs energy (ΔG^o) by the following reaction;

$$\Delta G^o = \sum \left(n_i G_i^{\ o} \right)_{prod} - \sum \left(n_i G_i^{\ o} \right)_{react} = -RT \ln(K)$$

In order for the reaction to proceed from reactants to products, the change in Gibbs energy must be negative. It follows that the greater this negative value, the more stable the products are in relation to the reactants.

Table 2.2 – Gibbs energy calculations for hydroprocessing reactions

Sample Reaction *	Type	ΔG^o (500 K) (KJ)	ΔG^o (700 K) (KJ)
$C_7H_{8\,(l)} + 3\ H_{2\,(g)} \rightarrow C_7H_{14\,(l)}$	HYD	-61.76	0.828
$C_7H_{8\,(l)} + H_{2(g)} \rightarrow C_6H_{6\,(l)} + CH_{4\,(g)}$	HCK	-37.82	-37.54
$C_4H_4S_{\,(g)} + 4\ H_{2\,(g)} \rightarrow C_4H_{10\,(g)} + H_2S_{\,(g)}$	HDS	-1639	-1195

** All reactions carried out at 50 atmospheres (Bale et al., 1996)*

From the results presented in Table 2.2, it is evident that all three hydroprocesses are favoured thermodynamically at the lower temperature condition. It is also important to realise that despite the greater change in Gibbs energy at these lower temperatures, there is no suggestion that the products presented in the reactions are the most stable species, only that there is greater stability for the products at lower temperatures. In order for these reactions to take place, an activation energy barrier must be overcome through an elevation in temperature, the addition of a catalyst, or both. When the necessary increase in temperature makes the reaction unfavourable, a catalyst is of no use.

Thermodyamic investigations of Mo-supported catalysts in the literature indicate that the optimal reaction temperature for hydrogenation of multi-ring aromatics to isoparaffins and cycloparaffins occurs around 598 K, based on calculated equilibrium constants (Demirel and Wiser, 1998). Reactions that break carbon-heteroatom bonds, such as thiophene HDS, are also exothermic, leading to considerable generation of heat. Following the principle of Le Chatelier, increasing the partial pressure of hydrogen will serve to promote the reaction in the direction illustrated (from reactants to products).

2.2 Hydrotreating Catalysts

Transition metal based catalysts have been widely used in the petroleum industry for the hydroprocessing of heavy oil fractions (Kim et al., 1994). Molybdenum (Mo) is usually the preferred transition metal based on its overall effectiveness in promoting boiling point conversion, Conradson carbon conversion and hydrodesulfurization (HDS) (Del Bianco et al., 1993; Panariti et al., 2000a). MoS_2 nanoclusters with a triangular morphology have been recently found to offer a layered structure and interrupted domains which provide abundant edges and active sites in comparison to other metals (e.g. Ni, Co, Fe, etc.). It is well established that the MoS_2 edge structures, along with morphology, active sites and molecular interactions play a key role in the higher activity of Mo when compared to other elements (Lauritsen et al., 2004).

Catalysts developed for hydrotreating include cobalt and molybdenum oxides on alumina, nickel oxide, nickel thiomolybdate, tungsten and nickel sulfides and vanadium oxide (Gary and Handwerk, 2001). These catalysts are also bifunctional, in that they have

a hydrogenating function from the metal (or metal sulfide) and they possess a cracking function from the alumina. Molybdenum oxides on γ-alumina (a high-area robust porous support) catalysts are among the most commonly used catalysts in hydroprocessing because they have proven to be selective, easy to regenerate, and resistant to poisons when they are activated by converting the hydrogenation metals from the oxide to the sulfide form. Molybdenum sulfide, MoS_2, is several orders of magnitude less active than Mo metal, but it has the unique advantage of not being poisoned by sulfur compounds typically present in heavy feeds. The molybdenum sulfide is highly dispersed on the support because the catalytic metal is expensive and it is efficient to have most of the metal exposed at a surface and accessible to reactants (Gates, 1992). MoS_2 catalyst is also unusual in that it can still function with massive amounts of deposits (e.g. Ni and V sulfides from organometallic constituents in the oil and coke) covering its surface and plugging its pores, sometimes even when the mass of deposits outweigh the mass of original fresh catalyst (Gates, 2007).

The addition of a second transition metal (Co, Ni etc.) to a sulfide such as MoS_2 has also been shown to lead to a significant enhancement of hydrogenation and HDS activity (Eijsbouts et al., 2005; Topsøe, 2007). Recent research into HDS reactions at high temperature and pressure with MoS_2 (or WS_2) catalysts promoted by cobalt and nickel has been reported (Guevara-Lara et al., 2007). These bi-functional supported catalysts are typically used in a combi-bed with a hydrogenation active Ni-Mo-catalyst in the inlet layer, followed by the more HDS-active (and less hydrogen consuming) Co-Mo-catalyst (Rostrup-Nielsen, 2004). The Ni-Mo catalyst works best when inhibiting nitrogen compounds have been removed from the feedstock. Cobalt is a multiple function promoter. It makes molybdenum oxide better dispersed on the carrier and thus facilitates the oxide to be easily reduced and sulfided in the formation of the active phases (Li et al., 1999). In the case of hydrogenation, cobalt also promotes the dissociation of adsorbed CO and activation of H_2. Most recently, new discoveries regarding molybdenum sulfide based hydrotreating catalysts have been presented by researchers at Haldor Topsøe in Denmark, where insight is revealed into the mechanistic, structural and particle size effects of the catalysts (Besenbacher et al., 2008).

Among non-conventional catalysts, metal carbides have been tested for hydroprocessing. One author cites rather peculiar trends in their intrinsic activity making them unsuitable for hydroprocessing (Ancheyta et al., 2005). However, another source describes transition metal carbides as being suitable for hydrotreatment applications due to their high HYD properties (Breysse et al., 2003). Molybdenum carbide has been reported as being as active as ruthenium in liquid or gas hydrogenation reactions and appears to be resistant to sulfur poisoning (Oyama, S.T., Catal. Today 15, 179 (1992)) but acts slightly differently than conventional sulfided catalysts regarding selectivity.

2.2.1 Catalyst Preparation

For hydrotreating catalysts, moist powders are agglomerated and shaped into pellets using a bowl granulation process. Hydrothermal treatment follows to achieve the desired texture, structure and homogeneity of the catalyst. Calcination is carried out under oxygen flow at 773 K prior to impregnation. Calcination enables control of the pore size diameter while obtaining the desired mechanic resistance. The general preparation method for a MoS_2 HDS catalyst involves impregnating a support, typically γ-alumina, silica or a composite type of support (eg. TiO_2-Al_2O_3). γ-Alumina has been regarded as a superior support for Mo-based catalysts due to its ability to increase the degree of dispersion of Mo species increasing thus the concentration of catalytically active sites (Komatsu and Yashima, 1986). The active phase of the catalyst is partially deposited by impregnation on one of these pre-shaped supports. Composite types of supports are typically prepared using the CVD (Chemical-Vapour-Deposition) method (Yoshinaka and Segawa, 1988). After drying, calcination and removal of the decomposition products, the catalyst is treated with hydrogen gas and some sulfur-containing compounds to convert the surface oxides into the well dispersed sulfides (MoS_2) that are the catalytic active species on the support. The sulfiding reaction is highly exothermic and care must be taken to prevent excessive temperatures during activation (Gary and Handwerk, 2001).

The high concentrations of heteroatoms, metals (e.g. nickel, vanadium and iron) and coke precursors typically found in heavy oil have a major influence upon catalyst

performance and must, therefore, also be considered in catalyst design and/or catalyst selection. Many catalyst preparation reports omit important details (for proprietary reasons) and are therefore difficult to reproduce exactly. Preparations require details of morphology, grain size and specific macroscopic properties of the catalyst, ultimately leading to an improvement in catalytic activity, selectivity and production.

2.2.2 Reaction Kinetics and Mechanisms

Although a catalyst can only increase the rate of a thermodynamically feasible reaction, kinetic limitations imposed by certain systems (namely, high activation energies) create the need for such a promoting agent. A catalyzed reaction can give the same final products as a noncatalyzed reaction; however a great variety of intermediate products may be obtained depending on the catalyst used. For this reason, and acknowledging the tight product specifications for marketing oils, great effort has been placed into tailoring hydrotreating catalysts for a wide variety of complex feedstocks.

Heavy oil hydroprocessing demands knowledge of simultaneous mass and energy transfer, fluid dynamics, chemical reaction rates and a comprehensive understanding of the complex chemical reactions in multiphase flow systems. Fluid dynamics is related to the reactor type (fixed bed, ebullated bed, etc.) which is important for the rate of mass and energy transfer between and/or within the phases. Chemical kinetics is important in determining reactor size, reactor dynamics (i.e. control mechanism), product yield and quality. Mechanism of the catalytic reactions (chemisorption, diffusion in porous media and catalytic reactions) and phase equilibrium (thermodynamics) relations are also important elements to hydroprocessing (Speight, 2004).

Hydrodesulfurization (HDS) is the most common industrial process for sulfur removal and, because of changing environmental regulations and specifications for fuel oil production, considerable efforts have been made in the last few years to develop better catalysts for this process. More than a quarter of a century ago the kinetics of HDS over dispersed supported Mo-based sulfide catalysts was well understood (Vrinat, 1983), although much debate exists regarding the reaction pathway (Sullivan and Ekerdt, 1988). These catalysts generally still remain accepted as the industry standard for HDS.

This thesis will address hydrodesulfurization by focusing on the complete hydrogenation of thiophene (C_4H_4S). Thiophene (Figure 2.2) is representative of organic sulfur compounds that are hydrogenated in commercial hydrodesulfurization of petroleum naphtha (Hill, 1977). Thiophene is a 5-membered planar ring and is the simplest aromatic in the feedstock.

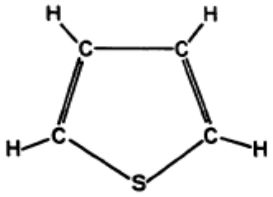

Figure 2.2 – Representation of a thiophene molecule

The HDS process results in the transformation of thiophene into butane and hydrogen sulfide via a series of intermediate steps, which are illustrated in the proposed reaction mechanism. The resulting overall reaction may be presented as follows:

$$C_4H_4S \text{ (Thiophene)} + 4\,H_2 \rightarrow H_2S + C_4H_{10} \text{ (n-Butane)}$$

The rate expressions proposed for thiophene HDS have a general form:

$$r = \frac{kK_T P_T K_H P_H}{(1 + K_T P_T + K_S P_S)^2}$$

where r is the reaction rate, k is the rate constant; K_i are equilibrium constants; P_i are pressure values; and the subscripts T, H, S refer to thiophene, hydrogen, and H_2S, respectively. This expression implies first-order adsorption of both thiophene and hydrogen and adsorption inhibition by thiophene and H_2S. The open literature on the kinetic modeling of hydrodesulfurization is vast however, due to the complexity of the reaction mechanism.

A mechanistic pathway is proposed (Figure 2.3) that is consistent with the analysis of the observed kinetics of thiophene HDS (Gellman et al., 1987). Interpreting their data leads to three conclusions. First, the hydrogen coverage of the catalytic surface varies in the temperature range 523-698 K resulting in non-Arrhennius-type temperature dependences for the rates of production of butane and butene. At a temperature of 613 K the coverage is at the low end of the hydrogen adsorption isotherm and thus varies as the half-order power of the hydrogen pressure. Second, the rate-determining step in the production of butadiene occurs prior to any hydrogenation steps. This results in the observed first-order dependence on thiophene pressure and apparent independence of hydrogen pressure. Finally, the hydrogenated products are produced via an intermediate whose coverage saturates its available adsorption sites, resulting in an independence of thiophene pressure.

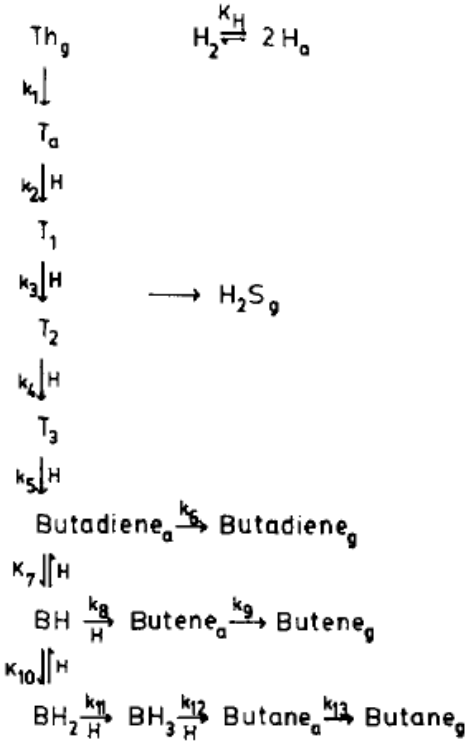

Figure 2.3 – A reaction mechanism for thiophene HDS (Gellman et al., 1987)

Gellman, Neiman and Somorjai also found that butadiene production was unaffected by adsorbed sulfur, suggesting that the thiophene and butadiene adsorption sites or configurations are different from those of the partially hydrogenated intermediates.

Figure 2.4 presents another more comprehensive mechanism for thiophene HDS (Sullivan and Ekerdt, 1988).

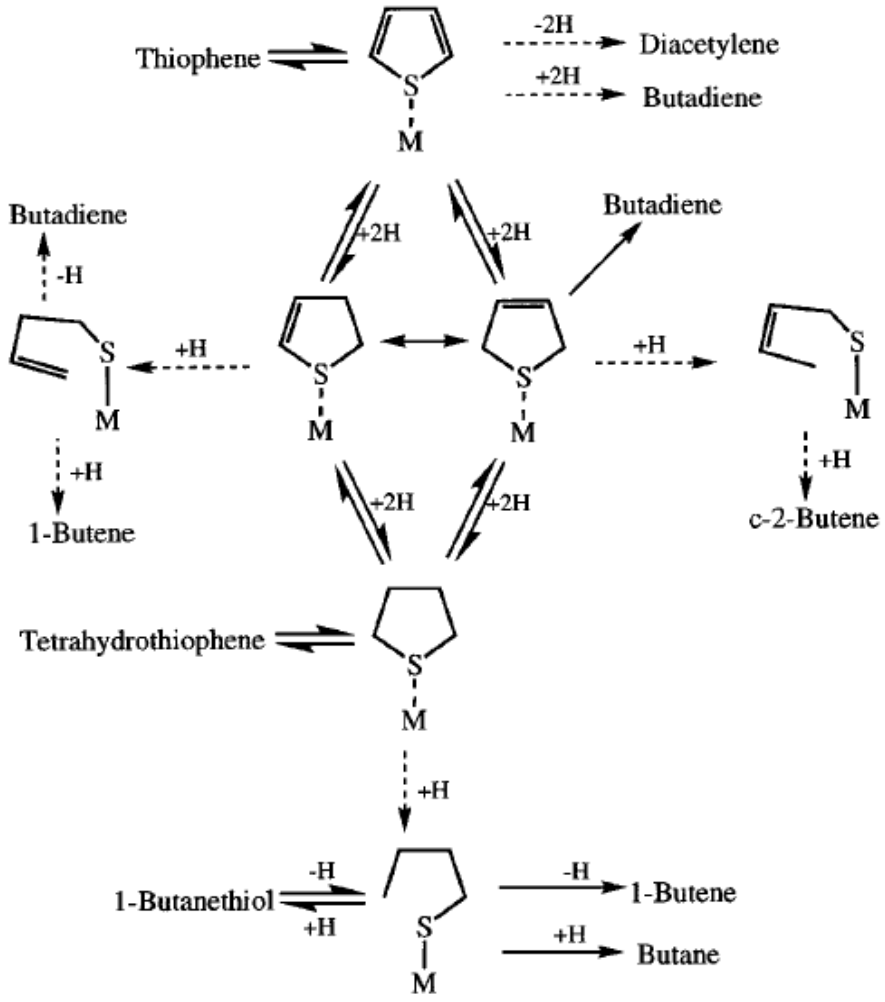

Figure 2.4 – Alternate mechanism for thiophene HDS (Sullivan and Ekerdt, 1988)

Sullivan and Ekerdt analyzed the products of thiophene HDS on MoS_2/SiO_2 at 530 K. Figure 2.5 has been extracted from their report to illustrate some of the observed behaviour.

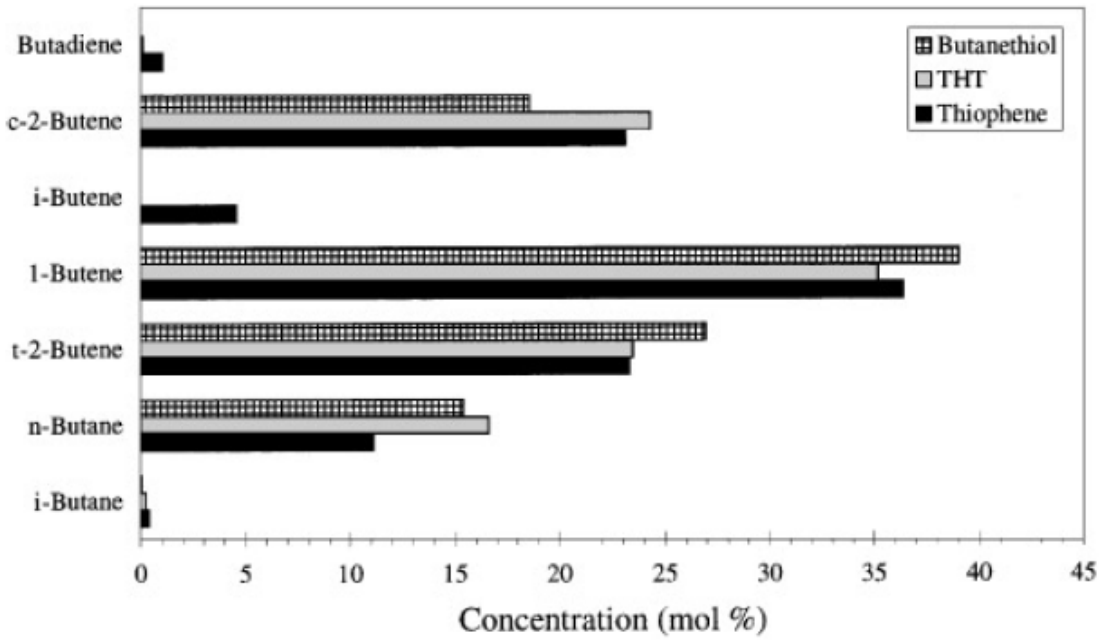

Figure 2.5 – C_4H_x products of thiophene, THT, and 1-butanethiol HDS at 530 K (Sullivan and Ekerdt, 1988)

The experimental temperature of 530 K was selected in order to minimize secondary hydrogenation and isomerization reactions. Based on this (and other) information, the HDS of thiophene is proven to occur through many possible intermediates, such as those in the aforementioned complex reaction mechanisms.

Lauritsen, Nyberg, Norskov, Clausen, Topsoe, Laegasgaard and Besenacher combat these proposed mechanisms based on their findings through the use of atomically resolved scanning tunnelling microscopy (STM), which offers atomic-scale insight into the interactions with hydrogen and thiophenes (Lauritsen et al., 2005). The STM images proved that thiophene molecules can adsorb and react on the fully sulfided edges of triangular single-layer MoS_2 nanoclusters. The fully sulfur-saturated sites were found to be capable of adsorbing thiophene, and when thiophene and hydrogen reactants are co-

adsorbed there, a reaction path is revealed which leads to partial hydrogenation of the thiophene followed by C-S bond activation and ring opening of thiophene molecules. These should be acknowledged as important first steps in the hydrodesulfurization of thiophene. Their proposed reaction scheme and calculated energies associated with the individual steps in the reaction path are illustrated in Figure 2.6 (a) and (b), respectively.

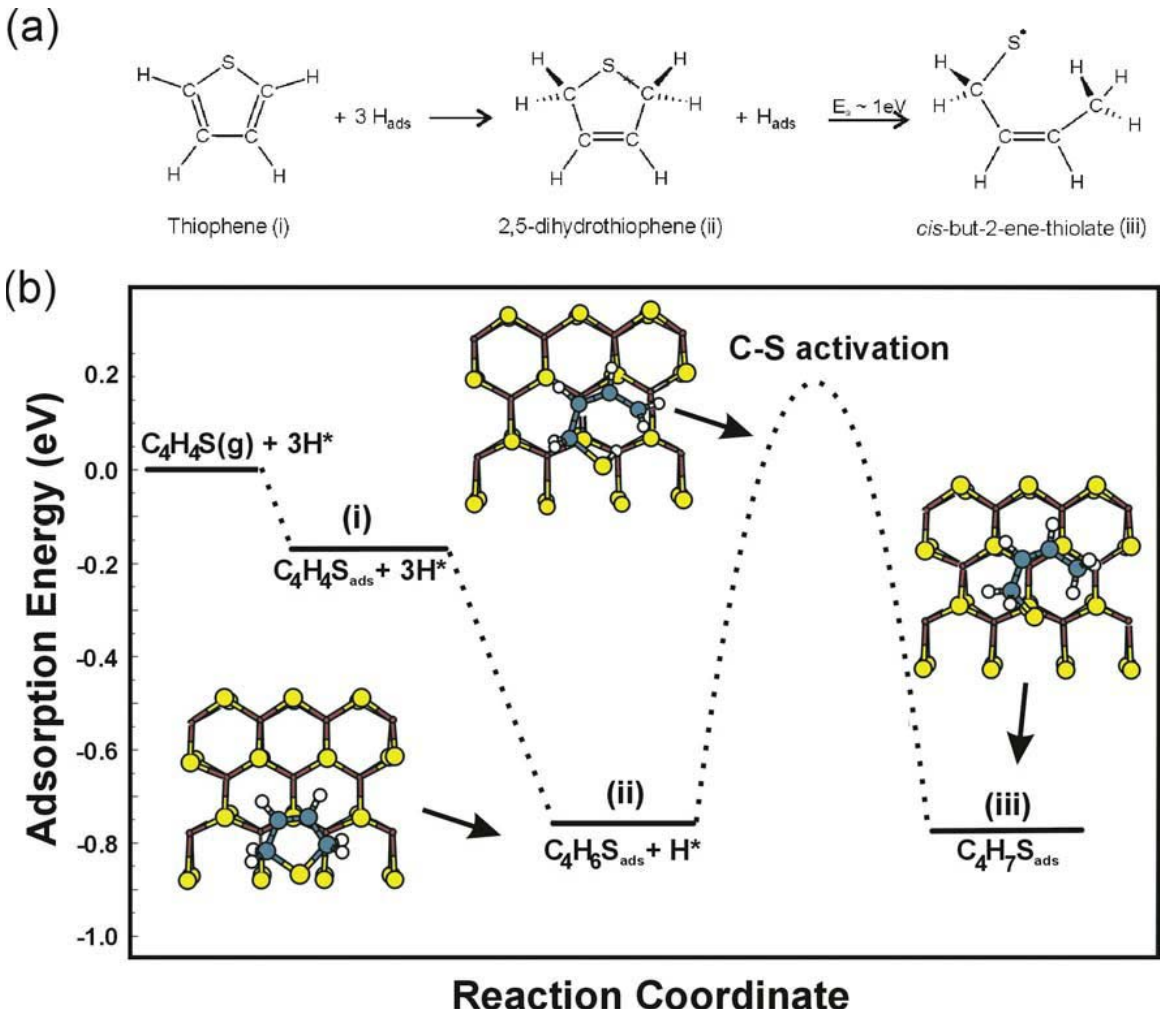

Figure 2.6 – (a) The Proposed Reaction Scheme of Thiophene Intermediates
(b) The Calculated Energies Associated with the Individual Steps in the Reaction Path
(Lauritsen et al., 2005)

It is the STM characterization which offers insight into the chemistry associated with the metallic character of the brim sites located adjacent to the MoS_2 edges. Based on their findings, thiophene HDS may proceed by a mechanism very different from the previously presented schemes of Gellman, Neiman & Somorjai and Sullivan & Ekerdt.

The fact that this process and many others are not fully understood prohibits the development of the actual reaction mechanisms, thereby preventing the formation of an optimum catalyst configuration. Until the complexities of sulfur-containing aromatic compound hydrogenation are better understood, maximizing reaction efficiencies and selectivities cannot be achieved.

2.2.3 Supported Catalyst Deactivation

The supported catalyst system deactivates due to coke deposition and metal poisoning that occurs in three phases. The first phase is coke deposition on the fresh catalyst system. The second phase is represented by the constant deactivation rate that is influenced by metal deposition from the feedstock, during which nickel and vanadium fill up the pores and block active sites. The third is the rapid deactivation caused by the final constriction of the catalyst pore mouth by metal deposition. Therefore, in processing heavier oils, large pore volumes and tolerance to the feedstock constituents are required if a high level of efficiency is to be achieved. Large pore diameters are required to lower diffusion limitations. Highly porous, low surface area catalysts have favourable transport properties and have high metals capacities and resistance to pore plugging but the hydrotreating activity of these catalysts is relatively low. Less porous, high surface area catalysts have a higher hydrotreating activity, but are now more susceptible to deactivation through pore-mouth plugging. An optimum balance in metals capacity and hydrotreating activity is therefore necessary to optimize the catalyst load and maximize its life cycle. In order to overcome the pore-plugging problem of supported catalysts, ultra-dispersed (unsupported) catalysts have been developed and are discussed in Section 2.3.

2.3 Ultra Dispersed (Unsupported) Catalyst Technologies

Over the past 25 years, the interest in the development of dispersed catalysts for conversion of heavy feeds to distillate has increased significantly. This is because catalyst activity is not only controlled by the composition of the catalyst under a given set of reaction conditions, but also by the degree of catalyst dispersion. The use of UD catalysts offers several advantages. These catalysts have large surface to volume ratio due to their submicron size which leads to improved catalytic performance which occurs on the high surface area of the small particles, ultimately yielding improved processing economics. Additionally, mobilizing the particle (suspended like a heavy molecule), as well as the heavy molecules in the reactor, increases the contacting probabilities and increases the reactor volume effectively available for the transformations. Another characteristic advantage of UD catalysts is that as there is no fixed bed, preferential channelling common to FBR operations is avoided. Longer run times for conversion may also be possible as the need to replace a deactivated catalyst bed is unnecessary. If the UD catalysts are used for an in-situ recovery technique, one potential disadvantage is dealing with catalyst recovery and contamination of the product. However, recovering supported catalysts from an in-situ technique would likely pose a far greater challenge.

With respect to converting heavy feeds with supported catalysts, it is important to recognize that the porosity of the catalyst is inversely proportional to the surface availability. This means the larger the pore radii the lower the surface area, which implies fewer sites to anchor active species. Observing the fact that the pore must be approximately six times (or greater) the size of the molecules targeted to convert in order to maximize the rate of access to the sites and put the reaction under catalytic (chemical) rate control, implies a very large reduction in available sites when dealing with large asphaltene molecules typically present in heavy feeds. Recalling that the asphaltene average size is between 3 to 6 nm, the pores in the porous catalyst are required to be around 40 nm and the largest agglomerates (> 10 nm) would still have trouble penetrating the pores. It is acknowledged that there are many molecules with lower sizes, but they are easier to process, whereas the heaviest molecules if not quickly converted would readily

produce deposits and pore plugging given their higher tendency to condense their structures and to agglomerate.

The concept of the existence of an active surface area (ASA) representing a small fraction of the total surface area (TSA) was developed (Laine et al., 1963) in order to have a comparative value for catalyst reactivity. A porous catalyst with mono-modal 20 nm pore radii would likely have a total surface area (TSA) no greater than 60 m^2/g (Pereira-Almao, 2006). If this catalyst surface area was covered with a monolayer, there would never be more than that surface of active sites available for reaction. However, the active surface area (ASA) would typically be much less. This is estimated to be an order of magnitude less due to the degree of metal dispersion.

For an ideal porous catalyst with a mono-modal porous distribution and assuming cylindrical pores:

$$S = \frac{2V_p}{r_p}$$

where S represents the surface area per unit weight (m^2/g), V_p represents the pore volume per unit weight (m^3/g) and r_p represents the average pore radius (m)

Assuming spherical particles whose agglomeration constitutes the mass of the catalyst:

$$S = \frac{3}{\rho r_p}$$

where ρ represents the density of the support (g/m^3)

A supported catalyst density of 2.5 x 10^6 g/m^3 and an average pore radius of 20 nm therefore yields S = 60 m^2/g.

Figure 2.7 illustrates the relationship between active surface area and particle size for UD catalysts assuming non-porous particles (to be overly conservative) with a spherical geometry.

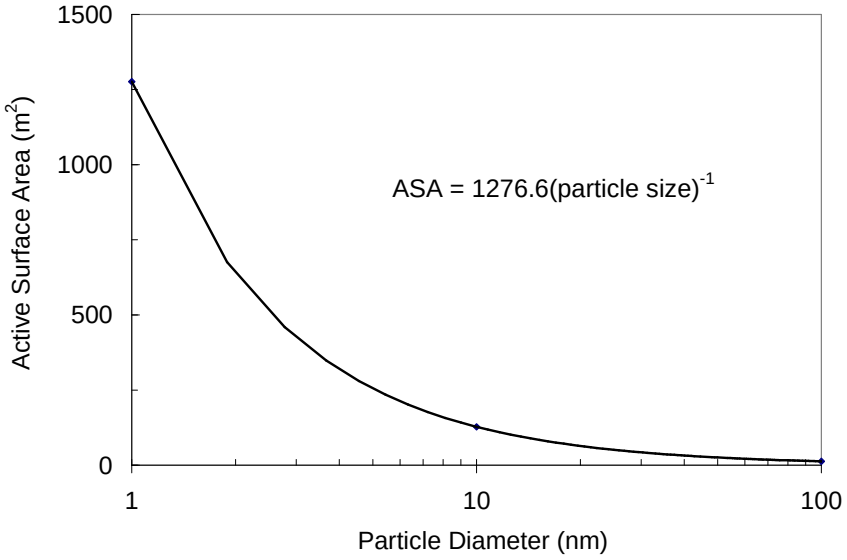

Figure 2.7 – Active surface area vs. particle size for UD particles

From the figure it may be witnessed that for particle diameters of 100 nm the active surface area is comparable to that of a conventional catalyst with tremendous gains in active surface area as the particles are further reduced in size based on the shape of the power law correlation. For comparison, INCO has used carbonyl-based CVD technology to create a nano nickel catalyst powder with an average nickel particle size of 60 nm and an active surface area between 30 - 100 m^2/g (INCO Special Products, 2006). From Figure 2.7, a 60 nm particle corresponds to an active surface area of approximately 22 m^2/g. However, once again, this model operates with the assumptions that the particles are spherical and have no porosity; porosity which leads to penetration and channels which, along with other geometry considerations, would increase the active surface area to values equivalent to or greater than that of the nano nickel powder.

Some of the methods that have been used to produce materials of nanometer structure include acidification of organometallic compounds (Osseo-Asare et al., 1995), thermal decomposition of organometallic compounds (Lisitsyn et al., 1989), metal evaporation (Davis and Klabunde, 1982), the reduction of metal salts (Boutonnet et al., 1982; Cauliez et al., 1991), and sonochemical decomposition of metal carbonyl compounds (Suslick et al., 1995).

Several patents for dispersed catalyst technologies in heavy oil upgrading applications may be found in the literature (Bearden and Aldridge, 1979; Derouane and Varghese, 1986; Moll and Quarderer, 1979). The M-Coke hydroconversion process for heavy oil states that Mo concentrations of less than 1000 ppm will result in effective conversion (Bearden and Aldridge, 1979). One hydrogenation process, which uses a Mo-catalyst derived from the same precursor salt used in this research, ammonium heptamolybdate (AHM), claims proportions of 100-10000 ppm of Mo (based on the substance being hydrogenated) may yield good results (Moll and Quarderer, 1979). At these concentrations it may not even be economically necessary to include a catalyst recovery step, conditional that catalyst remaining with the products no longer has a significant impact on the product specifications or quality.

Not surprisingly, increasing Mo catalyst concentration increases the reduction of heteroatoms in the product and lowers the Conradson Carbon Residue (CCR) value in petroleum residue. The CCR (ASTM-189) value is considered by some to give an approximate indication of the coke forming propensity of the fuel. A Mo concentration of 200 ppm for coke suppression has been suggested as a lower limit for hydrotreating this heavy hydrocarbon fraction with dispersed Mo catalysts (Marchionna et al., 1994). Due to the capability of dispersed catalysts to control coke formation, slurry processes are generally considered an interesting alternative to the conventional hydrocracking technologies (Panariti et al., 2000a; Panariti et al., 2000b).

2.4 Ultra Dispersed Catalysts Prepared from Microemulsions

Microemulsions have been defined as being colloidal *'nano-dispersions'* of water-in-oil (w/o) or oil-in-water (o/w) stabilized by a surfactant film (Lopez-Quintela, 2003). For w/o emulsions, small water droplets are dispersed in a continuous oil phase through surfactant addition and stirring forming reverse micelles as illustrated in Figure 2.8. These thermodynamically stable dispersions look like a homogeneous solution but at the molecular scale, they appear to be heterogeneous. Microemulsions feature nano-spherical mono-sized droplets from 10 to 100 nm depending on the type of surfactant.

These are the nano-reactors used to carry out the chemical reactions or compartmentalize the pre-cursor metal compounds (i.e. water soluble salts) necessary to synthesize nano-materials. The size of the micelle, and therefore the size of the particle formed in its core, is easily controlled by varying the water to surfactant ratio. When the amount of water and oil is kept at fixed values, an increase in the amount of surfactant increases the number of droplets, which decreases the number of metal ions per droplet and consequently the particle size (Pileni and Lisiecki, 1993). It has also been found that a decrease in nanoparticle formation rate (longer residence time, lower space velocity) gives rise to a larger final particle size (de Dios et al., 2005).

It should be pointed out that the system is strongly sensitive with respect to decomposition temperature, particularly in the case of non-ionic surfactants such as those used in this research (e.g. TWEEN 80 and SPAN 80). Other parameters, such as chemical reaction rate, concentration and temperature ramping, have been demonstrated to also affect size (de Dios et al., 2005).

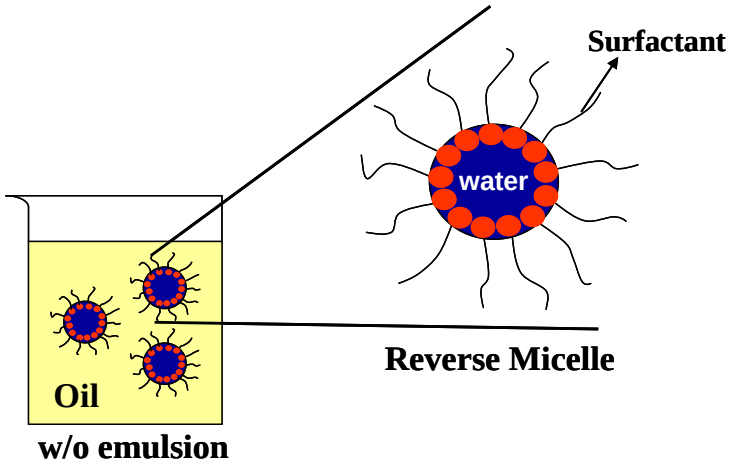

Figure 2.8 – The microscopic structure of a water-in-oil microemulsion

The first implementation of water-in oil (w/o) microemulsions to produce metal nanoparticles was introduced in 1982; nanoparticles (3-5 nm) which were intended to be adsorbed onto a support for catalytic purposes (Boutonnet et al., 1982). Although extremely small dispersed particles can be prepared with this technique, they do not readily form kinetically well stabilized colloids as nanoparticles have a propensity to

agglomerate and sediment. The method usually employed for the preparation of supported metal catalysts using microemulsions is the impregnation technique. It is possible to prepare small metal particles using this technique but it is quite difficult to obtain a narrow particle size distribution due to the morphology of the catalyst support which has some effect on the structure and size of the metal particles (Eriksson et al., 2004). The mechanisms to control the final size and size distribution of these particles are still not fully understood.

There are three main ways of preparation in order to obtain nanoparticles from microemulsions. The first is by mixing two microemulsions; one containing the precursor and the other a precipitating agent. The second is by adding a precipitating agent directly to the microemulsion containing the metal precursor. The third is to decompose the metal precursor in the microemulsion at high temperature. The work presented herein focuses on the latter.

With respect to the decomposition of organometallic compounds from dispersions of o/w mediated routes, there are a limited number of oil-soluble Mo compounds and these compounds have limited solubility in heavy feeds with high associated costs. Under a thermal treatment, less expensive aqueous salts, which are dissolved in the water pools of w/o emulsions, can be easily decomposed to give rise to a slurry of fine submicron solid particles, which can be successfully used in the upgrading of heavy feeds (Del Bianco et al., 1993).

2.5 Mo-Based Ultra Dispersed Catalyst Synthesis from a Water-in-Oil Emulsion

Prior to the 21st century there was little published research on Mo-based nanoparticle synthesis for hydroprocessing reactions from the decomposition of w/o emulsions. Recently however, studies have been performed that indicate that decomposition temperature, residence time, water-to-oil ratio, and surfactant concentration all have an effect on the size of the molybdenum oxide particles produced for such reactions (Müller et al., 1972; Vasquez and Pereira-Almao, 2006; Wang, 2004).

As previously stated, for the purposes of establishing simple preparation and characterization procedures, ultra dispersed catalysts were prepared in the less active

oxide form (MoO_2 and MoO_3) from the decomposition of ammonium heptamolybdate tetrahydrate (herein referred to as AHM). The desired sulfide form for the catalyst can ultimately be formed during the hydrogenation process from the sulfur naturally present in the heavy oil or by presulfiding the catalyst. MoS_2 is by far the most easily obtained compound as, in both sulfiding and reducing atmospheres, at moderate temperatures (573 - 873 K) the molybdenum oxides MoO_3 and MoO_2, as well as the higher moly sulfides (MoS_4 and MoS_3), are transformed to MoS_2 (Grange and Delmon, 1974). Thermodynamic validation of this assertion will be presented in Section 4.1.6 through the use of predominance diagrams.

A variety of reaction mechanisms for the decomposition of AHM in atmospheres containing air and/or hydrogen have been proposed (Hanafi et al., 1981; Said and Halawy, 1994; Yong, 1990). Various thermal analysis techniques from previous investigations suggest that regardless of the atmosphere used or the mechanism of decomposition, MoO_3 forms in the temperature range of 533 to 633 K (Yong, 1990). This temperature range is of particular interest as it meets the temperature requirements of typical hydroprocessing reactions, specifically hydrotreating (i.e. reactions governing the removal of hetero-atoms such as sulfur, nitrogen and metals). Complete thermal decomposition of AHM for this temperature range may be presented by the following reaction:

$$(NH_4)_6 Mo_7 O_{24} \cdot 4H_2O \rightarrow 7MoO_3 + 7H_2O + 6NH_3$$

It should be noted that ammonia gas (one of the products of the above decomposition reaction) begins to thermally decompose at temperatures in the vicinity of 456 K (see Thermodynamics Section 4.1.6) to produce hydrogen, although the reaction kinetics are unknown given the presence of a Mo catalyst. Research has been conducted on ammonia decomposition/dehydrogenation in the presence of water vapour with a Ni, Ru, and Pd base formula (Friedlander et al., 1977) and an Ir formula (Choudhary et al., 2003), however no publications were found that investigated the presence of a Mo-base formula.

2.6 UD Catalyst Applications for In-Situ Upgrading

A potentially more economic alternative to upgrading heavy crude oil, using large high pressure reactors above ground, is upgrading the oil prior to production, either in an oil-bearing reservoir, near a producing well, or in the producing well-bore. Successful in-situ catalytic upgrading projects have already been proposed (Weissman and Kessler, 1996). These involve placing heterogeneous catalysts in or near a production well, passing oil and co-reactants, such as hydrogen, water, or carbon monoxide, over the catalyst, achieving sufficient temperatures and pressures for a reasonable degree of upgrading, and producing the upgraded oil. Until a couple years ago however, the injection of UD catalysts into an oil bearing reservoir or in the producing well-bore has not been investigated. The Alberta Ingenuity Centre for In-Situ Energy launched an initiative in December 2005 proposing this idea as a central one for producing novel in-situ upgrading coupled with thermal EOR methods. This work, and results from others yet unpublished, pioneers this paradigm-breaking technology for heavy oil upgrading catalysis.

In order to be useful for in-situ upgrading, the UD catalysts need to have significant catalytic activity in the presence of aqueous brine solutions and at temperatures, pressures, and hydrogen partial pressures outside of their typical design parameters. Some success at hydroprocessing of heavy crude oils in water has been demonstrated using supported catalyst, but at surface processing conditions and at a diminished catalytic activity (Laurent and Delmon, 1994), or at very high pressures and temperatures to achieve reasonable activity (Gregoli et al., 1989). Another important consideration to any *in situ* project is the effect of steam. Once reaction temperatures are reached, connate water can exert considerable steam partial pressures. At 566 K the saturated steam pressure is 76.7 atm or 1127 psi (Lide, 2003). Thus, it is expected that in-situ processes have to operate at pressures considerably above the saturated steam pressure in order to have significant reactive gas partial pressures, or the steam must not be present in the reaction zone.

In situ processing has several advantages over conventional surface upgrading technology. *In situ* upgrading can be applied on a well-by-well basis, so that the large

volumes of production needed for surface processes are not required. *In situ* processes can easily be adjusted to take into account declining production rates. There is no need to build large, costly pressure vessels, as the reservoir formation serves as the reactor. *In situ* upgrading can be applied both on land and off-shore, in remote locations, and in places where a surface upgrader would be inappropriate. *In situ* processing also differs from most conventional surface processes in that full-range whole crude oils are treated, and not specific boiling range fractions as is commonly done in refineries. This is particularly important for the heavier components, which should more easily undergo reactions in their natural solubilized forms. Finally, the coke or sludge by-products containing concentrated amounts of the removed impurities may be left behind in the reservoir alleviating environmental concerns and reducing disposal costs. One obstacle to *in situ* processing with UD catalysts is the possibility that once in place, the UD catalysts will not be retrievable; and if so, will likely be significantly deactivated due to contacting with brine and deposition of metals from the crude.

Chapter Three: Materials, Methodology and Design

This chapter presents the materials, laboratory apparatus and methodology used for the following three experimental set-ups: molybdenum-based UD catalyst synthesis (Section 3.1), pelletized catalyst reactivity (Section 3.2), and UD catalyst reactivity in a porous media (Section 3.3). Each set-up is introduced by a listing of all materials required for its operation, including the material properties and their importance. This is followed by the methodology used to operate each unit, containing an illustration of the laboratory apparatus with associated operating procedure. The experimental design listing the operating conditions for the individual runs of each unit concludes each of these sections. Theory behind the techniques employed for solid and effluent product (i.e. liquids and gases) characterization is also introduced in Sections 3.4 and 3.5, in addition to precursor material characterization in Section 3.6.

The preparation procedure of UD catalysts from the decomposition of a water soluble precursor salt in water-in-oil (w/o) emulsions and the method for their reactivity, both in pelletized form and in their natural dispersed state, is presented in this chapter. All experiments were conducted in a continuous mode, suitable for on-line application to conventional hydroprocessing facilities or to *in situ* upgrading.

3.1 Molybdenum-based UD Catalyst Synthesis

3.1.1 Materials

The water soluble salt ammonium heptamolybdate tetrahydrate $(NH_4)_6Mo_7O_{24} \cdot 4H_2O$ (AHM) from Strem Chemical (98.98%) was used as the molybdenum metal precursor material for catalyst synthesis. The primary reason for the selection of this salt over other candidates is the cost of material. AHM (54.3% Mo by wt.) at 99.98% purity is listed at $198.80 per 100 grams, whereas ammonium molybdate $(NH_4)_2MoO_4$ (48.9% Mo by wt.)at 99.98% purity lists for $747.00 per 100 grams (Aldrich Chemical Company, 2007). Aqueous soluble salts are also far less expensive than those which are oil soluble (and not as rare); the determining factor for selecting water as the dispersed phase in the emulsion preparation. A typical oil soluble molybdenum salt, as an example, is

molybdenumhexacarbonyl $Mo(CO)_6$ (36.4% Mo by wt.). This compound at 99.9% purity lists at $1184.00 per 100 grams (Aldrich Chemical Company, 2007) and molybdenum carbonyl also happens to be a well recognized toxin.

In addition to aqueous precursor solutions, w/o emulsions were prepared with a non-ionic surface-active agent (i.e. surfactant) and a continuous high boiling point hydrocarbon phase. Surfactant was added to each mixture to reduce the interfacial tension between the continuous oil phase and water droplets. Nonionic surfactants, such as SPAN 80 (sorbitan monooleate) and TWEEN 80 (polysorbate 80), are very common in the literature and are mainly used to prevent possible counter-ion interactions (Lopez-Quintela et al., 2004). The surfactant selected for the Ultra-Dispersed Catalyst Preparation Unit (CPU) is based on its hydrophilic-lipophilic balance (HLB) number. The HLB system is used for describing the characteristics of a surfactant. It consists of a scale to which HLB values are experimentally determined and assigned. If the HLB value is low, there is a low number of hydrophilic groups on the surfactant and it is more lipophilic (oil soluble) than hydrophilic (water soluble). For example, SPAN 80 (sorbitol monooleate) has an HLB value of 4.3 and is oil soluble. The corollary can be illustrated by TWEEN 80 (polysorbate 80), which has an HLB value of 15.0 and is water soluble due to a large number of hydrophilic groups on the surfactant. For the CPU, SPAN-80 (Sigma-Aldrich) was selected based on the literature for w/o emulsions, which recommends a surfactant with an HLB value between 3 and 9 (Eijsbouts, 1999) to form stable emulsions (not microemulsions). However, it should be noted that the HLB number neglects the effects of the oil type, salinity, pressure, temperature and other additives, which have a dramatic influence on the emulsion phase behaviour (Wormuth et al., 2002).

MCT-10 lubricant base oil (Imperial Oil) was selected for use in the preparation of the w/o emulsions. It was selected for two specific properties; its high boiling point (613 K, 340^{o}C), as the oil could not be allowed to fractionate at the catalyst decomposition temperatures under investigation (473-598 K), and its translucence, which was intended to aid in achieving successful dynamic light scattering characterization results for the colloidal suspension products. The properties and TBP curve for MCT-10

are presented in Table 3.1 and Figure 3.1, respectively. Nitrogen gas (Praxair, 99%) was also required.

Table 3.1 – Imperial Oil MCT-10 lubricant base oil characteristics

Viscosity @ 293 K	67.55 cP
Viscosity @ 313 K	26.42 cP
Viscosity @ 333 K	12.51 cP
Viscosity @ 353 K	6.93 cP
Pour Point	261 K
Density @ 311 K	0.87 g/cm^3

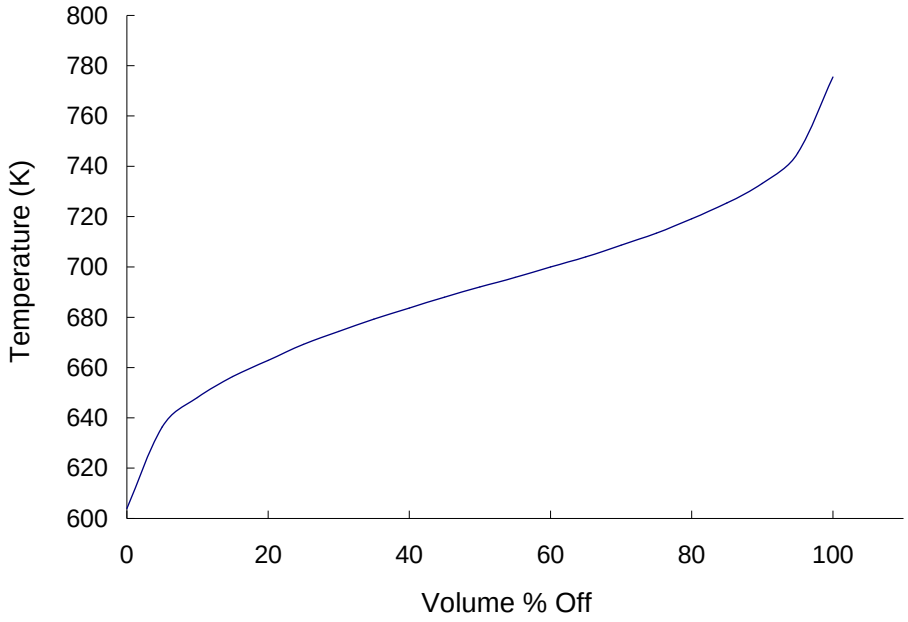

Figure 3.1 – MCT-10 TBP distillation curve

3.1.2 Methodology

The CPU features a horizontally positioned reactor (HR) similar to previous research on UD Mo-oxide synthesis from the decomposition of a w/o emulsion (Wang, 2004), but unlike work featuring a vertical reactor (VR) (Vasquez, 2006). A comparison

between the HR and VR configurations was performed in order to study the influence of the flow dynamics regime on particle synthesis. The texture (i.e. size and shape), crystalline structure, surface area and particle size were determined using scanning electron microscopy, X-ray diffraction, nitrogen physisorption and dynamic light scattering, respectively. The emulsions were formulated with high boiling point lubricant base oil, whose gas fraction may be neglected at the temperature range studied, and all were injected at constant emulsion flow rates.

Unsupported molybdenum catalysts were prepared by flashing and decomposing w/o emulsions consisting of SPAN 80, base oil, AHM, and distilled water. All experiments were conducted at atmospheric pressure and all emulsions were prepared using 150 g of oil, 16.8 g of water (corresponding to 10% w/o by wt.) and 1.87 g of AHM salt (corresponding to 10% salt-in-water and 7820 ppm Mo in oil). The addition of SPAN 80 increased with successive batches of runs, ultimately climbing to 9 g of surfactant per 150 g of oil (5% of emulsion by wt., batch 3) to achieve the desired droplet/particle size. A high surfactant concentration was used due to the inherent instability of the emulsion at lower concentrations. The mixtures were blended in a homogenizer (IKA Ultra-Turrax T25 Basic) for 6 minutes at speeds of 6500 RPM (batch 1-2) and 24000 RPM (batch 3) to produce the inverse micelle emulsions.

Figure 3.2 is a schematic of the CPU used to study the behaviour of emulsion decomposition and particle synthesis in a HR configuration. The reactor was heated to temperatures ranging from 473 K to 598 K (experiments conducted in 25 degree increments) using insulated heating tapes, while being monitored and controlled using a 3-point type-K temperature probe and a PID temperature controller with solid-state relays (Model SSRL240DC10, OMEGA Engineering Inc.). The reactors used in the decomposition of the emulsion consist of 9.5 mm (0.375 inch) diameter, 0.0889 mm (0.035 inch) wall thickness and 381 mm (15 inch) long stainless steel tubes, heated in two sections with ribbon heating tapes.

Using a precision high pressure dual-syringe pump (Teledyne ISCO, Electric Valve Dual Pump), blank emulsions (with no dissolved salt) were pumped through the reactors at constant flow rates of 250 cm^3/hr until steady-state temperatures were achieved. Once

steady-state was achieved, and the remaining blank emulsion pumped into the system, the second of the two pumps was activated and the metal-based emulsion was injected at flow rates duplicating the blank emulsion settings to avoid temperature fluctuation in the decomposition zone. The liquid product was collected at the exit of the flash separator for dynamic light scattering analysis. The solids suspended in the liquid product were separated using a high-speed (6000 RPM) centrifuge (MPW-350/110 V, MPW Instruments) and were washed with solvents (toluene and hexane) and dried to obtain a solid product free of most hydrocarbon. Initial flow rates for emulsion injection were set to that of previous work using a vertical reactor (VR) configuration (200 cm^3/hr) to obtain equivalent residence times (Vasquez, 2006). However, an adjustment was made following run-6 in order to achieve a uniform reactor temperature profile, as it was found faster flow rates (250 cm^3/hr) aided process control. An increased flow rate also reduces the potential for catalyst precipitation in the HR (a non-issue for the VR set-up).

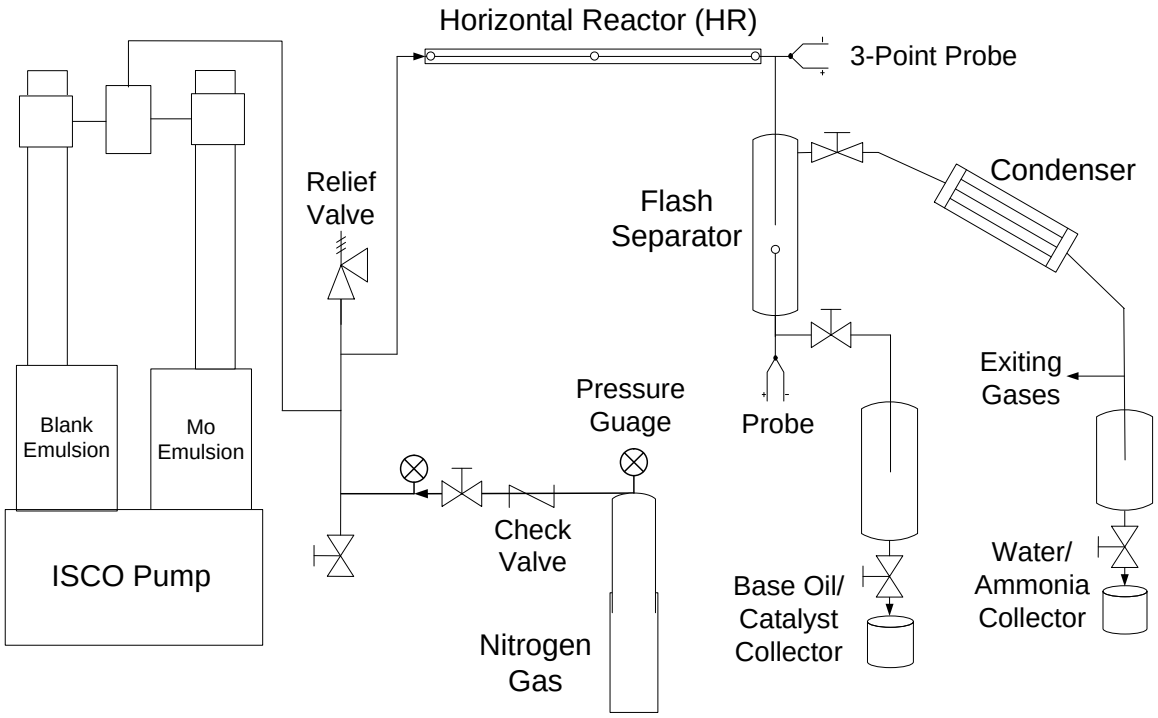

Figure 3.2 – Schematic of UD Catalyst Preparation Unit (CPU)

Using information gathered in the literature, Table 3.2 presents a comparison of the operating conditions used to synthesize highly dispersed molybdenum oxide particles.

Table 3.2 – Comparison of operating conditions for UD Mo-catalyst synthesis

	(Wang, 2004)	(Vasquez, 2006)	Thompson (batch 3)
Flow Rate	210 – 420 cm^3/hr	200 cm^3/hr	250 cm^3/hr
Residence Time	0.7 – 1.4 min	5.2 min	4.1 min
Water:Oil (by wt.)	10 – 20 %	10%	10%
AHM:Water (by wt.)	10 – 30 %	10 – 20 %	10 %
Surfactant Conc.	3 g / 100 g oil	6 g / 100 g of oil	6 g / 100 g of oil
Mixing Speed	4700 RPM	24000 RPM	24000 RPM
Mixing Time	6 minutes	6 minutes	6 minutes
Sonication Time	10 – 20 min	5 min	10 min
Flow Orientation	→	↓	→

3.1.3 Experimental Design

The preparation of UD catalysts was divided into 3 batches as is indicated in Table 3.3, which lists the variable operating conditions for all experimental runs. All emulsions were prepared with 6 minutes of stirring time, a nitrogen flow rate of 5 SCCM, and water and salt concentrations previously stated in Section 3.1.2. In preparation for dynamic light scattering particle size characterization, samples were placed in a sonication bath for 10 minutes. Runs 1-7 were trial runs to prepare for unit malfunctions and optimize control settings. The AHM salt used for these runs was not fully soluble in the aqueous solution and was therefore replaced for successive runs. For Runs 24-31 (i.e. Batch 3), the beakers used for emulsion preparation were placed in cold water baths during mixing to prevent the temperature from reaching values over 363 K at high mixing speeds. Duplicate runs were performed for 498 K and 573 K (runs 31 and 27, respectively) to test the precision of the unit, with results indicating less than an eleven per cent deviation for each test condition.

Table 3.3 – Operating conditions for CPU experimental runs

Run No.	Batch No.	Reactor Temp. (K)	Flow Rate (ml/hr)	Mixing Speed (RPM)	Surfactant Conc. g/100g oil	Comments
1	n/a	523	200	6500	1.5	trial run
2	n/a	523	200	6500	1.5	trial run
3	n/a	523	200	6500	1.5	trial run
4	n/a	523	200	6500	1.5	trial run
5	n/a	523	200	6500	1.5	trial run
6	n/a	523	200	6500	1.5	trial run
7	n/a	523	300	6500	1.5	temp control problems
8	n/a	523	250	6500	1.5	temp control problems
9	1	523	250	6500	1.5	successful
10	1	498	250	6500	1.5	successful
11	n/a	473	250	6500	1.5	white precipitate (salt) in oil
12	1	548	250	6500	1.5	successful
13	1	573	250	6500	1.5	successful
14	1	598	250	6500	1.5	successful
15	1	623	250	6500	1.5	successful
16	n/a	548	250	6500	1.5	aborted – plug formed
17	2	548	250	6500	1.5	successful
18	2	598	250	6500	1.5	successful
19	2	523	250	6500	1.5	successful
20	2	498	250	6500	1.5	successful
21	2	573	250	6500	1.5	successful
22	2	573	250	6500	1.5	successful
23	2	523	250	6500	1.5	successful
24	3	523	250	21500	6	successful
25	3	573	250	21500	6	successful
26	3	498	250	24000	6	successful
27	3	573	250	24000	6	Successful – duplicate run
28	3	598	250	24000	6	Successful
29	3	548	250	24000	6	Successful
30	3	473	250	24000	6	Successful
31	3	498	250	24000	6	Successful – duplicate run

3.2 *Pelletized* UD Catalyst Reactivity

3.2.1 Materials

Toluene (Fisher-Scientific, 99.9%) was selected as a feedstock to study the reactivity performance of the synthesized UD catalyst particles in converting the model molecule into hydrodearomatized products. The catalysts for reactivity tests were

selected from two CPU experimental runs, one where the catalysts were prepared at low temperature (498 K) and one at high temperature (598 K). Hydrogen gas (Praxair, 99%) was also required.

3.2.2 Methodology

Reactivity tests were performed using a high pressure stainless steel catalytic reactivity test apparatus (Figure 3.3) connected to a gas chromatography (GC) system (Hewlett Packard HP 6890 Series) using hydrogen as the carrier gas.

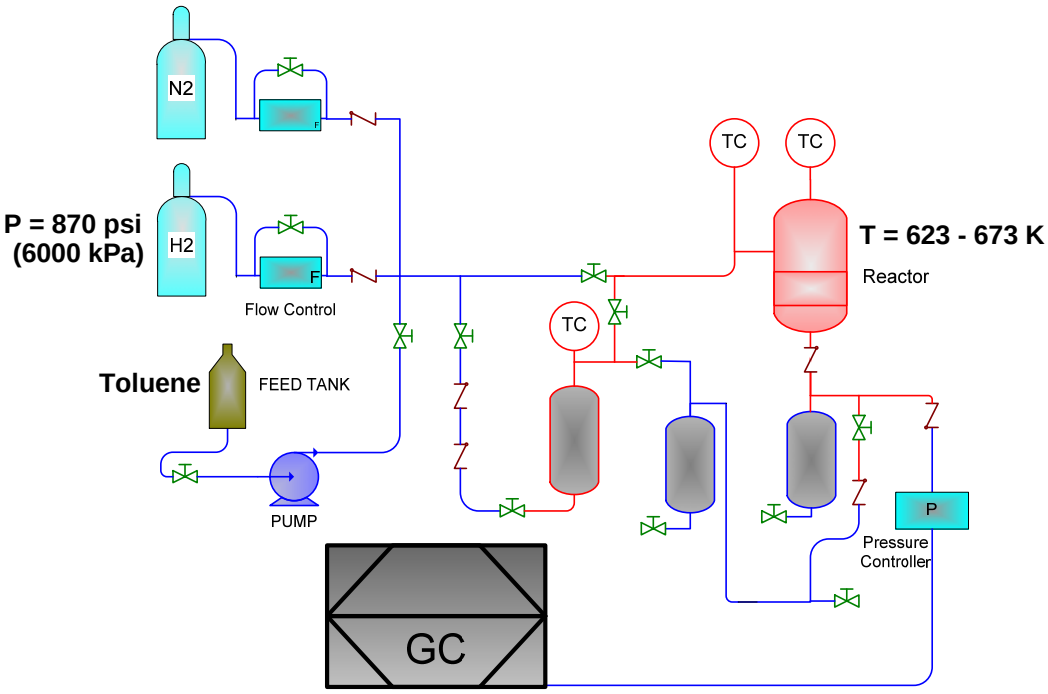

Figure 3.3 – Schematic of (*Pelletized*) Catalyst Reactivity Unit (CRU)

Toluene hydrodearomatization/hydrogenation was used as a test reaction to allow estimation of both cracking as well as hydrogenating capabilities of the catalysts. Although the catalysts are ultimately intended to be used in an ultra-dispersed state, for the purposes of the reactivity testing they were centrifuged from the oil media, washed with toluene twice and hexane once, dried, and pressed at 6.895×10^7 Pa (10,000 psi) into

pellets prior to being loaded in the reactor. Surface area analysis was performed on two different pellets produced from UD catalyst synthesis. These pellets were used for reactivity testing. Testing was performed in a continuous mode studying toluene conversion and product yields at two temperatures, namely 623 K and 673 K.

3.2.3 Experimental Design

Two reactivity tests were performed; the first using pelletized catalyst produced from run-26 (Catalyst A, synthesized at 498 K – low temperature) and the second using pelletized catalyst from run-28 (Catalyst B, synthesized at 598 K – high temperature). Table 3.4 presents the operating conditions for the (*Pelletized*) Catalyst Reactivity Unit (CRU) runs. A sample spreadsheet used to achieve one of the mass balances for the Catalyst B CRU run may be found in Appendix C.

Table 3.4 – Operating conditions for the evaluation of synthesized catalysts

Produced from decomposition temperatures of 498 K (A) and 598 K (B) using a toluene feedstock, H_2 flow rate = 128 SCCM and a total system pressure of 6000 kPa

Catalyst	Condition	Temp (K)	Catalyst (mg)	WHSV[1] (h^{-1})	TOS[2] (h)
A (498 K)	1	623	154*	3.7*	118
	2	673	154*	4.1*	20
	3	673	154*	1.4*	17
B (598 K)	1	623	246*	3.4*	152
	2	673	246*	3.4*	21
	3	623	246*	3.4*	82
	4	673	246*	3.4*	37
	5	623	246*	3.4*	28

[1] weight-hourly space velocity, [2] time-on-stream, * mass of catalyst changing with time

Both reactivity experiments were performed in a continuum, i.e. the same catalyst sample was kept in the reactor for all three conditions of run (A) and a second batch of catalyst was kept in the reactor for all five conditions of run (B). Only temperature and time-on-stream (TOS) at each temperature were changed intentionally during run (B), whereas weight-hourly space velocity (WHSV) was also changed for run (A).

3.3 UD Catalyst Synthesis and Performance in Porous Media

3.3.1 Materials

The porous medium adopted to study the transport of molybdenum-based particles dispersed in a heavy hydrocarbon phase was silica sand native to the Athabasca region in Alberta, Canada. The particle size distribution was obtained through sieve analysis (see Table 3.5). Mesh sizes are often used in classifying the particle size distribution of a granular material and have therefore also been provided. Brine was prepared in accordance to the field brine composition native to the Athabasca region for the purpose of wetting the sand prior to oil injection to simulate actual reservoir properties (*see Appendix D for the types and amounts of salt added to the distilled water*).

Table 3.5 – Porous media particle size distribution

Mesh	Sieve Opening (μm)	Amount (g)
+ 80	+ 177	26.61
+ 120	+ 125	44.36
+ 170	+ 88	17.63
+ 200	+ 74	4.10
+ 270	+ 53	2.25
+ 400	+ 37	0.59
- 400	- 37	0.33
Total		95.80

Sieve stack loaded with 100.00 grams of sand initially

Emulsions for the Sand-Packed Reactivity Unit (SPRU) were prepared using a heavy feedstock consisting of a blend of Athabasca bitumen and Shell vacuum gas oil (VGO). The bitumen was blended with the lighter hydrocarbonaceous VGO in order to reduce the viscosity of the feedstock to 32829 cP (@ 293 K) to facilitate its transfer into the holding tank of the injection pump. Optical microscopy revealed the absence of clay particles in the feedstock, supporting the belief that the bitumen was likely produced from steam-assisted gravity drainage (SAGD) operations (typically, 0.1 % clay content). The simulated distillation curve for the feedstock may be observed in Figure 3.4. A surfactant of HLB 8 (mixture of SPAN 80 and TWEEN 80) was used for the porous media runs. This formulation was assigned from experimental determination (Scott, 2007).

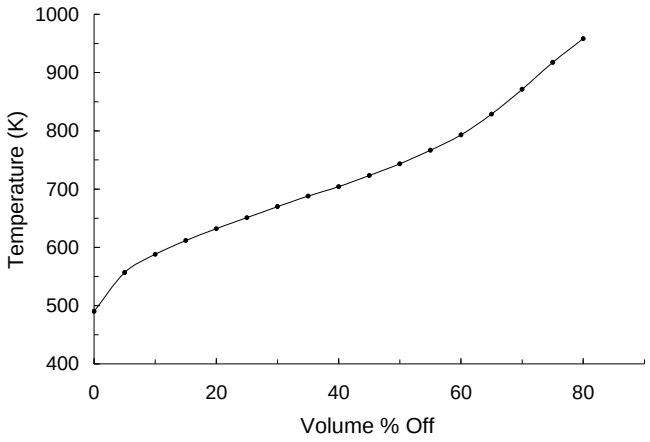

Figure 3.4 – SPRU heavy oil feedstock TBP distillation curve

3.3.2 Methodology

Reactivity tests were carried out in the SPRU to test the performance of UD catalysts in their natural dispersed state. For these experiments, a blended heavy oil sample consisting of 70% Athabasca bitumen and 30% Shell VGO was emulsified. The emulsion was prepared in 100 gram batches with the following composition: 89 grams blended heavy oil, 10 grams of aqueous solution (0.923g AHM salt, corresponding to 5630 ppm Mo in oil) and 1 gram of surfactant (HLB 8). Emulsions were prepared in a homogenizer (IKA Ultra-Turrax T25 Basic) following the 3-stage procedure depicted in Figure 3.5.

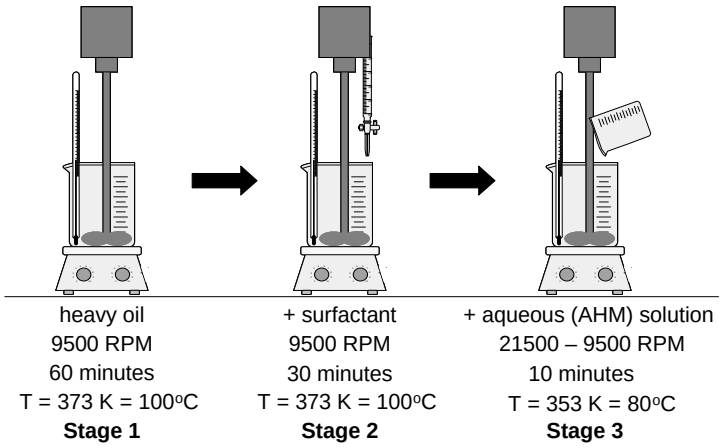

Figure 3.5 – Emulsion preparation procedure for SPRU

For Stage 3 of the emulsion preparation procedure, following salt water addition, emulsions were stirred for 10 minutes with the following stirring procedure: setting 5 (21500 RPM) for 3 minutes, setting 4 (17500 RPM) for 2 minutes, setting 3 (13500) for 2 minutes, and setting 2 (9500 RPM) for 3 minutes. The stirring speed was reduced in order to keep the temperature of the emulsion below 80^{o}C (353 K) to prevent evaporation of the water phase. It was discovered that left to stir at the higher settings, temperatures in excess of 120^{o}C (393 K) could be reached.

For these experiments, horizontally positioned porous media filled reactors were used. The reactors consisted of two sections of stainless steel tubing, each 12.7 mm (0.5 inch) diameter, 0.0889 mm (0.035 inch) wall thickness and 140 mm (5.5 inch) long, connected by a stainless steel union tee yielding a total reactor volume of 27.3 cm^3. A porosity of 41.9 per cent was measured for the unconsolidated sand packs yielding a void volume of 11.4 cm^3. The sand pack was held in place through the use of stainless steel frits (thin pellet-like 200-mesh discs) at each end of the reactor. Reactors were heated to temperatures ranging from 573 K to 653 K using two insulated heating tapes (one on each side of the union tee), while being monitored and controlled by two type-K temperature probes (probes 3 and 4 - see Figure 3.6 for locations) using the same PID temperature controller from the CPU. The porous media in the reactors were prepared by injecting 12 pore volumes (PVs) of prepared brine solution followed by 12 PVs of feedstock oil using a high pressure syringe pump (Teledyne ISCO), duplicating test condition flow rates so as to not create channelling in the sand pack. Two flow rates were investigated; 3 cm^3/hr and 1 cm^3/hr, corresponding to residence times of roughly 4 and 12 hours, respectively.

A decomposition zone was designed to feed the porous media reactor. A stainless steel section of tubing 6.35 mm (0.25 inch) in diameter (with 0.0889 mm (0.035 inch) wall thickness) and 38.1 mm (1.5 inch) in length, coupled with a union tee, provided adequate volume (1.70 cm^3) (therefore adequate residence time) to decompose the pre-cursor salt prior to entering the reactor. This was based on findings from the CPU, which suggested a minimum decomposition time of 5 minutes for temperatures above 493 K. Temperatures in the decomposition zone were monitored using two type-K temperature

probes (probes 1 and 2 - see Figure 3.6) and measured temperatures ranging from 353-593 K, adequate to completely decompose the salt prior to entering the sand pack, and with a large temperature gradient from the entrance of the zone to the exit

Blank emulsions (with no dissolved salt) were pumped through the reactors at constant flow rates until steady-state temperatures and gas chromatography data were achieved with the purpose of providing a baseline for comparison to catalytic results. Using the syringe pump, the emulsions were injected into the reactors and subjected to catalytic hydroconversion to determine the hydrogenating and hydrocracking capabilities of the UD catalyst while traveling through an unconsolidated sand pack. Hydrogen gas at a flow rate of 50 SCCM and pressure of 500 psi was introduced to achieve the desired partial pressure of hydrogen for the hydroprocessing reactions. In addition to the characterization of the product gases using the GC system, simulated distillation was performed on the liquid products to determine the degree of upgrading. Mass balances were also performed for the successful runs during steady-state operation.

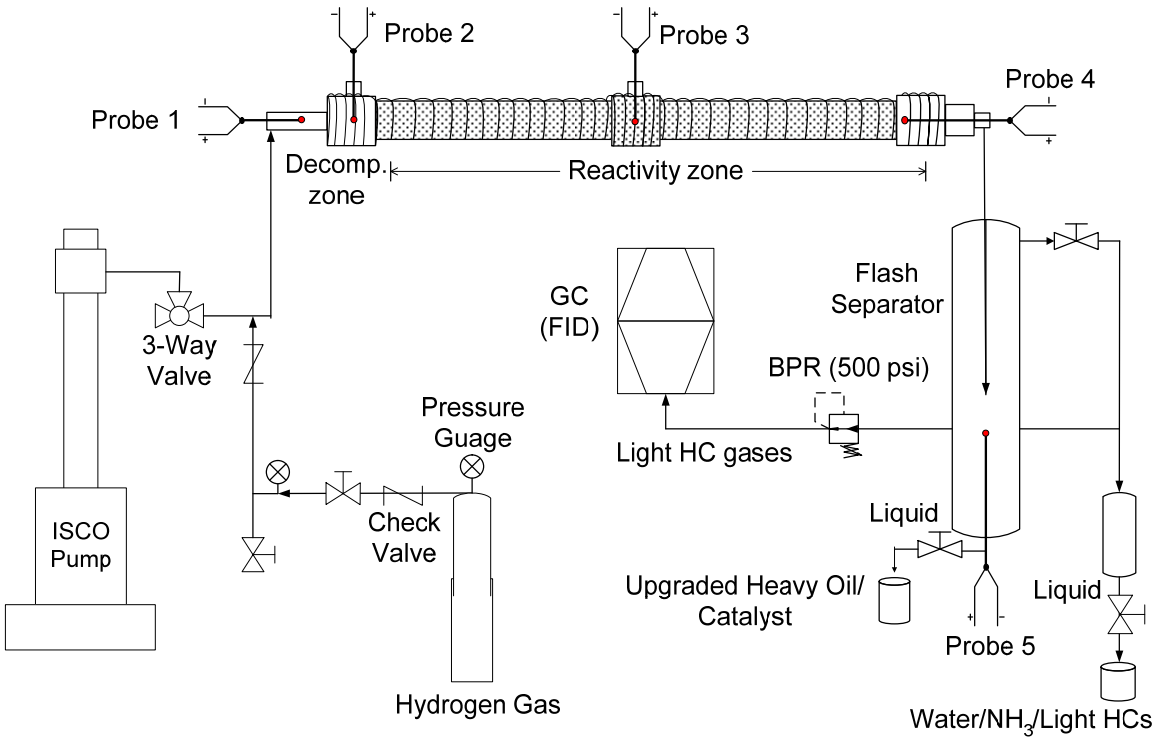

Figure 3.6 – Schematic of Sand-Packed Reactivity Unit (SPRU)

3.3.3 Experimental Design

The SPRU successfully yielded results at two temperatures (573 K and 633 K) and two residence times (4 hours and 12 hours). The operating conditions for all SPRU experiments are listed in Table 3.6, however only runs PM-6, PM-8 and PM-9 yielded successful operation without flash separator failure or plug formation in the reactor.

Table 3.6 – Operating conditions for SPRU experimental runs

Run	Decomposition Temperature (K)	Residence Time (hrs)	Comments
PM-1	573	4	Flash separator not functioning properly
PM-2	593	4	Flash separator not functioning properly
PM-3	573	8	Flash separator not functioning properly
PM-4	653	4	Flash separator not functioning properly
PM-5	573	4	Plug formed in the inlet of the reactor
PM-6	**573**	**4**	**Successful operation, no blank run**
PM-7	653	4	Loss of temp control (> 780 K), aborted
PM-8	**573**	**12**	**Successful operation**
PM-9	**633**	**4**	**Successful operation**
PM-10	633	12	Plug formed for blank-emulsion run

3.4 Characterization of Catalyst Particles

The following section lists the techniques and instruments used to characterize the produced molybdenum-based particles from the synthesis unit.

3.4.1 Particle Size Determination

Particle size is an important parameter in determining the surface area of UD catalysts, assuming internal porosity within the catalyst particles is either very small or negligible for large molecules of heavy hydrocarbon fractions. Due to the submicron nature of the manufactured catalyst particles produced in the oil media for these experiments, the diameters of the Mo particles produced were determined using a dynamic light scattering technique. These measurements were then validated using scanning electron microscopy.

3.4.1.1 Dynamic Light Scattering

Dynamic light scattering (DLS) is a technique for measuring the particle size of colloidal suspensions. In DLS, the sample is illuminated with a laser beam and the intensity of the resulting scattered light produced by the particles fluctuates at a rate that is dependent upon the size of the particles. The intensity of the scattered light fluctuates due to the particles undergoing random, Brownian motion. Analysis of these intensity fluctuations enables the determination of the distribution of diffusion coefficients of the particles, which are converted into a size distribution using established theories.

The diffusion coefficient of colloidal spheres is well described by the Stokes-Einstein equation:

$$D = \frac{kT}{6\pi\mu_{solvent} r}$$

where, D = diffusion coefficient ($m^2 \cdot s^{-1}$)
T = temperature (K)
r = radius of the particle (m)
k = Boltzmann constant ($J \cdot K^{-1}$)
$\mu_{solvent}$ = solvent viscosity ($Pa \cdot s^{-1}$)

The Stokes-Einstein relation shows that Brownian motion is inversely proportional to size - a larger particle will diffuse more slowly than a small particle. Temperature and viscosity must be accurately known as temperature is directly proportional to diffusion rate - increased temperature will increase Brownian motion. The Stokes-Einstein relation also shows that increasing the solvent viscosity will reduce Brownian motion. Figure 3.7 demonstrates the impact of the viscosity parameter. It presents DLS analysis of particles synthesized from a 5 % w/o emulsion at 523 K (20 % AHM salt in water) and suspended in oil with a viscosity of 55 cP, corresponding to an average particle size (i.e. Z-ave) of approximately 500 nm. If this viscosity value was improperly entered as 30 cP, the reported size is 1000 nm. As evident in the figure, errors are particularly significant at lower viscosities due to the nature of the curve.

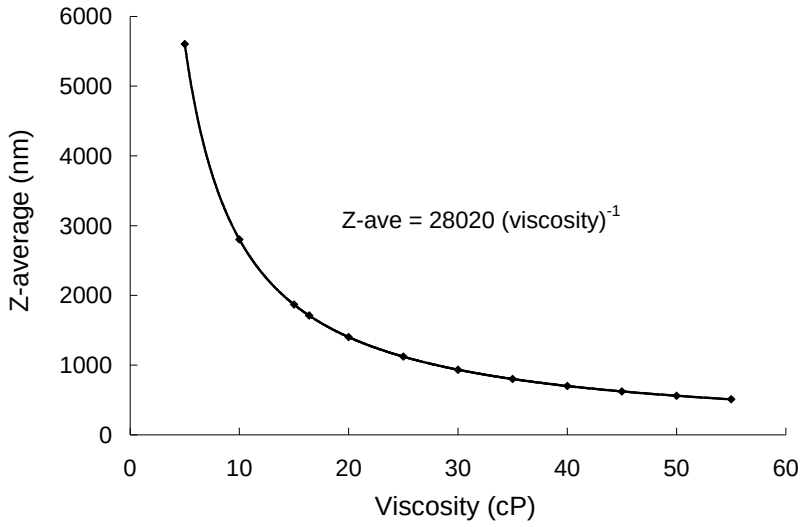

Figure 3.7 – DLS sensitivity analysis – average particle size vs. viscosity

The DLS measured diameter in water is called the Hydrodynamic Diameter and is illustrated in Figure 3.8. It dictates how the particle moves within the liquid with the assumption that all particles are spherical. 1/K (Debye length) is the thickness of the electrical double layer, or ion charge layer, and is dependent upon the ionic strength of the medium. In organic media an ion charge layer (i.e. Stern layer) is not present reducing the interaction of the particles with the solvent media, thus not affecting the direct measurement of the DLS.

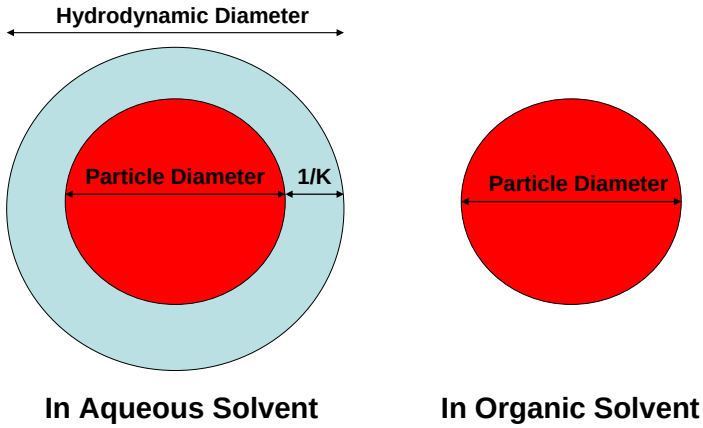

Figure 3.8 – Hydrodynamic diameter (effect of ionic strength)

Particles suspended in a liquid media tend to both agglomerate and settle with time. Sonication prepares the samples for measurement by dispersing the particles. However, there exists a critical time for sonication beyond which re-agglomeration occurs. A sonication time of 10 minutes for each sample was used to disperse the sub-micron particles as it was found that sonication periods under 10 minutes did not completely re-disperse the particles and periods greater than 20 minutes resulted in partial re-agglomeration (Wang, 2004). Particle concentration is also a significant parameter to DLS analysis as high particle concentrations result in increased particle size measurements due to agglomeration (see Section 4.1.5 for a detailed explanation of the agglomeration mechanism). These particle sizes can be increased to degrees beyond the measurement limitations of the instrument ($\geq$ 10 μm). High particle concentrations also lead to high sample opacities which also prevent the instrument from providing meaningful measurements. For these reasons, the catalyst particle/oil products produced from the preparation unit were dispersed with additional fresh (i.e. 'particle-free') base oil to obtain reasonable signal to noise ratios. Two dilution ratios were used to demonstrate the effect of increasing the particle concentration on the particle size measurement: 1 part (catalyst + oil) product plus 9 parts fresh base oil and 1 part (catalyst + oil) product plus 2 parts fresh base oil. The samples were transferred into 12 ml screw-cap glass vials and shaken for 5 minutes using a Burrell Model 75 Wrist Action Shaker (Burrell Scientific) before being placed in the sonication bath prior to DLS analysis.

DLS results are only comparable with other techniques if the samples are monomodal (i.e. only one peak), spherical and monodispersed (i.e. no width to the distribution), and the samples are prepared in the correct dispersant (Malvern Instruments, 2003). The width parameter is known as the polydispersity index (PDI). PDI values below 0.1 correspond to reasonably narrow monomodal samples suitable for such comparison. The DLS instrument (Malvern Instruments Zetasizer Nano S) was equipped with a 4.0 mW He-Ne laser (633 nm) and operated at an angle of 173º and at a temperature of 298 K to obtain the particle size distribution width (i.e. polydispersivity) and average particle size (i.e. Z-Ave) of the suspended particles.

3.4.1.2 Scanning Electron Microscopy

Scanning Electron Microscope (SEM) images were captured using an environmental SEM (Phillips XL-30 ESEM). This technique was used to confirm the measured particle sizes and size distributions obtained through DLS and to examine the particle morphology. The SEM is a microscope that uses electromagnets to bend an electron beam which is used to produce an image on a screen. From the impact of the electron beam on the sample, very short wavelength electron radiation is emitted and is captured to form images showing the various properties of the material. In comparison to an optical microscope, this microscope provides a much higher magnification, larger depth of focus, greater resolution, and ease of sample observation.

In preparation for SEM analysis, the particle samples produced from the synthesis unit were washed twice with toluene and once with hexane and were allowed sufficient time to dry at room temperature in a fume hood. This step was required to ensure all water, solvents, or other materials that could vaporize while in the vacuum were removed. The samples were then firmly mounted before being coated. The environmental SEM is capable of examining non-conductive samples without coating them with conductive material. However, after the particles were pulverised, the samples were sputter coated with gold to improve their electrical conductivity and, thus, image quality.

3.4.2 X-ray Diffraction

Compositional analysis was performed by X-ray powder diffraction (XRD). This method is based upon the fact that an XRD pattern is unique for each crystalline substance. Thus, if the pattern of an unknown sample matches that of an authentic and known sample, chemical identity can be assumed. XRD is a non-destructive technique and is the only analytical method that is capable of providing qualitative and quantitative information about the compounds present in a solid sample (Skoog et al., 1998). The quantitative methods (such as those which involve pattern modeling) however are computationally intensive and can only be applied with powerful analytical software.

X-rays are electromagnetic radiation generated when a focused electron beam accelerated across a high voltage field bombards a stationary or rotating solid target. As electrons collide with atoms in the target and slow down, X-rays are emitted. The high energy electrons also eject inner shell electrons in atoms through the ionization process. When a free electron fills the shell, an X-ray photon with energy characteristic of the target material is emitted. When X-ray photons collide with electrons in atoms of the sample, some photons from the incident beam will be deflected away from the direction of original travel. This scatter carries information about the electron distribution in materials. Diffracted waves from different atoms can interfere with each other and the resultant intensity distribution is strongly modulated by this interaction. Diffraction occurs as waves interact with a regular structure whose repeat distance is about the same as the wavelength. It happens that X-rays have wavelengths on the order of a few angstroms, the same as typical inter-atomic distances in crystalline solids. Crystalline solids have atoms which are arranged in a periodic fashion yielding diffracted waves consisting of sharp interference maxima (i.e. peaks) with the same symmetry as in the distribution of atoms. Peaks in an XRD pattern are directly related to the atomic distances (Krawitz, 2001). For a given set of crystal lattice planes (Figure 3.9), the condition for a diffraction (peak) to occur is expressed by Bragg's Law:

$$2d \sin\theta = n\lambda$$

where, λ = wavelength of the X-ray
θ = scattering angle
n = order of the diffraction peak
d = the inter-plane distance

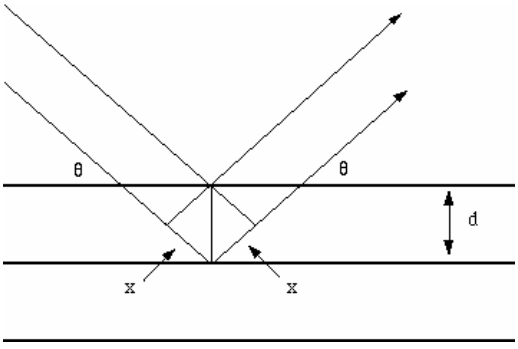

Figure 3.9 – Reflection of X-rays from two planes of atoms in a solid

XRD patterns were recorded on a Rigaku Multiflex X-ray diffractometer using copper K-alpha radiation (λ=1.54 angstroms) at 40 kV tube voltage and 40 mA tube current with a scanning speed of 2°/min over a 2θ range from 3° and 60°. The XRD patterns were referenced to powder diffraction files (International Centre for Powder Diffraction PDF 2001) using JADE XRD Pattern Processing analysis software (Materials Data Inc., 2003) for identification.

3.4.3 Surface Area Measurement

The solids obtained by centrifuging the liquid product were analyzed using nitrogen physisorption at 77.35 K (Micromeritics TriStar 3000) to determine surface areas. The specific surface area was calculated using the BET method. BET theory is a well-known rule for the physical adsorption of gas molecules on a solid surface. The concept of the theory is an extension of the Langmuir theory for monolayer molecular adsorption applied to multilayer adsorption with the following hypotheses: (a) gas molecules physically adsorb on a solid in layers infinitely; (b) there is no interaction between each adsorption layer; and (c) the Langmuir theory can be applied to each layer.

3.4.4 Thermodynamics

An investigation into the thermodynamics was conducted using the software F*A*C*T (Facility for the Analysis of Chemical Thermodynamics) in order to confirm the synthesised particle compositional findings gathered through XRD. Mono-metallic predominance diagrams were generated and are presented in Chapter Four. These diagrams illustrate the predominant molybdenum-based phase(s) present for a specified set of conditions (temperature, pressure, chemical potentials, etc.) when equilibrium between the different phases is established. The term predominance is used even though the compounds may have partial (or even total) miscibility. That is to say they have been treated as if they were immiscible or exist as pure separate phases. The boundary lines are therefore no longer truly phase boundaries, but are lines separating regions in which one species “predominates” (Kostorz, 2001). Predominance diagrams, which can assist in the

interpretation and evaluation of thermodynamic data, calculations and approximations, have been constructed in accordance to the detailed explanations provided by the authors (Pelton and Thompson, 1975) based on Gibbs energy minimization techniques.

3.5 Reactivity Tests – Characterization

3.5.1 Characterization of Gases – GC

Gas Chromatography (GC) was performed on the exiting gases produced from the reactivity units. Chromatography is the separation of a mixture of compounds (solutes) into separate components so that they can be identified and quantified. By separating the sample into individual components, it is easier to identify (qualitative) and measure the amount (quantitative) of the various sample components. GC is a technique whereby a moving gas (the mobile phase) carries the sample across a stationary phase (the solid support found within a GC column) (Skoog et al., 1998). To be suitable for GC analysis, a compound must have sufficient volatility and thermal stability. Gas chromatography was conducted using a Hewlett Packard HP 6890 Series GC System. Figure 3.10 presents a simplified illustration of the GC system.

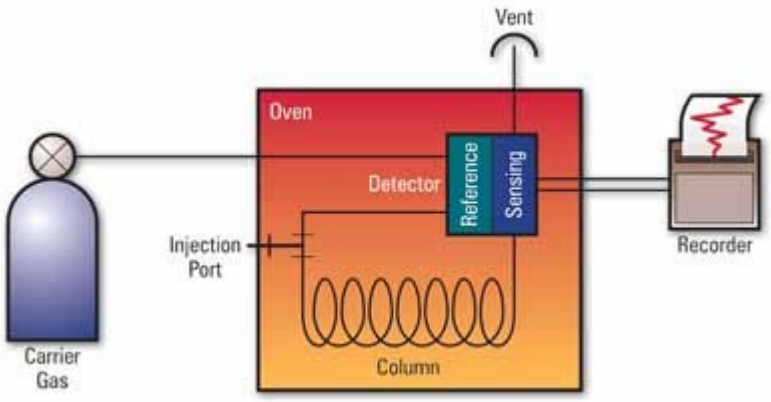

Figure 3.10 – Diagram of gas chromatography

There are many detectors which can be used in GC. Different detectors offer different types of selectivity. For this research, the GC system featured a flame ionization detector (FID) (Figure 3.11) for its usefulness in analysing organic compounds due to its high sensitivity, large linear response range, and low noise production.

The effluent from the column is mixed with hydrogen and air and ignited. Organic compounds burning in the flame produce ions and electrons which can conduct electricity through the flame. A large electrical potential is applied at the burner tip and a collector electrode is located above the flame. The current resulting from the pyrolysis of any organic compound may be measured. The FID is mass sensitive, which has the advantage that changes in mobile phase flow rate do not affect the response of the detector. However, it has the disadvantage of being a destructive technique.

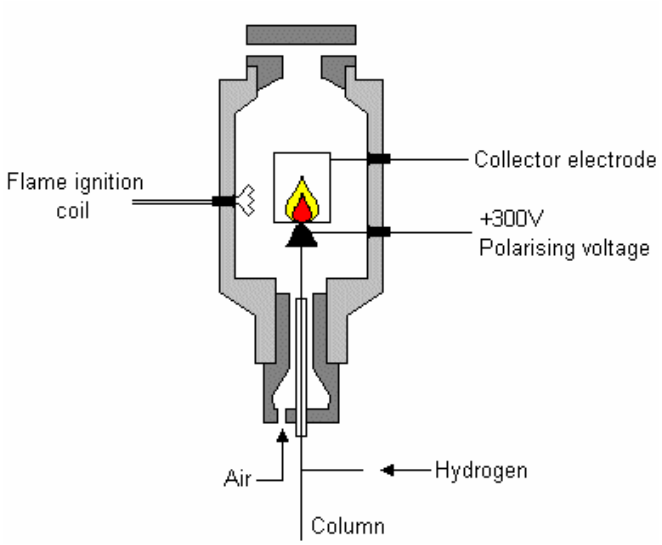

Figure 3.11 – The flame ionization detector

3.5.2 Characterization of Liquids

3.5.2.1 Water Content Measurement

Karl Fischer (ASTM D789) was used to determine the water/moisture content of the samples. Knowledge of the moisture content is important since it can interfere with the correct interpretation of the performance of the reactivity tests when characterizing

produced oil samples through simulated distillation. The Karl Fischer test procedure requires a small weighed sample (1 to 3 grams) to be placed in a drying oven at a predetermined temperature for a predetermined period of time. The time and temperature values were arrived at by testing a similar material and varying the temperature and bake time independently to determine optimal conditions for removal of all water in the sample. If the temperature is too low or the retention time too short all of the water might not be driven off. A temperature value too high can degrade the polymer and actually generate water in some cases. The water in the sample is vaporized and carried by dry oxygen free nitrogen into a reaction vessel with methanol. The methanol traps the water which is titrated to an end point to determine the amount present.

3.5.2.2 Simulated Distillation

Simulated Distillation (ASTM-7169) is a well established technique used to characterize petroleum fractions which have a wide boiling point distribution. For the purpose of this research, obtaining the boiling point distribution aids in determining the improvement in the quality (i.e. upgrading) of the oil, thereby demonstrating the performance of the SPRU. The simulated distillation system contains a temperature programmable inlet, a column and a flame ionization detector. The technique is carried out under constant flow to ensure constant response of the flame ionization detector.

3.5.2.3 Viscosity Measurement

Viscosity is a measure of the resistance of a fluid to deform under either shear stress or extensional stress. Viscosity describes the resistance of a fluid to flow and may be thought of as a measure of internal molecular friction. The viscometer (Brookfield DV-II+ Pro) is an instrument used for measuring the viscosity and flow properties of fluids. It measures the force required to rotate a disc or hollow cup immersed in the oil at a predetermined speed. It is paired with a temperature controlled water bath (Brookfield TC-502) to help insure accurate test results.

3.5.3 Characterization of Porous Media – ICP-AES

Inductively Coupled Plasma Atomic Emission Spectroscopy (ICP-AES) (Thermo Electron IRIS Intrepid II XDL) was the technique used to measure the molybdenum metal content of the porous media following reactivity testing. ICP is a very high temperature excitation source that efficiently vaporizes, excites, and ionizes atoms. The samples were passed through a nebulizer and were entrained in the flow of argon, a plasma support gas. By definition, a plasma is an electrical conducting gaseous mixture containing a significant concentration of cations and electrons. Analytical plasmas are very high in temperature, ranging from 6000-10000 K, comparable to the surface of the sun. The energy that maintains analytical plasma is derived from an electric or magnetic field and because it operates with pure argon, combustion is impossible.

The plasma torch consists of concentric quartz tubes. The inner tube contains the sample aerosol and argon support gas and the outer tube contains flowing gas to keep the tubes cool. A radiofrequency generator (1-5 kW @ 27 MHz) produces an oscillating current in an induction coil that wraps around the tubes. The induction coil creates an oscillating magnetic field. The magnetic field in turn sets up an oscillating current in the ions and electrons of the support gas (argon); ions which are initiated by a spark from a Tesla coil. This interaction between the ions and electrons and the fluctuating magnetic field causes the ions and electrons to flow in closed annular paths. The sand in the porous media runs was characterized for molybdenum metal content. To prepare these samples for ICP, the samples were first emptied from the stainless steel reactors and set on ceramic dishes before being placed in an oven set at 550^{o}C overnight to remove the organic fraction. The samples were then digested in 25 ml beakers with 10 ml of a 90% Distilled H_2O / 10% nitric acid (Fisher-Scientific, trace metal grade, 68 - 71%) solution. The beakers were covered with glass lenses and gently heated at 40^{o}C for several hours to liberate the molybdenum metal into the aqueous acidic solution. Once digestion was complete, the samples were transferred into syringes and passed through filter cartridges to prevent the sand from being aspirated into the instrument. Samples were carried into the torch by argon flowing at 1.5 L/min through the central quartz tube. Sample injection was carried out by nebulizing the samples by a stream of argon, and the resulting finely

divided droplets were carried into the plasma. The ICP sources were used to excite atoms for atomic-emission spectroscopy.

3.6 Characterization of Precursor Materials – TGA

Thermogravimetric Analysis (TGA) is a type of testing that is performed on samples to determine changes in weight in relation to change in temperature. Such analysis relies on a high degree of precision in three measurements: weight, temperature, and temperature change. The weight change over specific temperature ranges provides indications of the composition of the sample and thermal stability. The application for TGA in this work is in the assessment of composition of surfactants, AHM and materials such as coke produced from the SPRU.

The analyzer consists of a high-precision balance with a pan loaded with the sample. The sample is placed in a small electrically heated oven with a thermocouple to accurately measure the temperature. A computer is used to control the instrument. Analysis is carried out by raising the temperature gradually and plotting weight against temperature.

Chapter Four: Results and Discussion

The results presented in this chapter are divided into three sections. The first presents the characterization results from UD catalyst synthesis, including a look into the mechanism of particle agglomeration and a thermodynamics investigation to validate the compositional findings. The second illustrates the reactivity results using the pelletized particles in the conversion of toluene; results supporting the thermodynamic study. The third section presents the results obtained from the reactivity of UD catalysts within a porous media with simulated reservoir conditions to reveal the potential for *in situ* hydroprocessing.

4.1 UD Catalyst Synthesis

Figure 4.1 illustrates an example of temperature control achieved during experimentation using LabView 7.0 (National Instruments).

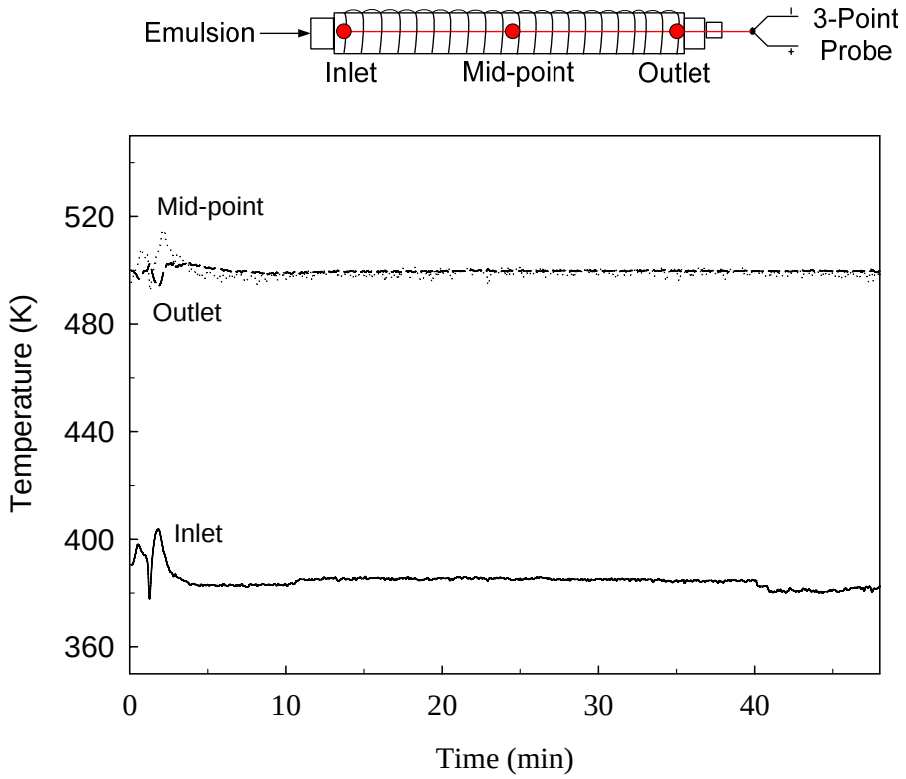

Figure 4.1 – Temperature profile achieved during UD catalyst synthesis at 498 K

The slight disturbance in the temperature profile which appears within the first few minutes of the recording is attributed to switching over from pumping the blank-emulsion to the molybdenum-emulsion. Following this transition, steady-state temperatures are observed.

The relevance of Figure 4.1 stems from its demonstration of steady state production of particles at constant pressure, temperature and residence time, which differs from most works in the literature that produce particles in batch mode and usually under conditions unlike those used in actual dispersed catalyst preparation. They are also not very well controlled or up-scalable. A continuous setup like the one presented in this thesis allows evaluation of catalytic particles under online production conditions and is easily up-scalable.

4.1.1 X-ray Diffraction

All XRD patterns of the synthesized catalyst particles were amorphous, corresponding to substances whose particles have no regular pattern, consistent with those obtained from the previous work (Vasquez and Pereira-Almao, 2006; Wang, 2004; Wang et al., 2004). Occurrence of the amorphous phases is inferred by observing the presence of broad and diffuse peaks in the XRD patterns. Figure 4.2 illustrates that these patterns are also partially composed of MoO_2 and MoO_3 species as observed from the broad peaks spanning 26 and 30 degrees 2-theta. The sharp peak observed near 12 degrees observed for the catalyst prepared at 473 K demonstrates that the AHM precursor salt did not fully decompose at this low temperature as this peak is characteristic of compounds containing molybdenum and ammonium (e.g. PDF#39-0035>ammonia molybdenum oxide, PDF#18-0117>ammonium molybdenum oxide, PDF#21-0571>molybdenum oxide ammonia hydrate, PDF#47-0872>molybdenum trioxide hydrate) (JADE, 2003).

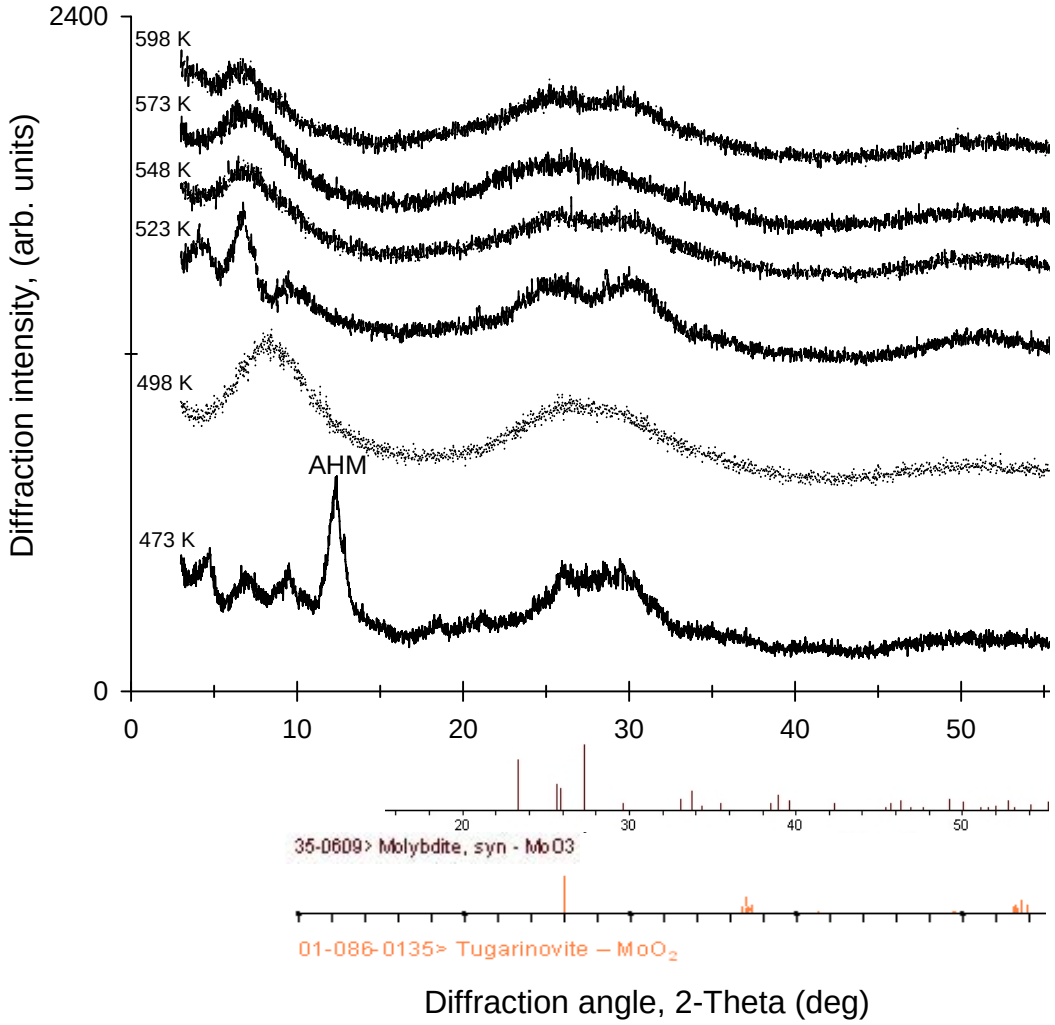

Figure 4.2 – XRD analysis of produced Mo-based particles (*Batch 3*)

4.1.2 Dynamic Light Scattering

Figure 4.3 illustrates typical DLS output in measuring both the average polydispersivities and average particles sizes of a single experimental run at two distinct dispersant ratios, each measured 4 times in succession with intervals of 3 minutes between readings. DLS analysis was conducted on particles synthesized at 498 K with product-to-base oil dispersant ratios of 1:9 and 1:2, corresponding to Z-Averages of 98.5 nm and 110.4 nm; respectively, and PDIs of 0.136 and 0.175; respectively. Figure 4.4 illustrates the effect of decomposition temperature on synthesized average particle size.

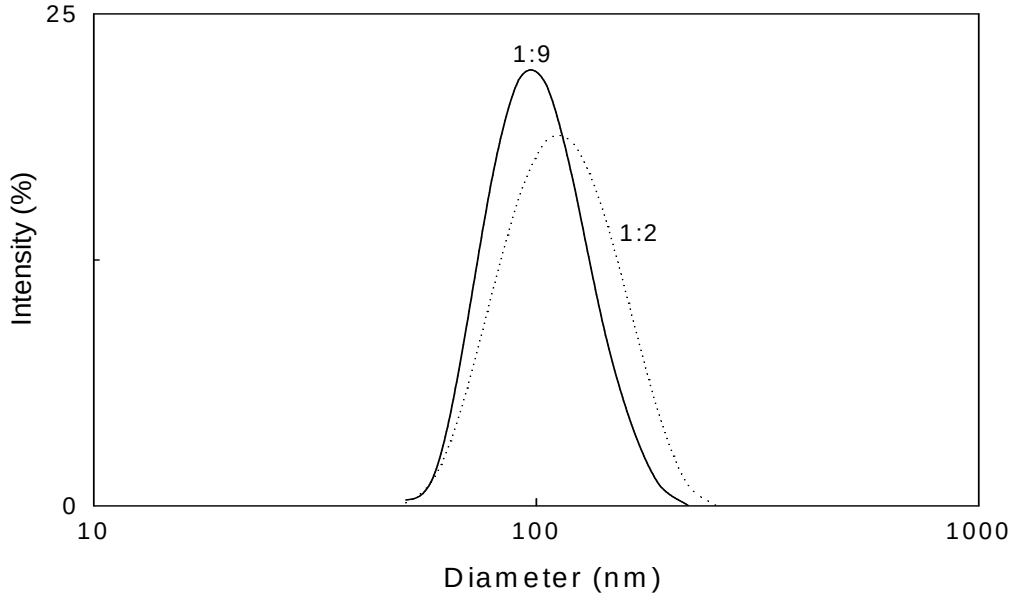

Figure 4.3 – DLS analysis of UD particles synthesized at 498 K with product-to-fresh base oil dispersant ratios of 1:9 and 1:2

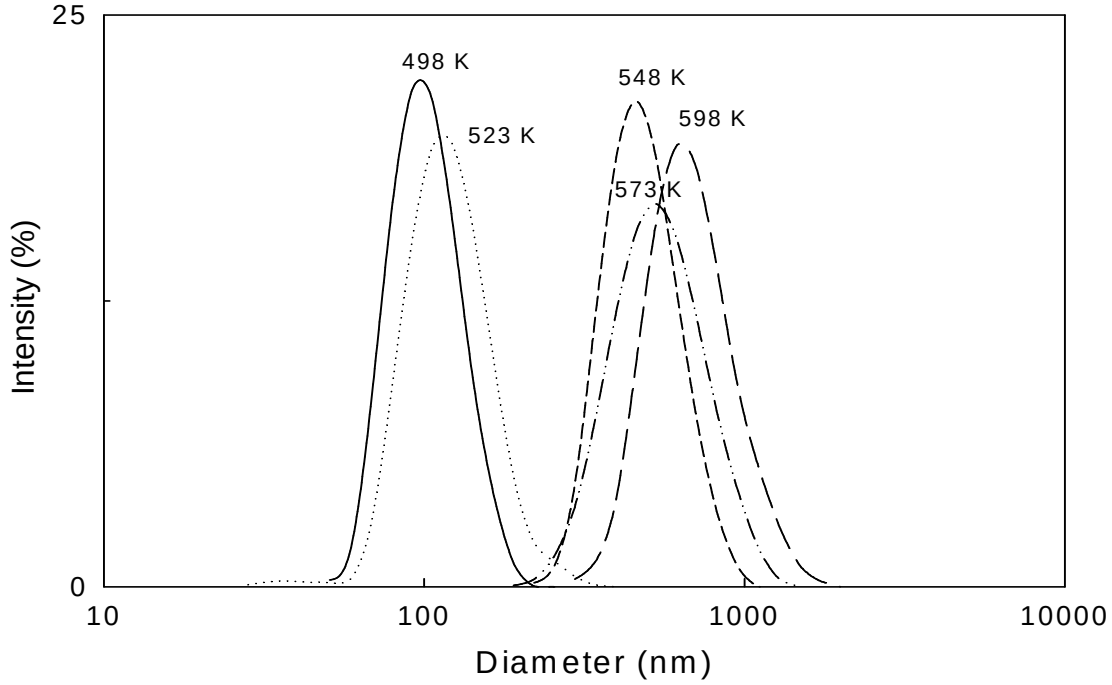

Figure 4.4 – Effect of temperature on DLS particle size and dispersivity with product-to-fresh base oil dispersant ratio of 1:9 (*Batch 3*)

Upon inspection, it is clear that the average particle size increases as the decomposition temperature increases. This finding is also reported in the open literature for a similar horizontally positioned reactor (herein referred to as HR) configuration (Wang, 2004) and for a unit with a vertically positioned reactor (VR) (Vasquez and Pereira-Almao, 2006). Experiments between the HR and VR configurations were conducted to determine if the flow type affected the results.

Table 4.1 – Comparison of DLS results between HR and VR configurations *using a (catalyst + oil) product-to-base oil dispersant ratio of 1:9*

Decomposition Temperature (K)	*Thompson* HR Z-Ave (nm)	*Vasquez, 2006* VR Z-Ave (nm)
498	99	n/a
498	111	n/a
523	115	399
548	463	498
573	438	610
573	473	n/a
598	659	n/a

For all tested decomposition temperatures it is also evident that the VR unit produced larger particles. However, it should be noted that the VR unit used an emulsion flow rate of 200 cm^3/hr resulting in a greater residence time of 5.2 minutes, compared to the residence time of 4.1 minutes for the HR set-up and previous work has shown that an increase in residence time leads to an increase in particle size (Wang, 2004)

As stated previously, sonication time has an impact on particle size measurement; a measurement which is also extremely sensitive to physical parameters such as viscosity. High particle concentrations in the dispersant may lead to agglomeration and sedimentation. Use of DLS for characterization of nanocatalysts in organic solvents such as base oil is novel and the results are subject to varied interpretation.

4.1.3 Scanning Electron Microscopy

Figure 4.5 shows a representative image of molybdenum-based particles synthesized with the CPU at 498 K (run-26). This image appears to indicate that primary or minimum particle sizes ranging between 30 and 50 nm have agglomerated into larger particles (several hundred nm). The spherical particle shapes observed suggest that the particles are suspended as a different phase (inorganic) within a liquid and possibly submitted to numerous collisions.

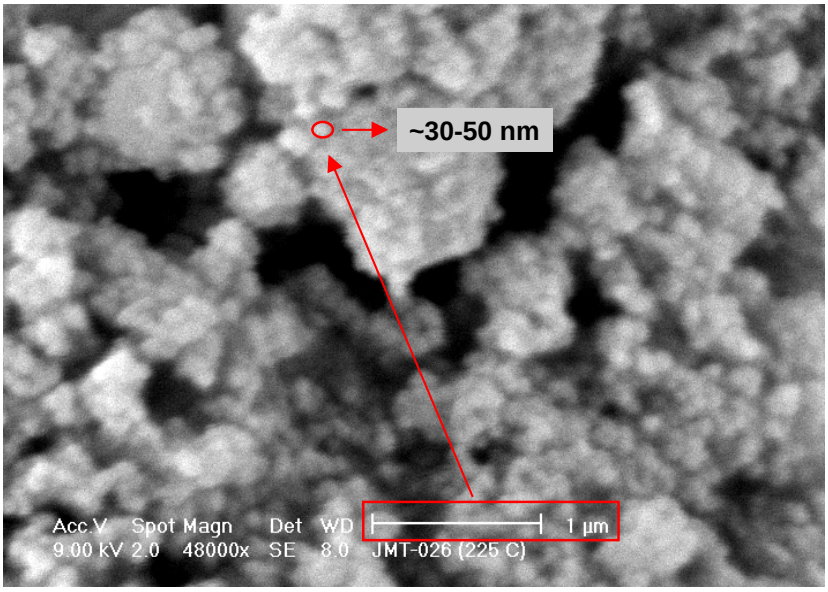

Figure 4.5 – SEM image of produced particles at 498 K (CPU Run-26)

4.1.4 Surface Area Measurement

The average surface area of the particles (in powder form) produced from HR synthesis at 498 K and 598 K was found to be approximately 30 $m^2 g^{-1}$, as determined by a multi-point BET analysis. After pelletizing at 10,000 psi, the BET surface areas of the catalysts were 7 $m^2 g^{-1}$ and 10.7 $m^2 g^{-1}$ for the 498 K and 598 K runs, respectively. It is expected that the run producing the larger particle sizes according to DLS (i.e. 598 K) would have a corresponding smaller BET surface area, but this is not the case. This can possibly be attributed to oil entrained in the solid sample before measurement and the effects of pelletizing. The measured differences however are not considerable.

4.1.5 Activation Energy of Agglomeration Process

To reveal the nature of particle agglomeration (being either a physical or chemical process), an investigation into its energetics was performed following previously proposed theory (Pereira, 2007). It follows that particle concentration in the system at any given time is inversely proportional to the average particle size (agglomerated) at any given time during early stages of aggregation. This can be expressed as:

$$[\phi_i] \sim \frac{1}{[\bar{\phi}_t]} \tag{1}$$

It can be assumed that in a highly dispersed system of particles with small diameter and low concentration, the aggregation of particles can be treated like a simple chemical reaction:

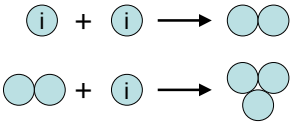

Using a power law expression the following expression for the entitled ‘agglomeration reaction’ is obtained:

$$-\frac{\partial[\phi_i]}{\partial t} = k[\phi_i]^{\alpha} \tag{2}$$

From Equation (1),

$$\partial[\phi_i] = \partial\left[\frac{1}{[\bar{\phi}_t]}\right] \qquad \text{or} \qquad \partial[\phi_i] = -\frac{\partial\bar{\phi}_t}{\bar{\phi}_t^{\,2}} \tag{3}$$

Substituting Equation (3) into Equation (2) provides:

$$\frac{\partial\bar{\phi}_t}{\bar{\phi}_t^{\,2} dt} = k^1\left[\frac{1}{\bar{\phi}_t}\right]^{\alpha}$$

If α = 1 it follows a first-order reaction rate expression:

$$\frac{\partial \bar{\phi}_t}{\partial t} = k^1 \bar{\phi}_t$$

If α = 2 it follows a zero-order reaction rate expression:

$$\frac{\partial \bar{\phi}_t}{\partial t} = k^1$$, where k^1 is a constant

Figure 4.6 presents Arrhenius plots of the particle diameter versus decomposition temperature. The activation energy for the process of particle growth was calculated to be 52 KJ mol^{-1} and 36 KJ mol^{-1} for the HR and VR units, respectively, based on first order reaction kinetics using the data available in Table 4.1.

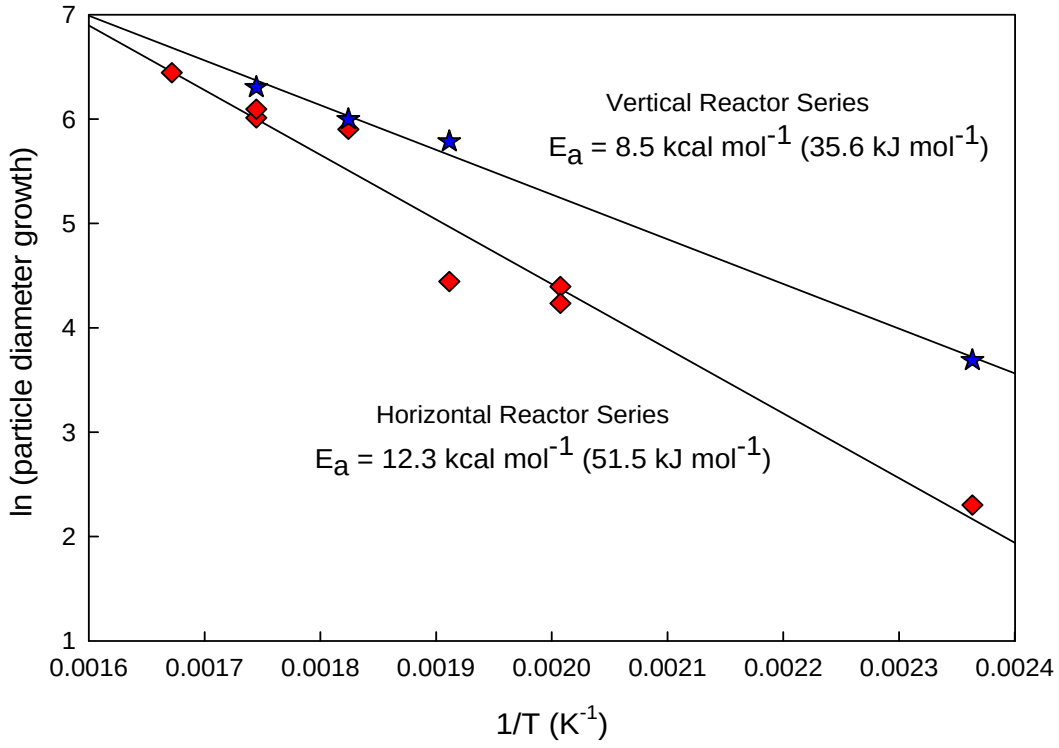

Figure 4.6 – Effect of decomposition temperature on particle size growth for HR and VR units at 1 atm based on first order reaction kinetics

It should be noted that the order does not have a significant impact on determining activation energy. It is assumed that the diameter of the first particles formed at an average value of 30 nm for the HR unit and 100 nm for the VR unit based on the smallest particle sizes measured through DLS (Figure 4.3 and Figure 4.4 for the HR series); sizes which are confirmed through SEM analysis of the dried agglomerated particles (Figure 4.5 for the HR series). DLS and SEM supporting results for the VR series may be found elsewhere (Vasquez and Pereira-Almao, 2006). In the case of horizontal flow through the reactor at a temperature of 473 K, as previously stated, full decomposition of the precursor did not occur and is therefore not considered in the analysis of the agglomeration process.

The process of nano-particle agglomeration may occur via reconstitution of large structural domains. For such a case the process is of a chemical nature and it is expected that with the formation of multiple bonds leading to stable solid larger particles that a highly exothermic reaction occurs with a high activation energy value.

An activation energy of this low requirement (between 30 and 60 KJ/mol) indicates that physical adsorption (resulting from simple Brownian collisions) with the participation of weak intermolecular forces, more than chemical binding, is the determining mechanism of agglomeration in the agglomeration process of nano-scale preformed catalytic particles. Both SEM and DLS analyses show that a distribution range of particle sizes is produced at every condition.

It is also assumed that these particles grow as a function of the concentration of particles, the residence time of the particles in the high temperature zone, the liquid nature and fraction in the decomposition zone, the geometry of that zone, and the temperature of the media. It is also expected that the viscosity of the media has an inverse effect on the particle growth. To keep these variables constant for evaluating the single effect of temperature is difficult, but it is presumed that, within a short range of temperature variation explored, these variables do not produce a significant impact to the qualitative conclusions derived from these results.

4.1.6 Thermodynamics

A thermodynamic analysis on the preparation of UD hydroprocessing catalysts based on Mo was undertaken through Gibbs energy minimization techniques. In particular, this methodology was used to develop predominance diagrams for Mo compounds at typical synthesis conditions (P = 1 atm, T = 498 – 598 K, in atmospheres containing carbon, hydrogen, oxygen and nitrogen) and at typical hydroprocessing conditions (P = 20 atm, T = 623 – 673 K, including atmospheres containing sulfur). The F*A*C*T platform as described in Section 3.4.4 was used for this purpose. The thermal decomposition of AHM for the synthesis temperature range is approximately presented by the following reaction at the conditions under consideration:

$$(NH_4)_6 Mo_7 O_{24} \cdot 4H_2O \rightarrow 7MoO_3 + 7H_2O + 6NH_3 \quad (4)$$

From the dominant products of the AHM decomposition, four further possible reactions are considered.

Reaction 1. (Catalytic) ammonia decomposition (to produce hydrogen)

$$2NH_3 \leftrightarrow N_2 + 3H_2 \quad (5)$$

Reaction 2. The gas-solid reaction between MoO_3 and NH_3

$$3MoO_3 + 2NH_3 \leftrightarrow 3MoO_2 + N_2 + 3H_2O \quad (6)$$

Reaction 3. The reduction of MoO_3 by produced hydrogen

$$MoO_3 + H_2 \leftrightarrow MoO_2 + H_2O \quad (7)$$

Reaction 4. The reduction of MoO_2 by produced hydrogen

$$MoO_2 + 2H_2 \leftrightarrow Mo + 2H_2O \quad (8)$$

Following this thermodynamics analysis of catalyst preparation, the potential Mo-containing catalyst phase changes given the specified hydroprocessing conditions are examined. A computational plan for the development of thermodynamically stable Mo-species with increasing elemental complexity is provided in Figure 4.7. The section will conclude with a crude simulated in-situ catalyst synthesis example.

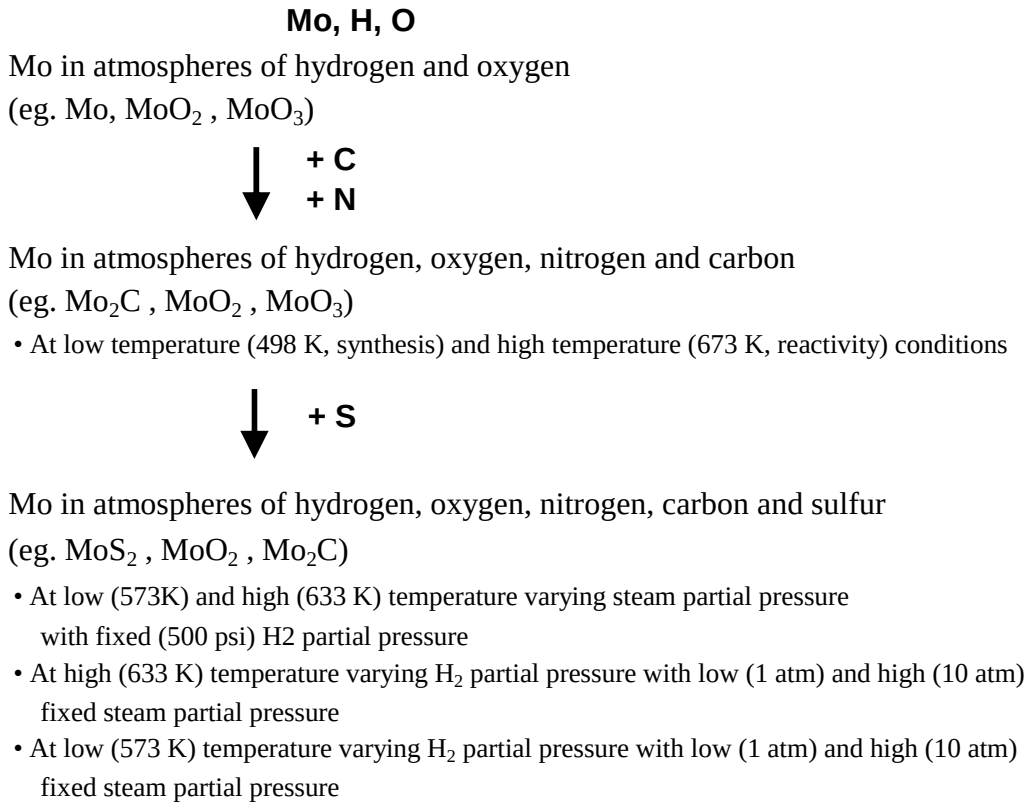

Figure 4.7 – Sequential procedure for determining Mo-containing predominant phases

4.1.6.1 Hydrogen Production from Ammonia Decomposition

Reaction 1 examines the complete thermal decomposition of ammonia gas to produce the hydrogen that may reduce the molybdenum oxide in a mainly water vapour atmosphere. Table 4.2 provides information on the complete ammonia decomposition at various conditions of temperature and pressure on the premise that the products are only N_2 and H_2. The equilibrium constant ($\Delta G^o = -R\,T\,\ln K_{eq}$) provides a relationship among the partial pressures of N_2, H_2 and NH_3, but this may be insufficient to establish the equilibrium composition of the gas phase when ammonia partially decomposes. N-H molecules other than NH_3 may exist as well, such as N_2H_4 and N_2H_2. Furthermore, species other than diatomic nitrogen and hydrogen may also be of potential significance (e.g. atomic H and N) at extreme conditions of high temperature and/or low pressure. The

technique of Gibbs energy minimization is particularly useful in processing thermodynamic data when many potential species are involved since the procedure does not begin with potentially false assumptions about which ones are important (i.e. have a high concentration).

Table 4.2 – Complete decomposition of ammonia to N_2 and H_2

$$2\ NH_{3\ (g,\ 1atm)} \longrightarrow N_{2\ (g,\ 1\ atm)} + 3\ H_{2\ (g,\ 1\ atm)} \quad \textit{(Reaction 1)}$$

T (K)	ΔH^o (KJ)	ΔG^o (KJ)	ΔV^o (liter)	ΔS^o (J/K)	K_{eq}
300	91.9	+32.4	49.2	198.2	$2.3x10^{-6}$
400	96.1	+12.0	65.6	210.3	0.028
456	98.2	0	74.9	215.2	1
500	99.7	-9.5	82.1	218.0	10
600	102.8	-31.6	98.5	224.0	580
700	105.2	-54.2	115.0	228.0	11400

Gibbs energy minimization for the ammonia decomposition is accomplished by numerically distributing nitrogen and hydrogen among all possible (or known) N- and/or H-containing molecules until the Gibbs energy can be made no lower. Proof that the Gibbs energy minimum has been found is provided by showing that the final proportion of molecules satisfy all possible equilibrium constants generated with the same Gibbs energy data as used in the minimization.

F*A*C*T output for equilibrium ammonia decomposition at 500 K and 1 atm:

$$NH_3 \rightarrow 1.8407\ \text{mol}\ \{0.68511\ H_2 + 0.22837\ N_2 + 0.086519\ NH_3 + 0.57210x10^{-20}\ H + 0.82039x10^{-22}\ NH_2 + 0.51544x10^{-22}\ N_2H_4 + 0.26511x10^{-28}\ N_2H_2\}$$

The value 1.8407 in the above expression represents the total moles of gas following decomposition of 1 mole of pure ammonia (NH_3). The numbers immediately preceding each (equilibrium) product species are the mole fractions. The output (equilibrium product) concentrations were truncated at a mole fraction of 10^{-30}. The very low stability of N in relation to N≡N is revealed in atomic N failing to meet this very low cutoff concentration.

The equilibrium can be checked for the ammonia, hydrogen, nitrogen equilibrium. For example, using the mole fractions (the same as partial pressures in this case since the total pressure is 1 atmosphere), the standard Gibbs energy change can be calculated and compared to the value in Table 4.2 above.

$$K_{eq} = \frac{[N_2][H_2]^3}{[NH_3]^2} = \frac{[0.22837][0.68511]^3}{[0.086519]^2} = 10 \qquad (9)$$

$$\Delta G^o = -\,R\,(500)\,\ln K_{eq} = -9493 \text{ J/mol} \qquad (10)$$

It can be seen that the equilibrium fractions of the product species coupled with the calculated total number of moles of gas satisfies the conservation of mass for N and H fixed by the input condition (1 mole of NH_3).

The Principle of Le Chatelier is also observed by the increase in the total number of moles of gas as the temperature increases under conditions of constant pressure. The same principle would also show that the total number of moles of gas increases as well under conditions of reducing the pressure at a fixed temperature.

N_2H_2 formation and its associated equilibrium constant for the reaction of $N_2 + H_2$ is illustrated in Table 4.3 in order to further establish that the equilibrium constant calculations above are correct.

Table 4.3 – Verification of equilibrium output

using N_2H_2 production as an example

$$N_{2\ (g,\ 1atm)} + H_{2\ (g,\ 1\ atm)} \leftrightarrow N_2H_{2\ (g,\ 1atm)}$$

T (K)	ΔH^o (KJ)	ΔG^o (KJ)	ΔS^o (J/K)	K_{eq}
500	209	266	-113	1.67×10^{-28}
600	208	277	-115	7.24×10^{-25}
700	207	289	-116	2.79×10^{-22}

For the isothermal reaction at 500 K, $K_{eq} = \frac{[N_2H_2]}{[N_2][H_2]} = \frac{[0.26511\times10^{-28}]}{[0.22837][0.68511]} = 1.69\times10^{-28}$

The equilibrium constant produced (1.69×10^{-28}) confirms what appears in Table 4.3 (1.67×10^{-28}). The computed mole fraction of products associated with ammonia decomposition at varying pressures is illustrated. The CPU is run at 1 atmosphere of total system pressure (Figure 4.8), but typical reservoir conditions could be represented by 20 atmospheres (Figure 4.9).

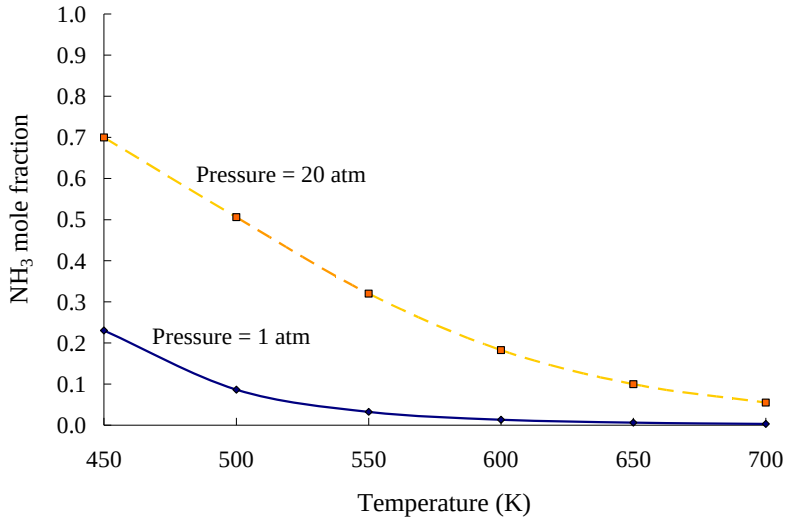

Figure 4.8 – Residual NH_3 associated with its equilibrium thermal decomposition

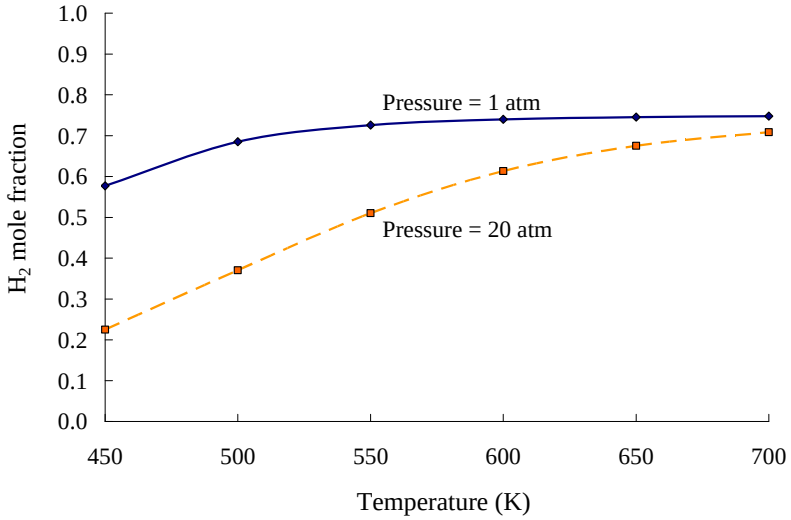

Figure 4.9 – H_2 production from equilibrium thermal decomposition of pure NH_3

4.1.6.2 The Reduction of Molybdenum Trioxide by Ammonia

In investigating the thermodynamics of the gas-solid reaction between MoO_3 and NH_3 (i.e. Reaction 2), the most stable products produced from these reactants (through F*A*C*T equilibrium calculations) are in keeping with the stoichiometry presented, namely $3\ MoO_3 + 2\ NH_3 \rightarrow 3\ MoO_2 + N_2 + 3\ H_2O$, within the temperature range studied (500 – 700K). This highly thermodynamically favoured reaction (see Gibbs energy output in Table 4.4) is most likely the main cause of molybdenum trioxide reduction to a dioxide, although hydrogen produced as an intermediate from ammonia decomposition may be part of the mechanism in this temperature range (Friedlander et al., 1977). Thermodynamics cannot be conclusive in making this distinction.

Table 4.4 – Gas-Solid reaction between MoO_3 and NH_3

$3\ MoO_{3\ (s,\ 1atm)} + 2\ NH_{3\ (g,\ 1atm)} \leftrightarrow 3\ MoO_{2\ (s,\ 1atm)} + N_{2\ (g,\ 1atm)} + 3\ H_2O_{\ (g,\ 1atm)}$ *(Reaction 2)*

T (K)	ΔH^o (KJ)	ΔG^o (KJ)	ΔS^o (J/K)	K_{eq}
500	-163	-301	277	$2.76x10^{31}$
600	-164	-328	275	$4.01x10^{28}$
700	-165	-356	272	$3.63x10^{26}$

4.1.6.3 The Stability of MoO_x in Hydrogen and Steam Atmospheres

From Table 4.5, it is clear that MoO_3 is relatively easy to reduce to MoO_2, however the reduction of MoO_2 to molybdenum metal requires extremely low partial pressures of water vapour even though the partial pressure of hydrogen may be 1 atmosphere (Table 4.6).

Table 4.5 – The reduction of MoO_3 to MoO_2 by produced hydrogen

$MoO_{3\ (s,\ 1atm)} + H_{2\ (g,\ 1atm)} \leftrightarrow MoO_{2\ (s,\ 1atm)} + H_2O_{\ (g,\ 1atm)}$ *(Reaction 3)*

T (K)	ΔH^o (KJ)	ΔG^o (KJ)	ΔS^o (J/K)	K_{eq}
500	-87.4	-97.1	19.4	$1.40x10^{10}$
600	-88.8	-98.9	16.9	$4.10x10^{8}$
700	-90.1	-101.0	14.8	$3.17x10^{7}$

Table 4.6 – The reduction of MoO_2 to Mo by produced hydrogen

$MoO_{2\ (s,\ 1atm)} + 2\ H_{2\ (g,\ 1atm)} \leftrightarrow Mo_{\ (s,\ 1atm)} + 2\ H_2O_{\ (g,\ 1atm)}$ *(Reaction 4)*

T (K)	ΔH^o (KJ)	ΔG^o (KJ)	ΔS^o (J/K)	K_{eq}
500	98.6	56.4	84.3	1.27×10^{-6}
600	95.6	48.3	78.8	6.25×10^{-5}
700	92.5	40.7	74.0	9.24×10^{-4}

A predominance diagram has been constructed to illustrate this matter (see Figure 4.10). To help explain the manner in which this predominance diagram was generated, the equilibrium constant for Reaction 4 is defined as follows:

$$K_{eq} = \frac{p(H_2O)^2}{p(H_2)^2} \tag{11}$$

By taking the logarithm of both sides of the equation and re-arranging the terms, a linear relationship can be observed:

$$\log p(H_2) = \log p(H_2O) - \frac{\log K_{eq}}{2} \tag{12}$$

The relationship in Equation 12 is now in the form of a straight line ($y = mx + b$). The straight line in this example can be regarded as the phase boundary between the Mo and MoO_2 fields on an isothermal diagram in log partial pressure space in the belief that these are coexisting pure separate phases. From this treatment, the lines are constructed in Figure 4.10.

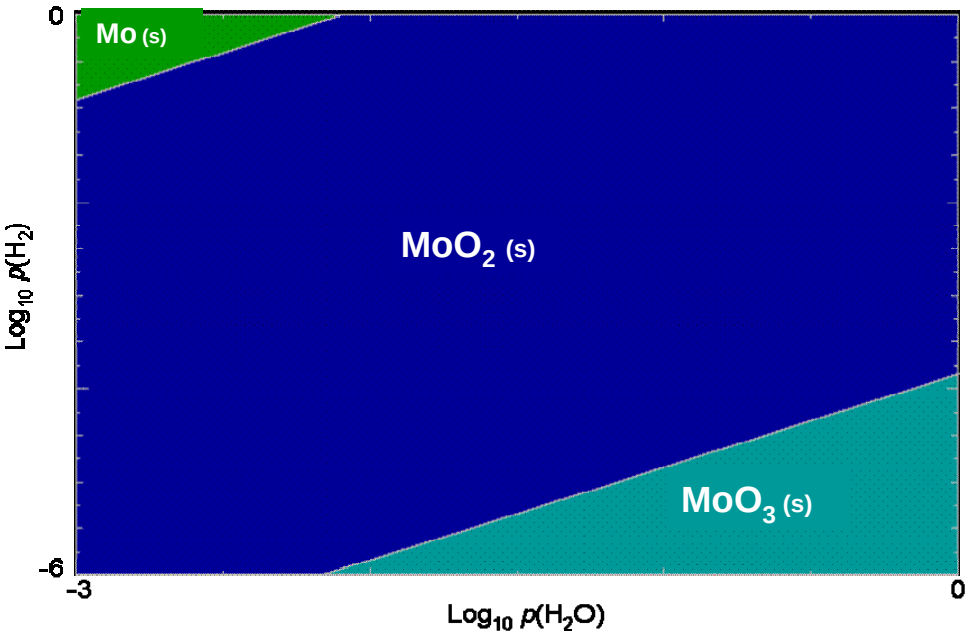

Figure 4.10 – Stability of MoO_x in hydrogen and water (*steam*) atmospheres (598 K)

4.1.6.4 Consideration of other Mo structures from AHM decomposition

Given that nitrogen is introduced into the system to help deliver the emulsion to the reactor in the CPU and given that carbon is present in the system from the base oil and from toluene for the reactivity tests, there is also the possibility that other molybdenum-containing phases may form, such as Mo_2C (s). Below is a list of compounds that are considered in the construction of isothermal predominance diagrams (Table 4.7). These compounds are the basis of Gibbs energy computations leading to the development of Figure 4.11 and Figure 4.12.

Table 4.7 – Other Possible Mo-Species Potentially Involved in AHM Decomposition

SPECIES		SPECIES		SPECIES		SPECIES	
1	Mo (s)	7	Mo_2N (s)	13	MoO_3 (g)	19	MoO_2H_2 (g)
2	Mo (l)	8	MoO (g)	14	Mo_2O_6 (g)	20	$Mo_2(OH)_4$ (g)
3	Mo (g)	9	MoO_2 (s)	15	Mo_3O_9 (g)	21	Mo(CO)6 (s)
4	Mo_2 (g)	10	MoO_2 (g)	16	Mo_4O_{12} (g)	22	Mo(CO)6 (g)
5	MoC (s)	11	MoO_3 (s)	17	Mo_5O_{15} (g)		
6	Mo_2C (s)	12	MoO_3 (l)	18	MoOH (g)		

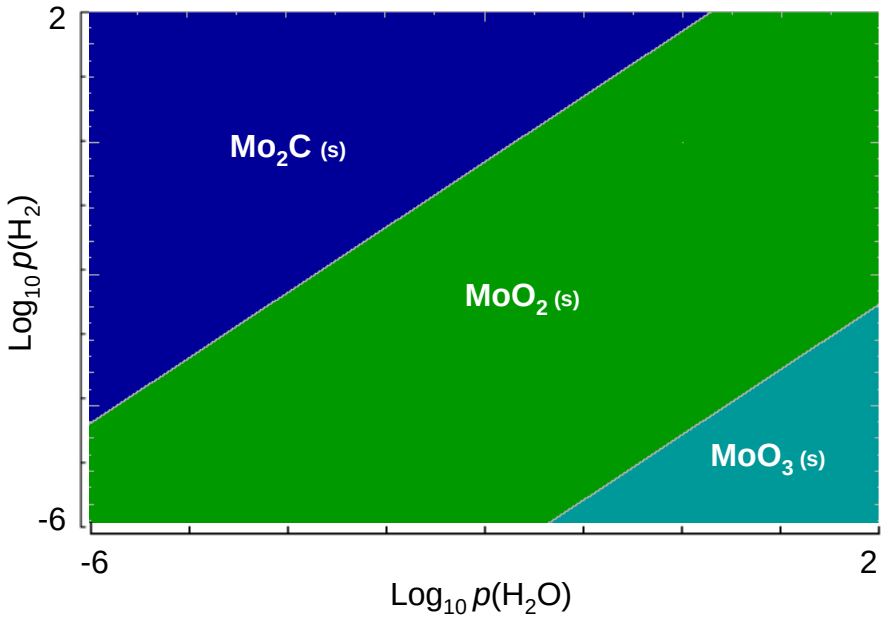

Figure 4.11 – Isothermal predominance diagram of Mo in atmospheres of C-H-O-N varying hydrogen and water vapour partial pressures with the following conditions: $p(N_2)$ = 1 atmosphere, $C_{(s)}$ activity = 1, T = 498 K

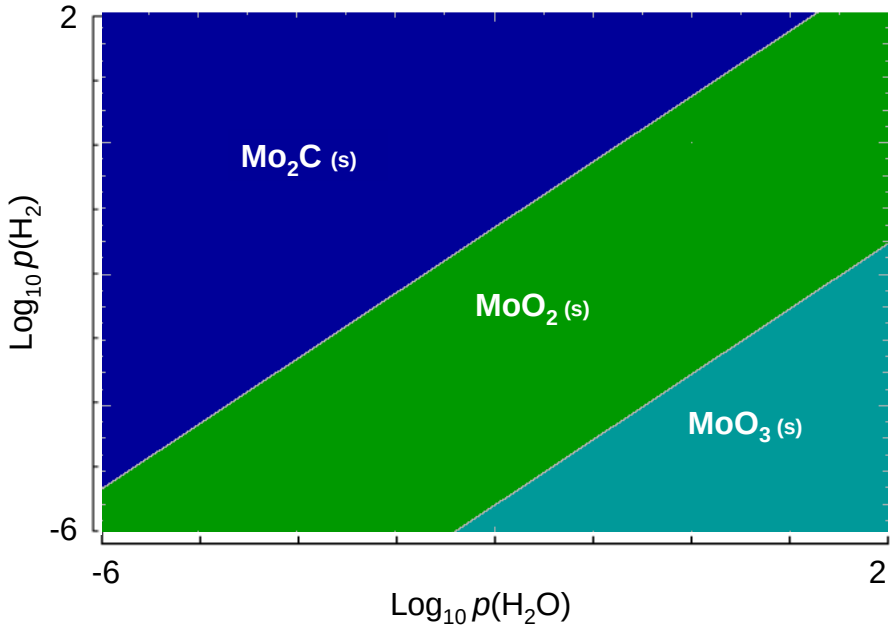

Figure 4.12 – Isothermal predominance diagram of Mo in atmospheres of C-H-O-N varying hydrogen and water vapour partial pressures with the following conditions: $p(N_2)$ = 1 atmosphere, $C_{(s)}$ activity = 1, T = 673 K

From Figure 4.11 it can be seen that for catalyst synthesis conditions (i.e. very low hydrogen partial pressure, roughly 1 atmosphere of water vapour pressure), the diagram denotes MoO_3 as the most stable Mo-containing phase, in agreement with that reported in the literature (Said and Halawy, 1994). This figure also demonstrates that lowering the water vapour partial pressure or increasing the partial pressure of hydrogen (perhaps from dehydrogenation of ammonia) may result in the formation of a different phase, namely MoO_2 or Mo_2C. Figure 4.12 demonstrates that increasing the temperature from 498 K to 673 K results in lower water vapour partial pressure requirements to form the trioxide phase, but with only a minor effect on the system. Figure 4.12 features temperature conditions similar to the reactivity tests carried out in this study using molybdenum oxide catalysts. As can be seen, increasing the hydrogen partial pressure to values associated with reactivity tests reduces the oxide to Mo_2C. This carbide phase is further promoted by lowering the water vapour pressure.

4.1.6.5 Diagrams for Catalytic In-Situ Hydroprocessing Applications

The first two of the following four figures, Figure 4.13 and Figure 4.14, illustrate the predominant Mo-containing phase(s) present applying the hydrogen partial pressure condition common to all SPRU experimental runs (500 psi) and at the two test temperatures, 573 K and 633 K, respectively. The diagrams also allow for potential sulfur species resulting from the naturally occurring presence of sulfur in the feedstock. These diagrams elucidate the most stable Mo-phase for a given steam (ordinate) and hydrogen sulfide (abscissa) partial pressure. These partial pressures range from 10^{-6} atm to 100 atm. It can be concluded that, for both temperatures, even very low concentrations of H_2S are sufficient to obtain MoS_2 in principle, with the lowest severity condition (i.e. 573 K) being the more susceptible to sulphidation as indicated by the larger size of the sulfide phase field. A lower concentration of hydrogen sulfide is therefore sufficient to obtain molybdenum sulfide at this lower temperature.

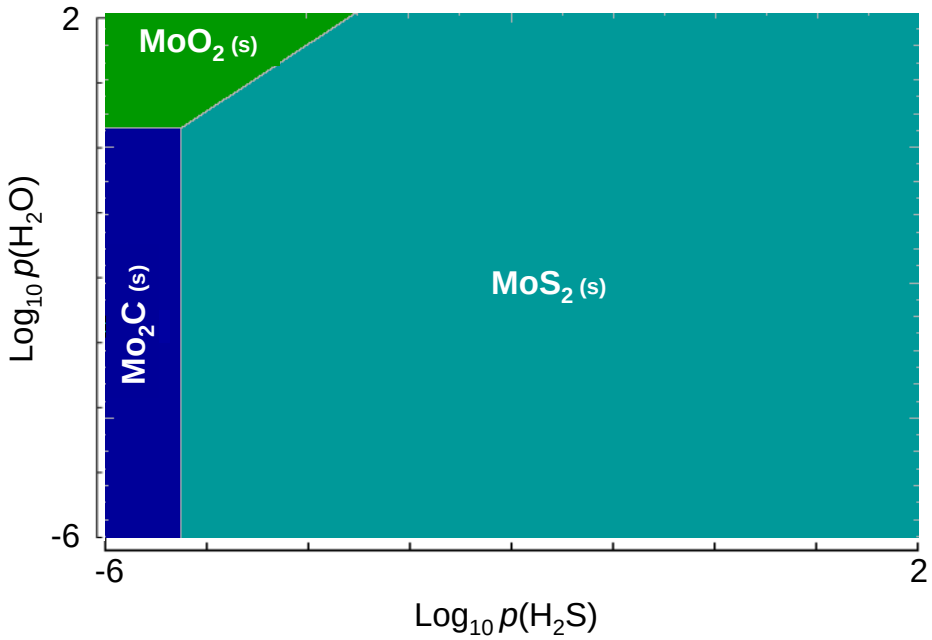

Figure 4.13 – Isothermal predominance diagram of Mo in atmospheres of C-O-H-N-S varying water vapour and hydrogen sulfide partial pressures with the following conditions: $C_{(s)}$ activity = 1, $p(H_2)$ = 34 atm (500 psi), $p(N_2)$ = 1 atm, and T = 573 K

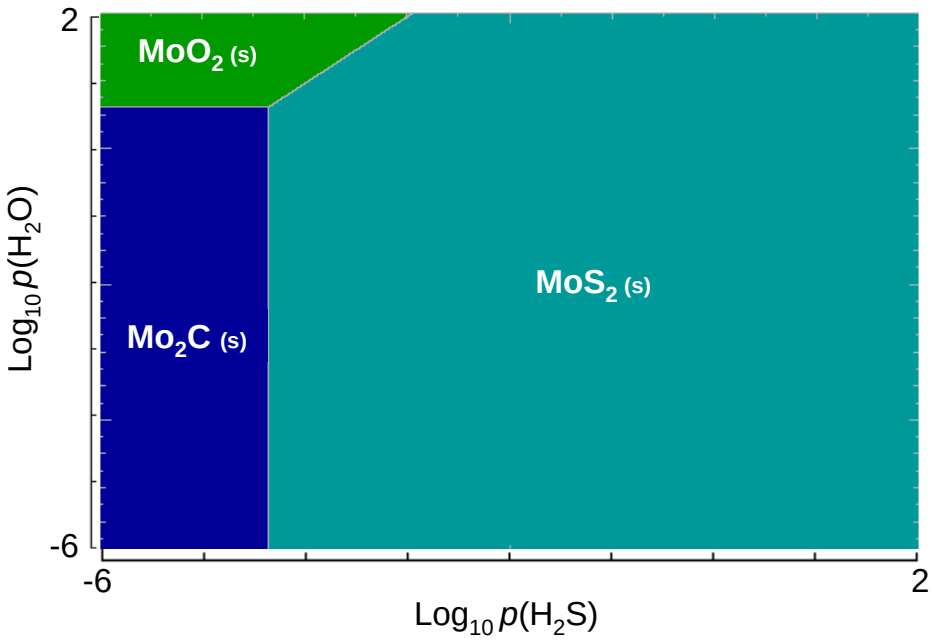

Figure 4.14 – Isothermal predominance diagram of Mo in atmospheres of C-O-H-N-S varying water vapour and hydrogen sulfide partial pressures with the following conditions: $C_{(s)}$ activity = 1, $p(H_2)$ = 34 atm (500 psi), $p(N_2)$ = 1 atm, and T = 633 K

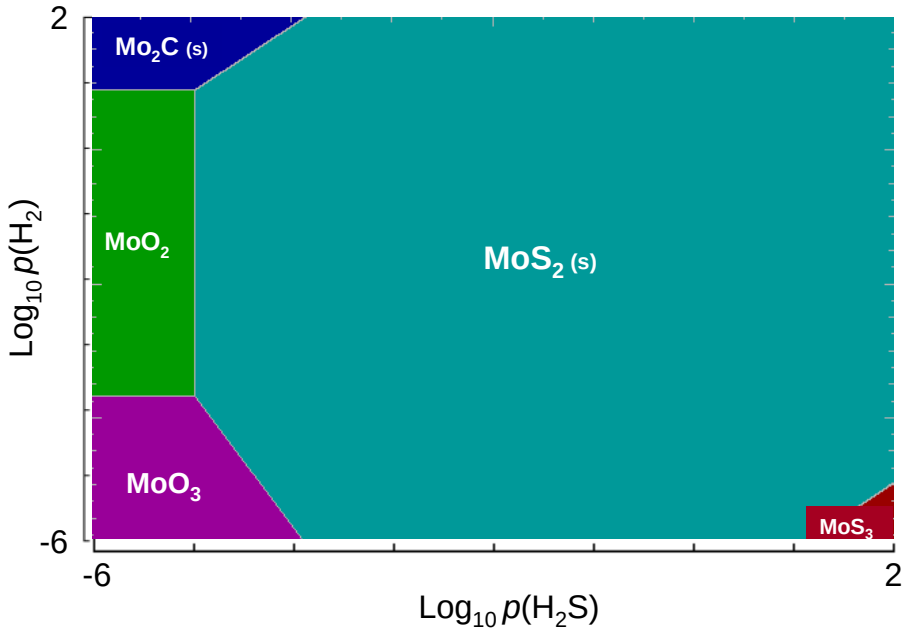

Figure 4.15 – Isothermal predominance diagram of Mo in atmospheres of C-O-H-N-S varying hydrogen and hydrogen sulfide partial pressures with the following conditions: $C_{(s)}$ activity = 1, $p(H_2O)$ = 1 atm, $p(N_2)$ = 1 atm, and T = 633 K (360°C)

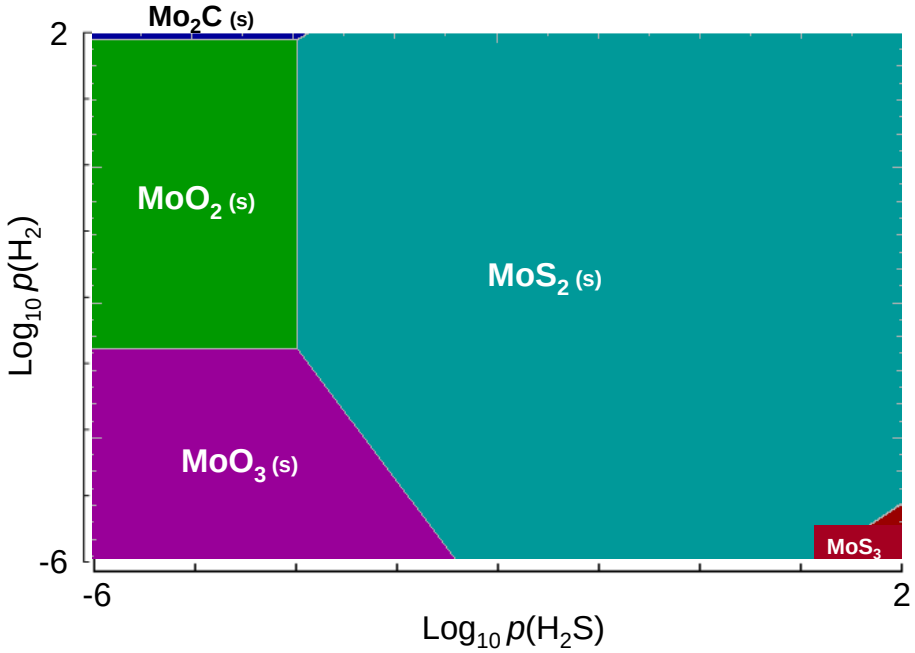

Figure 4.16 – Isothermal predominance diagram of Mo in atmospheres of C-O-H-N-S varying hydrogen and hydrogen sulfide partial pressures with the following conditions: $C_{(s)}$ activity = 1, $p(H_2O)$ = 10 atm, $p(N_2)$ = 1 atm, and T = 633 K (360°C)

In the previous two figures, Figure 4.15 and Figure 4.16, the ordinate was changed to the logarithm of the hydrogen partial pressure, while keeping the steam partial pressure constant at 1 atm and 10 atm, respectively. The influence of raising the steam partial pressure is evident by the near disappearance of the carbide phase at high hydrogen partial pressures. Here again, it is shown that in the presence of even a small concentration of hydrogen sulfide a molybdenum sulfide phase will form. From the conditions in Figure 4.16, Figure 4.17 displays the effect of lowering the temperature by 60 degrees to 573 K.

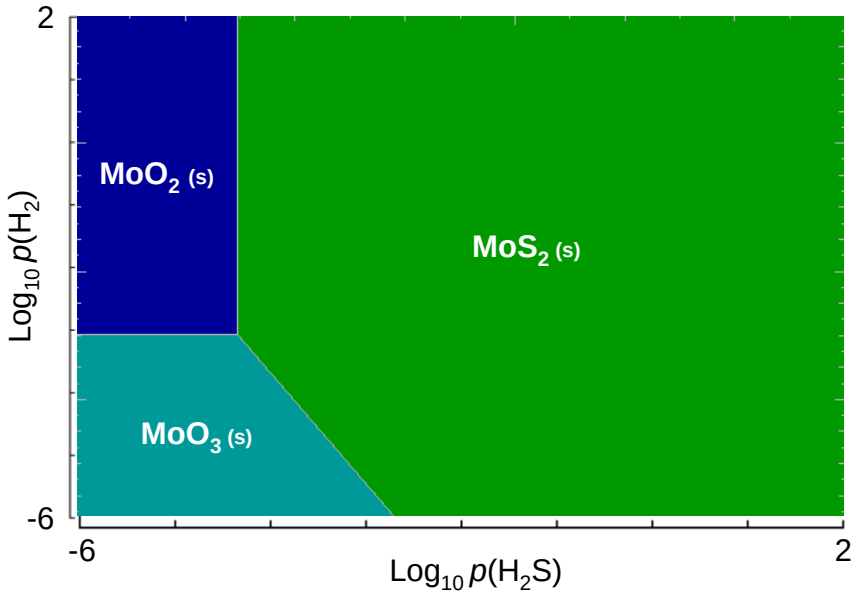

Figure 4.17 – Isothermal predominance diagram of Mo in atmospheres of C-O-H-N-S varying hydrogen and hydrogen sulfide partial pressures with the following conditions: $C_{(s)}$ activity = 1, $p(H_2O)$ = 10 atm, $p(N_2)$ = 1 atm, and T = 573 K (300°C)

4.1.6.6 Simulated In-Situ Catalyst Synthesis (*All Species Considered*)

The power of Gibbs energy minimization described in the preceding sections now is applied to a situation crudely representative of expected in-situ petroleum hydroprocessing conditions. This is depicted immediately below in Figure 4.18 where phase proportions in moles are underlined and mole fraction of gas phase species precede

each molecule. Many species other than the ones shown were considered in the minimization. MoO_3 is shown with zero moles and a carbon activity less than 1. This is given to justify the exclusion of MoO_3 from the most stable phase assemblage. Note particularly the appearance of MoS_2 and the reduction of MoO_3 to MoO_2. Nevertheless, the catalyst nanoparticles for in-situ upgrading can be prepared at the surface in a skid unit under controlled conditions to obtain the desired phase (Mo_2C, for example) and then delivered to the media.

$C_{10}H_{22}$ + 0.01 H_2S + 1 H_2O + 0.02 MoO_3 + 1 H_2 → *most stable products shown below*
(Supposed initial "in ground" conditions *crudely approximated*)

7.0338 mol (0.8515 CH_4
+ 0.1426 H_2O
+ 0.3990E-02 H_2
+ 0.1973E-02 CO_2
+ 0.3375E-04 C_4H_8
+ 0.7111E-05 C_2H_6
+ 0.3967E-06 CO
+ 0.5831E-07 H_2S
+ 0.4297E-09 C_3H_8
+ …… -------
+ …… -------)
500 K, 20 atm, treated as an ideal gas mixture

+ 3.996 mol C
500 K, 20 atm, solid (graphite), activity = 1

+ 0.01500 mol MoO_2
500 K, 20 atm, solid, activity = 1

+ 0.005000 mol MoS_2
500 K, 20 atm, solid, activity =1

+ 0.0000 mol MoO_3
500 K, 20 atm, solid, activity = 0.001357 < 1 (therefore does not appear)

Figure 4.18 – Most stable phase assemblage for crudely represented in-situ hydroprocessing conditions

4.1.6.7 Simulated In-Situ Catalyst Performance (*Withdrawal of Light Hydrocarbons*)

To very crudely simulate the effect of chemical kinetics, light hydrocarbons were somewhat arbitrarily withdrawn from the minimization. These include such species as CH_4, C_2H_6, etc. This still forces the atoms to assemble in a way that is more stable than

the input conditions but not in a way that is the most stable since the programming has no way of distributing atoms to the deliberately excluded species. This procedure attempts to recognize chemical kinetic considerations while still retaining what may be of thermodynamic significance. This approach is an extension from everyday thermodynamic computational practice. Thermodynamics by its nature must idealize the process(es) being examined. In the case of the rapid compression of gas, for example, equilibrium is achieved with respect to volume reduction but not with respect to heat transfer ("reversible adiabatic" change in state). Figure 4.19 provides an example of a metastable equilibrium.

$C_{10}H_{22}$ + 0.01 H_2S + 1 H_2O + 0.02 MoO_3 + 1 H_2 →

0.71045 mol (0.9968 H_2O
+ 0.3094E-02 C_8H_{18}
+ 0.1114E-03 C_9H_{20}
+ 0.5244E-05 $C_{10}H_{22}$
+ 0.3277E-05 H_2S)
(500 K, 20 atm, treated as ideal gas)

+ 0.0063384 mol (55.508 H_2O
+ 46.203 H_2
+ 0.1681E-05 H^+
+ 0.1635E-05 OH^-)
(500 K, 20 atm, treated as ideal aqueous solution)

+ 1.6624 mol C_6H_{14}
(500 K, 20 atm, liquid , activity = 1)

+ 0.007501 mol Mo_2C
(500 K, 20 atm, solid, activity = 1)

+ 0.004999 mol MoS_2
(500 K, 20 atm, solid, activity = 1)

Figure 4.19 – Gibbs energy minimization with light hydrocarbons withdrawn from the process to force a metastable equilibrium among more likely species

There are practically a limitless number of ways of arbitrarily withdrawing combinations of species. Figure 4.19 offers but a single example. The process of attempting to interpret in-reservoir conditions using a thermodynamic model would, at the very least, involve a great deal of computation and comparison with actual observation even if this approach is thought to be worthy of the massive effort involved.

4.2 *Pelletized* UD Catalyst Reactivity

Figure 4.20 (Catalyst A) and Figure 4.21 (Catalyst B) present the results from the pelletized UD catalyst reactivity tests and confirm that the produced molybdenum-based particles are active catalysts. It is difficult to compare the two reactivity tests as the mass of catalyst loaded in the reactor for each test was different and the WHSV was not common to both runs. The primary purpose of the reactivity test for Catalyst A was to provide some general insight on the catalyst activity at low synthesis temperature.

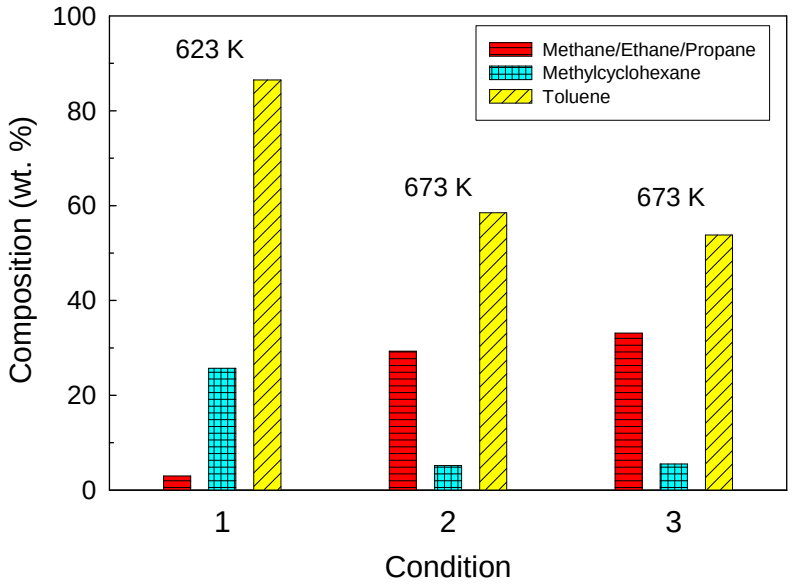

Figure 4.20 – Catalyst A reactivity test (synthesised at 498 K)

The WHSV between condition 1 and 2 for Catalyst A were very similar (3.7 h^{-1} and 4.1 h^{-1}, respectively) and therefore the effect of increasing temperature from 623 K to 673 K can be observed in Figure 4.20 (*See Table 3.4 for operating conditions)*. A greater conversion of toluene into lighter hydrocarbons (C_1-C_3) is illustrated, with a decrease in hydrogenated products, such as methylcyclohexane. Hydrocracking of toluene is therefore the predominant reaction over hydrogenation. In comparing conditions 2 and 3 for Catalyst A, the effect of adjusting the WHSV can be observed. As shown, there is minimal improvement by decreasing the space velocity from 4.1 h^{-1} to 1.4 h^{-1} (i.e. increasing the contact time). As expected, cracking reactions appear to take a

predominant role as the catalyst is at least partially composed of acidic molybdenum oxide(s). Unfortunately, there was insufficient sample collected following reactivity testing for Catalyst A to perform XRD characterization to determine the phase(s) present.

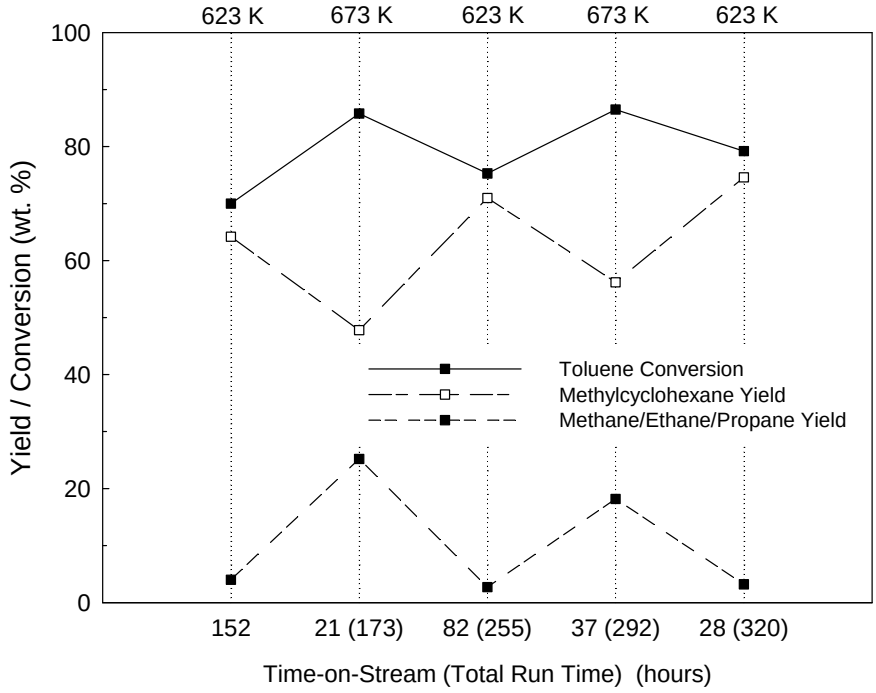

Figure 4.21 – Catalyst B reactivity test (synthesised at 598 K)

Figure 4.21 presents the reactivity results for Catalyst B (*See Table 3.4 for operating conditions)* showing total time-on-stream (TOS) values in parentheses along the abscissa. The values preceding the parentheses correspond to the time interval between the adjusted conditions (i.e. temperature change, as can be seen from the corresponding temperature values appearing on top). One conclusion that can be drawn from this figure is that as TOS increases the catalyst becomes more active, which could signify the progressive formation of more active phases initially inexistent or veiled. A second observation is that increasing the reaction temperature increases the cracking of both toluene and methylcyclohexane in favour of methane. It also appears that the hydrogenation of aromatics improves with time. This may possibly be attributed to a catalytic bi-functionality from new hydrogenating active phases formed during the

process, such as Mo_2C, which appears to be present in the catalyst based on XRD analysis as shown in Figure 4.22, which presents the effects of reactivity on the crystal structure of a pelletized catalyst.

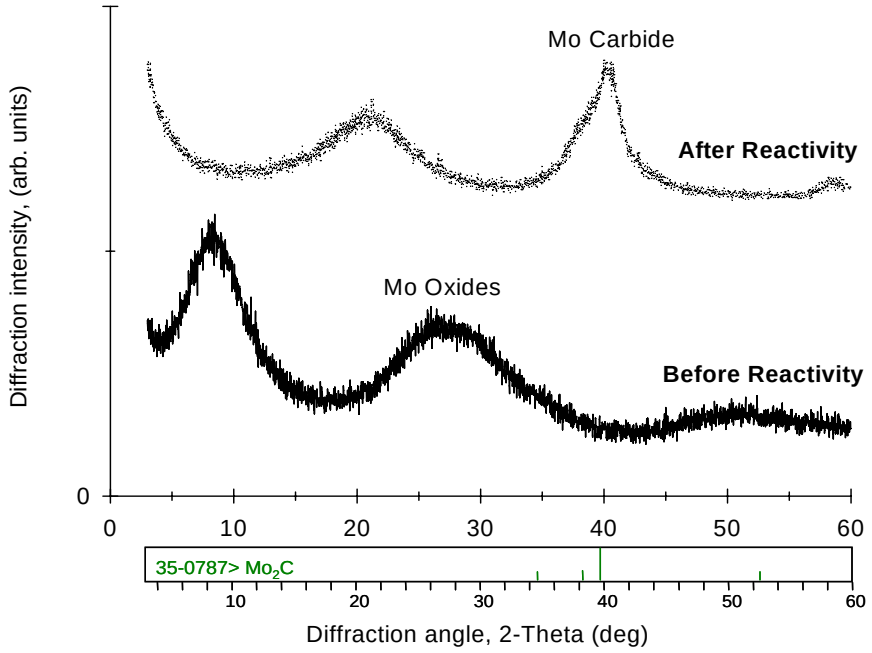

Figure 4.22 – Effect of reactivity on the composition of particles prepared at 498 K

For the catalyst before reaction, the broad amorphous peak from 26 to 30 degrees, common to all experimental runs, spans the region that includes the predominant characteristic peaks corresponding to the MoO_2 and MoO_3 species. The peak near 40 degrees for the catalyst after reaction closely corresponds to the published peak for the molybdenum carbide (Mo_2C) crystal structure (PDF#35-0787) (JADE, 2003). This argument is strengthened by reports that state molybdenum carbide is as active as noble metals (such as ruthenium) in liquid or gas hydrogenation reactions (Oyama, 1992). Another report describes transition metal carbides as having high hydrogenating properties (Breysse et al., 2003).

It should also be noted that although no catalyst particles were detected downstream of the reactor vessel, approximately half of the weight of the catalyst was

consumed during reaction for the reactivity test. This would increase the calculated WHSV values therefore providing less opportunity for toluene conversion. The weight loses may be associated to hydrocarbon moieties from the catalyst preparation stage that are progressively converted during the run time. Previous investigations regarding the catalytic performance of synthesized molybdenum oxide catalysts from water-in-oil emulsions list superior conversion of toluene into hydrodearomatized products in comparison to the results of this study (Wang, 2004; Wang et al., 2004), however the WHSV used by Wang et al. was reported as being 0.7 h^{-1}, thus allowing the catalyst significantly greater time to convert the feedstock. Nevertheless, product distributions between the two studies were very similar.

4.3 UD Catalyst Reactivity in Porous Media

This section presents the results obtained from the SPRU. Figure 4.23 illustrates an example of temperature control achieved during experimentation using LabView 7.0 (National Instruments) and Figure 4.24 provides the specific locations for the temperature probes used to generate these data.

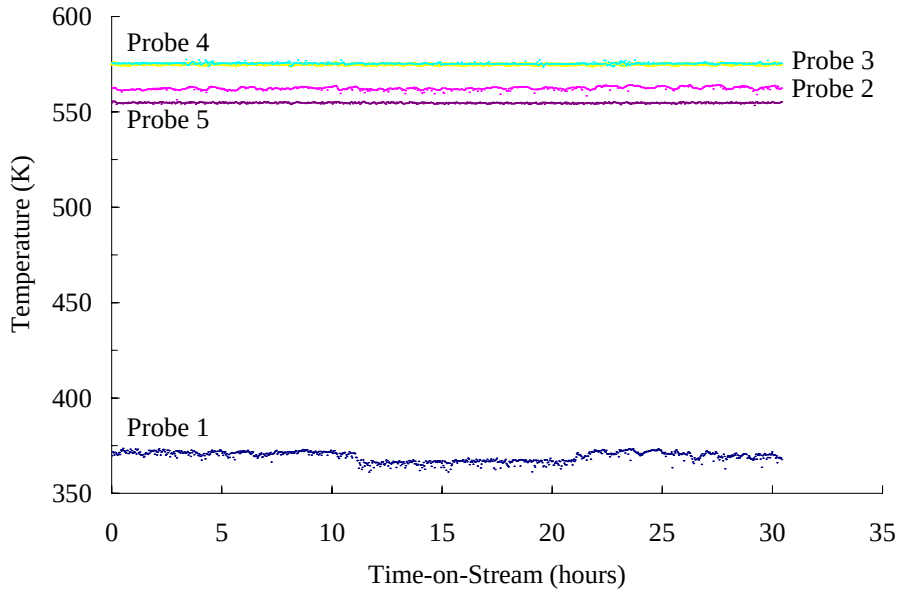

Figure 4.23 – Temperature control achieved for SPRU Mo-emulsion run PM-8

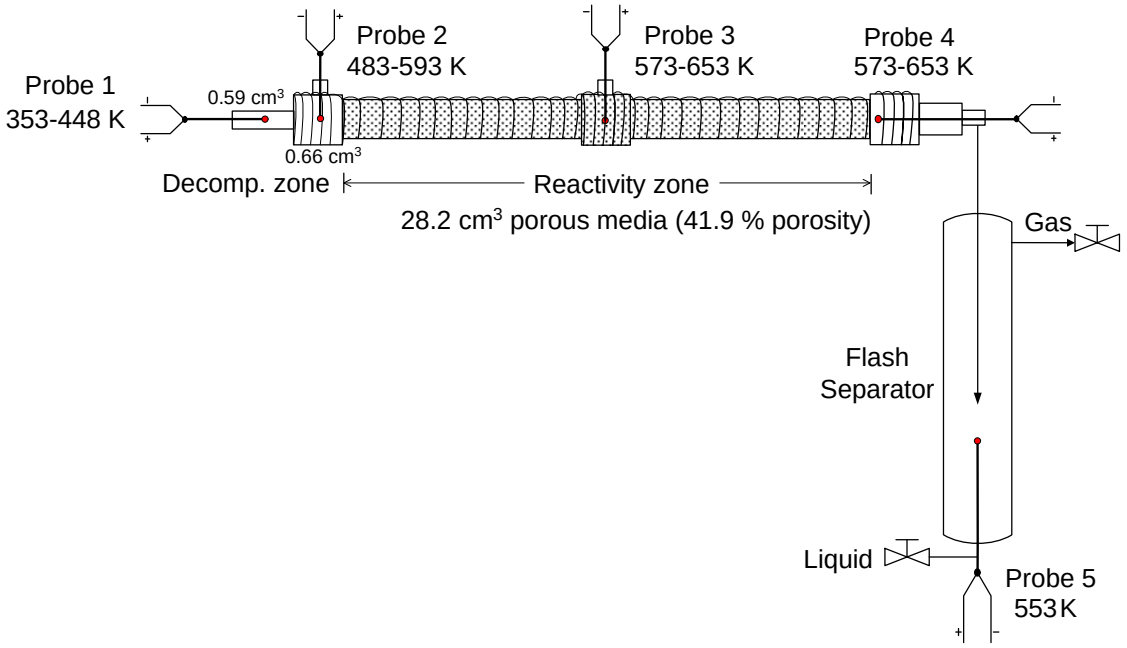

Figure 4.24 – SPRU probe locations with operating temperature ranges

The temperature control presented in Figure 4.23 is typical of all SPRU runs. Similar to the temperature control achieved with the CPU, its relevance stems from its demonstration of steady state production and reactivity of catalyst particles at constant pressure, temperature and residence time.

4.3.1 Viscosity Measurement

Table 4.8 presents the viscosity and water content measurements taken for the upgraded oil samples produced from the successful blank and metal-emulsion runs.

Table 4.8 – Viscosity and water content of feedstock and upgraded oil samples

Sample Name	**Viscosity *at 293 K* (cP)**	**Water Content (%)**
PM-Feed	32829	n/a
PM-6 Cat. (573 K - 4 hr)	16984	0.15
PM-8 Blank (573 K -12 hr)	105.6	0.36
PM-8 Cat. (573 K - 12 hr)	198.0	0.15
PM-9 Blank (633 K - 4 hr)	149.1	0.35
PM-9 Cat. (633 K - 4 hr)	111.0	0.16

In comparing the upgraded oil samples with the feedstock, it is evident that significant reductions in viscosity were achieved and the flash separation unit proved effective in removing the water fraction. The PM-8 blank emulsion run yielded a greater reduction in viscosity compared to its catalytic equivalent, possibly due to increased carbon retention (i.e. deposition) in the reactor for the blank run. The relative difference however is not overly significant. What is significant for in-reservoir upgrading is that increasing the reactivity temperature from 573 K to 633 K, while maintaining a residence time of 4 hours, has near equal impact for viscosity reduction as does maintaining the temperature at 573 K and increasing the residence time from 4 to 12 hours.

4.3.2 Simulated Distillation

Figure 4.25 shows the results from simulated distillation on the upgraded oil samples produced from the SPRU.

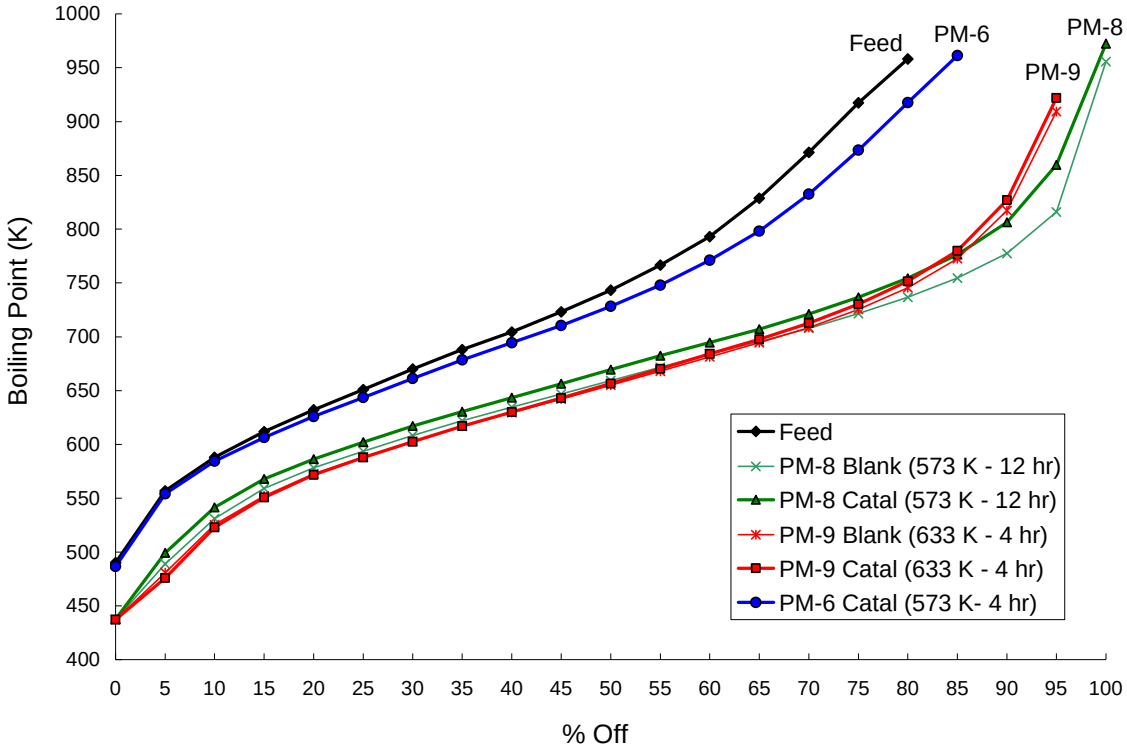

Figure 4.25 – Simulated distillation of feedstock and upgraded oil samples

Similar to the findings through viscosity measurement, increasing the reactivity temperature from 573 to 633 K has virtually an equivalent upgrading effect when compared to increasing the residence (i.e. reaction) time from 4 to 12 hours, with the increased residence time demonstrating slightly greater upgrading for the higher boiling point fractions. Once again, there appears to be only minor differences in upgrading between the blank and catalytic emulsion runs, with the blank runs producing a slightly higher quality product, particularly in the case of PM-8 (i.e. long residence time experiment). This finding is not surprising however, as thermal (non-catalytic) cracking at conversions higher than 30% may produce greater asphaltene precipitation and coke deposited in the system. Table 4.9 presents a table of mass balances for experiments PM-8 and PM-9 which appears to support this hypothesis. A lower recovery of liquid product (by wt.) is found for the higher temperature condition also due to increased cracking, leading to coke formation (hydrocarbon retention) in the system. Only slight upgrading of the heavy feed is observed for the lower residence time (4 hours) and temperature (573 K).

Table 4.9 – Mass balances for SPCU experimental runs PM-8 and PM-9

Sample	Temperature (K)	Flow Rate (cm3/hr)	Steady-State Sample Cut (hours)	Oil Weight (g)	Aqueous Weight (g)	Total Weight (g)	Fraction of Feed (%)
PM-8 Blank	573	1	29.75	24.6	3.1	27.7	92.9
PM-8 Moly	573	1	30.5	25.3	3.1	28.5	93.3
PM-9 Blank[1]	633	3	8.2	17.2	2.1	19.3	78.4
PM-9 Moly	633	3	12.0	28.4	3.9	32.3	89.8

[1]denotes steady-state may not have been reached - GC recording started 2.5 hours into cut

4.3.3 Characterization of Gases

Figure 4.26 displays the GC characterization of the SPRU effluent gases. The first observation which may be made is in reference to the conversion of aromatics in the light fractions that are collected as gases. Here, the lowest severity run (PM-6, 573 K - 4 hours) highlights a 19% composition of aromatics in the outlet gases without any presence of naphthenes (i.e. cycloparaffins). Runs (either with blank or catalytic

emulsions) at the higher temperature or longer residence time show a reduction of these aromatics and an increase of light alkane HCs (C_1-C_5), olefinic and naphthenic gases. It also appears that an increase in light alkane HCs occurs at the elevated temperature condition from the cracking of longer chain paraffins and alkyl branches.

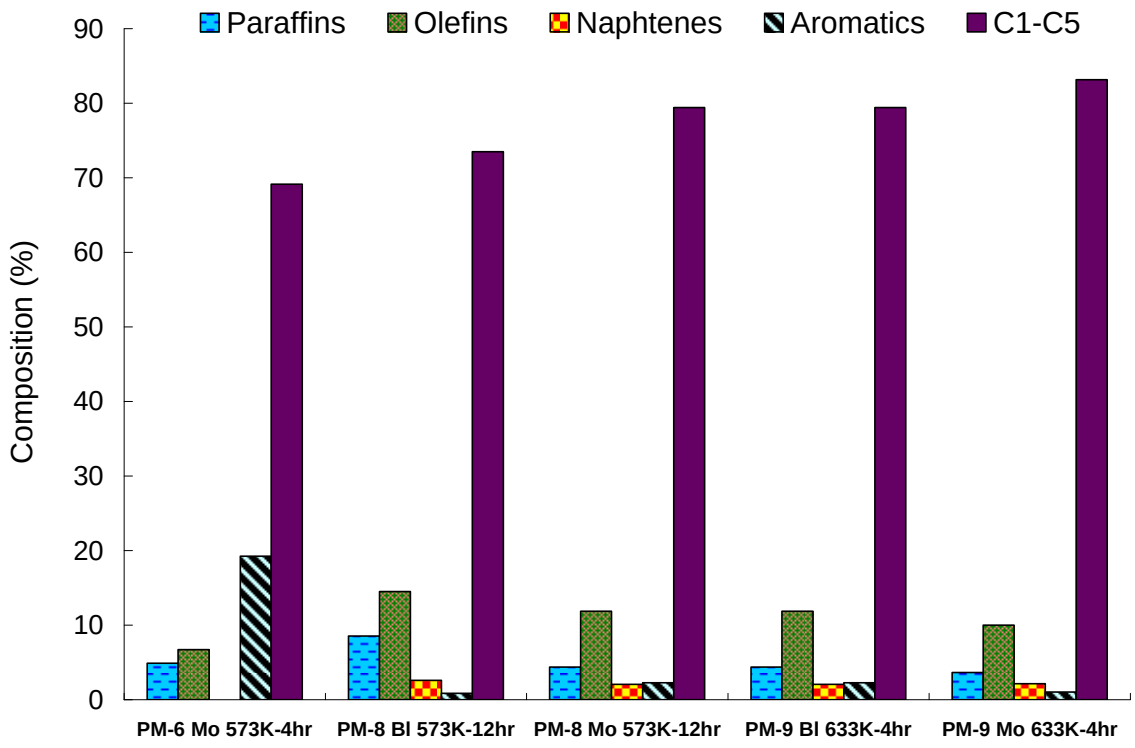

Figure 4.26 – Gas chromatography results of effluent gases from SPRU

4.3.4 Characterization of Porous Media – Molybdenum Content

Figure 4.27 and Table 4.10 illustrate the sampling points and molybdenum content characterization of the sand pack following reactivity, respectively, in order to determine the metal deposition profile.

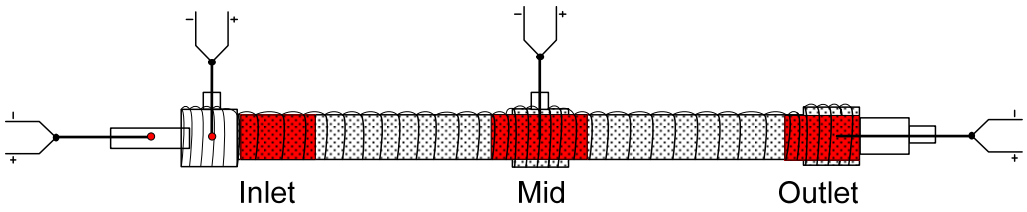

Figure 4.27 – Illustration of sampling points for sand pack following reactivity

Table 4.10 – ICP characterization of sand samples from the porous media reactor

Experimental Run	Moly Content (ppm)			Digested Weight (mg)		
	Inlet	Mid	Outlet	Inlet	Mid	Outlet
Clean Sand	10^{-3}	10^{-3}	10^{-3}	953	953	953
PM-6 (573 K, 4 hrs)	101.6	1.06	0.691	386	340	349
PM-8 (573 K, 12 hrs)	96.7	9.66	0.248	244	225	137
PM-9 (633 K, 4 hrs)	103.9	22.91	0.296	272	181	146

From inspection of Table 4.10, it is evident that all three experimental runs (PM-6, PM-8 and PM-9) demonstrate a similar trend; significant metal deposition on the sand at the inlet of the reactor. This phenomenon may be subject to interpretation, however a possible explanation is pore plugging resulting from increased catalyst particle sizes due to agglomeration. An unpublished work from AICISE on UD catalyst concentration effect on heavy ends (550^{o}C) conversion demonstrates that increasing the catalyst concentration beyond 1200 ppm results in significant losses to conversion most likely attributed to the effect of agglomeration (Trujillo, 2008). The catalyst concentration for the SPRU runs of 5630 ppm may therefore be significantly high enough to achieve aggregation of particles to the extent that agglomerates are unable to penetrate the sand-pack, supporting the high Mo metal concentration observed at the reactor inlet and extremely low concentrations at the outlet. This also serves to explain the frequency of plugging witnessed in several runs. The Mo-emulsions for this series of experiments were also given significant time to allow for particle aggregation in the decomposition zone prior to entering the sand-pack. This holds particularly true at the lower emulsion flow

rate (1 cm^3/hr), which developed a plug causing the unit to fail at 633 K (run PM-10). Another possible explanation for the observed high Mo content at the reactor inlet is chemical bonding of the metal to the porous media in the presence of high temperature and pressure. Regardless of the mechanism however, this may explain the fact that there was no further benefit by introducing molybdenum.

4.4 Precursor Materials Analysis – TGA

4.4.1 Surfactants

Figure 4.28, Figure 4.29 and Figure 4.31 present the TGA results for the surfactants SPAN 80, TWEEN 80 and HLB 8, respectively.

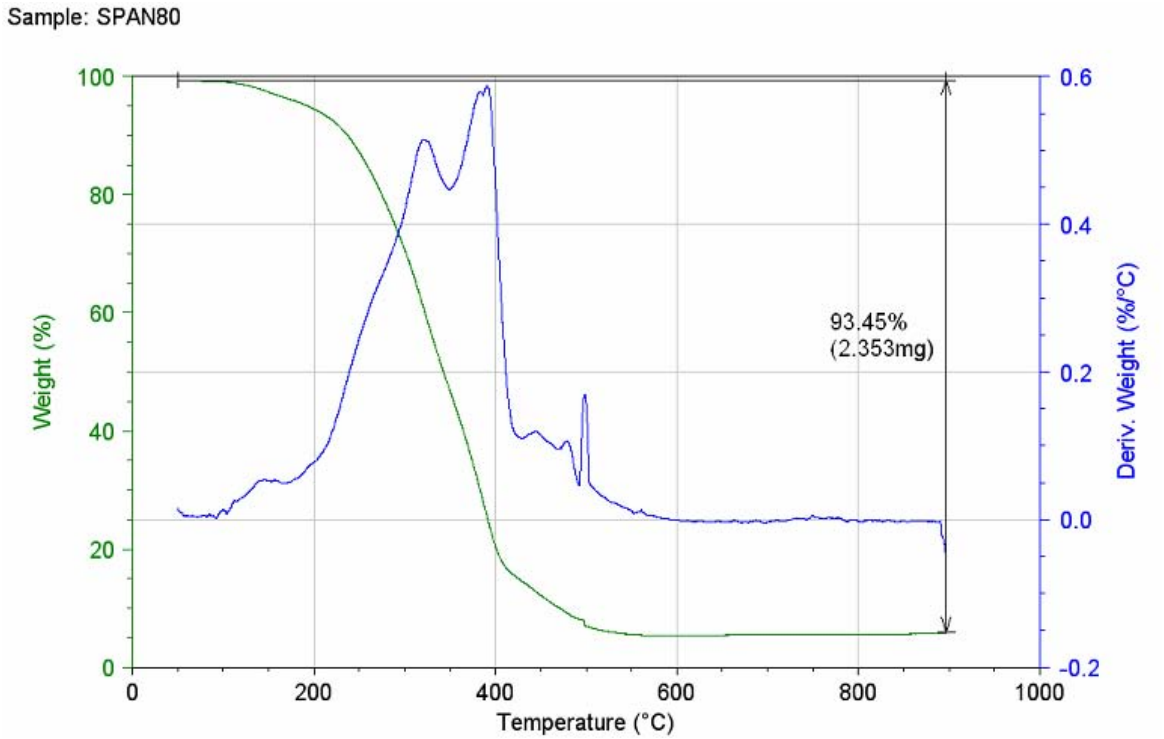

Figure 4.28 – TGA analysis of SPAN 80 in an inert atmosphere

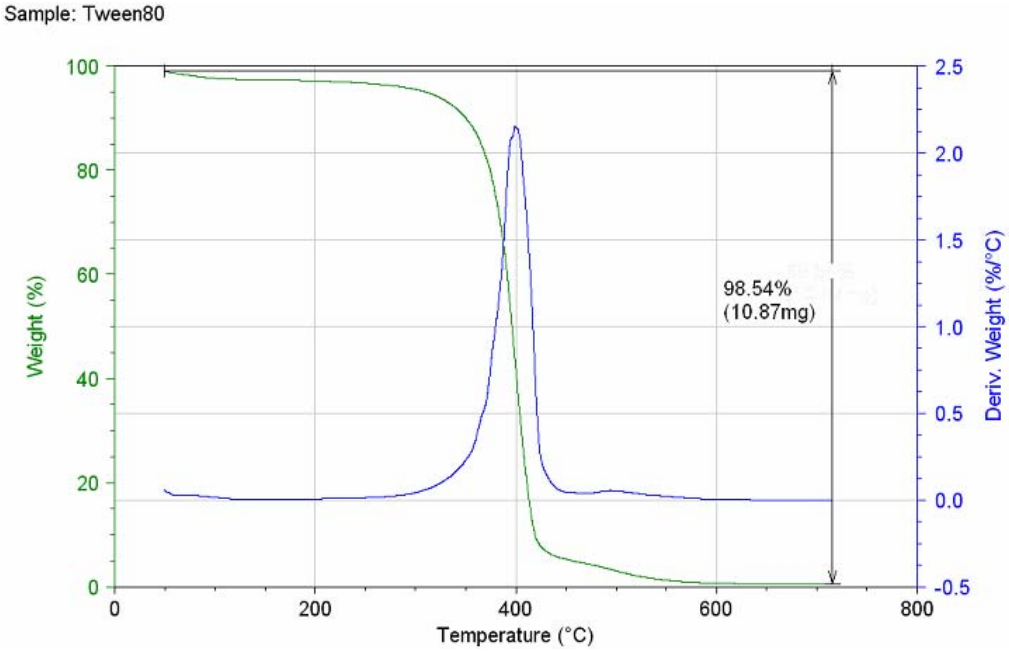

Figure 4.29 – TGA analysis of TWEEN 80 in an inert atmosphere

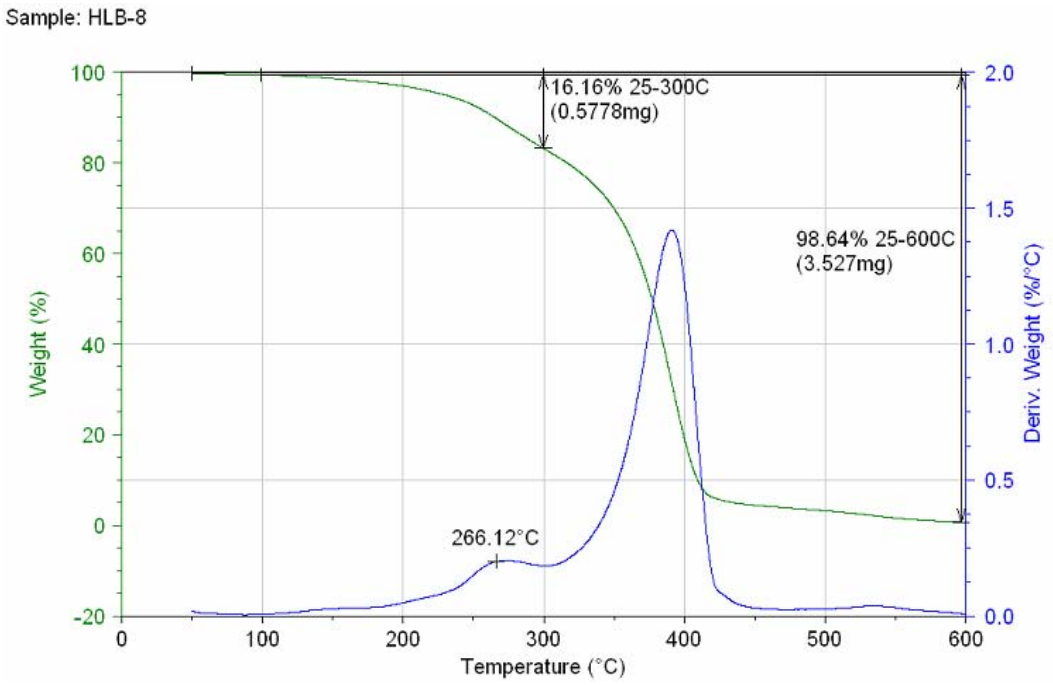

Figure 4.30 – TGA analysis of HLB 8 in an inert atmosphere

The TGA results indicate that many of the compounds that constitute the surfactant SPAN 80 decompose at higher temperatures than those reached during experimentation (i.e. > 360^{o}C or 633 K). This finding is even more pronounced for TWEEN 80 (and therefore also HLB 8), which show the majority of material decomposes near 400^{o}C (673 K). This suggests that some surfactant molecules are still present in the upgraded oil collected at the outlet of the units. It also seems likely that products from partial surfactant decomposition may possess properties which would affect particle dispersion.

4.4.2 Molybdenum Salt – AHM

Figure 4.31 relays the information obtained from the TGA of the Mo precursor material, AHM, in an inert atmosphere.

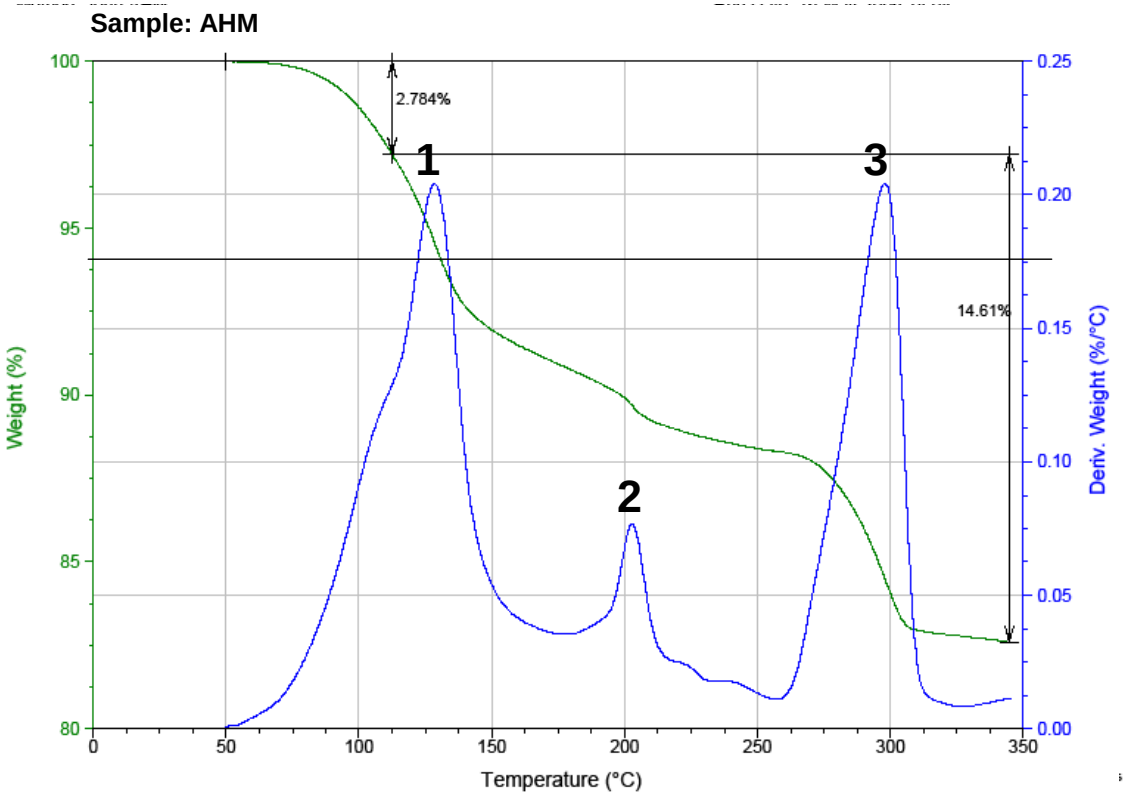

Figure 4.31 – TGA analysis of AHM in an inert atmosphere

Here, Peak 1 (130^{o}C) corresponds to the water liberated from the hydrated crystal salt, remembering that it is ammonium heptamolybdate tetrahydrate. Peak 2 (203^{o}C) likely corresponds to the salt decomposing into water vapour and ammonia molybdenum oxide (PDF#39-0035) or ammonium molybdenum oxide (PDF#18-0117) based both on the theoretical weights of remaining solid products for the staged decomposition of AHM presented in Table 4.11 and XRD results previously introduced in Figure 4.2. Peak 3 (295^{o}C) may be attributed to the escape of ammonia gas resulting from further decomposition of ammonia (or ammonium) molybdenum oxide.

Table 4.11 – Theoretical weight of solid products for staged AHM decomposition

$$(NH_4)_6 Mo_7 O_{24} \cdot 4H_2O \rightarrow 7MoO_3 + 7H_2O + 6NH_3$$

Peak	Material	Molar Mass (g/mol)	Weight off (%)
N/A	AHM (tetrahydrate)	1235.8	0
1	AHM (anhydrous)	1163.8	5.8
2	7 MoO3 • 6 NH3	1109.7	10.2
3	7 MoO3	1007.6	18.5

Chapter Five: Conclusion and Recommendations

5.1 Conclusion

The present study shows insight into the characterization of solid Mo-based UD catalyst particles for potential application to both *in situ* and above-ground hydroprocessing of heavy oil. The particles were prepared by the thermal decomposition of precursor emulsions using an inexpensive aqueous molybdenum salt (AHM) and in a continuous mode. Through DLS and SEM techniques, the particles were found to have average diameters in the nano-size range, as low as 30 nm. An activation energy estimate was performed seeming to reflect that simple collisions are at the basis of the agglomeration of these nanoparticles; agglomeration which results in the measurement of larger particles (agglomerates), regardless of reactor configuration being either horizontal or vertical.

The laboratory preparation of UD catalysts was then examined by thermodynamic computational means. Through Gibbs energy minimization and related phase (or predominance) diagrams, it is shown that MoO_3 (the expected product of decomposition) can be reduced to MoO_2 in the presence of hydrogen produced from the associated thermal decomposition/dehydrogenation of ammonia gas as well as by reaction with ammonia directly. The prediction of MoO_2 is consistent with XRD characterization of the solid particles produced by the laboratory work.

Gibbs energy minimization computations were then undertaken to infer the likely behaviour of MoO_3 when used as an in-situ catalyst. Although complete equilibrium cannot reasonably be expected to develop, the introduction of crude kinetic expectations by judicious species withdrawal gives indications that MoO_3 may convert to MoS_2 and/or Mo_2C. Reactivity results from pelletizing the UD catalysts and placing them in a FBR for toluene hydroconversion do in fact suggest the formation of Mo_2C as a new active phase due to the increase in the hydrogenation of naphthenic compounds. This is further strengthened by XRD characterization of the catalyst particles after reactivity, which showed evidence for Mo_2C formation.

The performance (i.e. viscosity reduction and oil upgrading) results of the SPRU runs indicate that increasing the temperature from 573 to 633 K is virtually equivalent to increasing the residence time from 4 to 12 hours. Catalyst deposition occurs at the reactor inlet in all cases, possibly from agglomeration effects due to high catalyst concentrations, resulting in no additional contribution to conversion.

In summary, this thesis demonstrates the value of laboratory characterization techniques and thermodynamics in helping to guide and interpret laboratory work as well as to give indications of what might be expected subsequently through experimentation and in the intended field application.

5.2 Recommendations

The effect that UD catalysts have once injected into a formation requires further study as the interaction of these catalysts with reservoir materials is complex. Reservoir sand (i.e. porous media) presents many obstacles in terms of fluid and particle dynamics. The effect of metal deposition in the reservoir from UD catalyst injection and the associated losses in formation permeability require a deeper investigation, not only from a performance perspective, but also from an environmental one. The prevention of agglomeration of UD particles (and therefore sedimentation and/or pore plugging) in the reaction zone, and in their travel back to surface for recovery, is a much needed study. Determination of the optimal surfactant(s) for maintaining/maximizing stable UD particle dispersion should be a subject of future research. Optimizing catalyst concentration, in order to achieve maximum conversion (upgrading) while maintaining dispersion stability and cost effectiveness, also requires continued investigation. As a final thought, perhaps another more effective means of achieving highly dispersed catalysts *in situ* is to transport volatile Mo compounds, such as $Mo(CO)_6$, into the reservoir with hydrogen gas while using thermodynamics as a tool to optimize the conditions to achieve the desired solid hydroprocessing active phase(s). However, this approach may not make economic sense and may potentially create a hazardous environment.

References

Absi-Halabi, M., A. Stanislaus, T. Al-Mughni, S. Khan and A. Qamra, "Hydroprocessing of Vacuum Residues: Relation between Catalyst Activity, Deactivation and Pore Size Distribution", Fuel **74**, 1211-1215 (1995).

Alberta Energy and Utilities Board, Burrowes, A. and F. Rahnama, "ST98-2007: Alberta's Energy Reserves 2006 and Supply/Demand Outlook 2007-2016" (2007).

Aldrich Chemical Company, "Aldrich Handbook of Fine Chemicals - 2007/08", Sigma-Aldrich Canada, Oakville, ON (2007).

American Society for Testing Materials, "Knocking Characteristics of Pure Hydrocarbons: Developed Under American Petroleum Institute Research Project 45", ASTM special technical publication, Philadelphia (1958).

Ancheyta, J., M. S. Rana and E. Furimsky, "Hydroprocessing of Heavy Petroleum Feeds: Tutorial", Catal. Today **109**, 3-15 (2005).

Bale, C. W., A. D. Pelton and W. T. Thompson, "Facility for the Analysis of Chemical Thermodynamics (F*A*C*T)", Version 2.1, Centre for Research in Computational Thermochemistry (C.R.C.T.), Montreal (1996).

Bearden, R. and C. L. Aldridge, "Hydroconversion of Heavy Hydrocarbons", United States Patent No. 4,134,825 to Exxon Research & Engineering Co. (1979).

Besenbacher, F., M. Brorson, B. S. Clausen, S. Helveg, B. Hinnemann, J. Kibsgaard, J. V. Lauritsen, P. G. Moses, J. K. Nørskov and H. Topsøe, "Recent STM, DFT and HAADF-STEM Studies of Sulfide-Based Hydrotreating Catalysts: Insight into Mechanistic, Structural and Particle Size Effects", Catal. Today **130**, 86 (2008).

Bezverkhyy, I., P. Afanasiev, C. Geantet and M. Lacroix, "Highly Active (Co)MoS_2/Al_2O_3 Hydrodesulfurization Catalysts Prepared in Aqueous Solution", J. Catal. **204**, 495 (2001).

Billon, A. and P. H. Bigeard, "Hydrocracking, in Petroleum Refining. 3 Conversion Processes", Institut Français Du Pétrole Publications, (2001).

Boutonnet, M., J. Kizling and P. Stenius, "The Preparation of Monodisperse Colloidal Metal Particles from Microemulsions", Colloids Surf. A **5**, 209 (1982).

Breysse, M., G. Djega-Mariadassou, S. Pessayre, C. Geantet, M. Vrinat, G. Perot and M. Lemaire, "Deep Desulfurization: Reactions, Catalysts and Technological Challenges", Catal. Today **84**, 129-138 (2003).

Cauliez, P. M., J. E. Jackson and J. L. Dye, "An Unusual Reduction of Ethylene Occurring During the Thermal Decomposition of Alkalides and Electrides", Tetrahedron Lett. **32**, 5039 (1991).

Chevron, "LC-FINING", http://www.chevron.com/products/sitelets/refiningtechnology/lcfin_7a.aspx (2007).

Choudhary, T. V., C. Sivadinarayana and D. W. Goodman, "Production of CO_x-Free Hydrogen for Fuel Cells via Step-Wise Hydrocarbon Reforming and Catalytic Dehydrogenation of Ammonia", Chem. Eng. J. **93**, 69-80 (2003).

Davis, S. C. and K. J. Klabunde, "Unsupported Small Metal Particles - Preparation, Reactivity, and Characterization", Chem. Soc. Rev. **82**, 153-208 (1982).

de Dios, M., F. Barroso, C. Tojo, M. C. Blanco and M. A. Lopez-Quintela, "Effects of the Reaction Rate on the Size Control of Nanoparticles Synthesized in Microemulsions", Colloids Surf. A **270-271**, 83-87 (2005).

Del Bianco, A., N. Panariti, S. Di Carlo, J. Elmouchnino, B. Fixari and P. Le Perchec, "Thermocatalytic Hydroconversion of Heavy Petroleum Cuts with Dispersed Catalyst", Appl. Catal. A **94**, 1-16 (1993).

Demirel, B. and W. H. Wiser, "Thermodynamic Probablility of the Conversion of Multiring Aromatics to Isoparaffins and Cycloparaffins", Fuel Processing Technology **55**, 83-91 (1998).

Derouane, E. G. and P. Varghese, "Hydrothermal Conversion of Heavy Oils and Residua with Highly Dispersed Catalysts", United States Patent No. 4,578,181 to Mobil Oil Corp. (1986).

Eijsbouts, S., "Life Cycle of Hydroprocessing Catalysts and Total Catalyst Management", Proceedings, The 2nd International Symposium on Hydrotreatment and Hydrocracking of Oil Fractions, Antwerpen, Belgium (1999).

Eijsbouts, S., L. C. A. van den Oetelaar and R. R. van Puijenbroek, "MoS_2 Morphology and Promoter Segregation in Commerical Type 2 Ni-Mo/Al_2O_3 and Co-Mo/Al_2O_3 Hydroprocessing Catalysts", J. Catal. **229**, 352-364 (2005).

Eriksson, S., U. Nylen, S. Rojas and M. Boutonnet, "Preparation of Catalysts from Microemulsions and their Applications in Heterogeneous Catalysis", Appl. Catal. A **265**, 207 (2004).

Friedlander, A. G., P. R. Courty and R. E. Montarnal, "Ammonia Decomposition in the Presence of Water Vapor: I. Nickel, Ruthenium and Palladium Catalysts", J. Catal. **48**, 312-321 (1977).

Gary, J. H. and G. E. Handwerk, "Petroleum Refining - Technology and Economics", New York (2001).

Gates, B. C., "Catalytic Chemistry", John Wiley & Sons, Inc., Newark (1992).

Gates, B. C., "Wiley Critical Content - Petroleum Technology", First Ed., Vol. 1 of 2, John Wiley & Sons, Inc., New Jersey (2007).

Gellman, A. J., D. Neiman and G. A. Somorjai, "Catalytic Hydrodesulfurization over the Mo(100) Single Crystal Surface", J. Catal. **107**, 92-102 (1987).

Grange, P. and B. Delmon, "The Role of Cobalt and Molybdenum Sulphides in Hydrodesulphurisation Catalysts: A Review", J. Less Comm. Met. **36**, 353-360 (1974).

Gregoli, A., U. M. Oko and F. Leder, "Process for Converting Heavy Crudes, Tars, and Bitumens to Lighter Products in the Presence of Brine at Supercritical Conditions", United States Patent No. 4,818,370 to Cities Services Oil and Gas Corporation (1989).

Guevara-Lara, A., R. Bacaud and M. Vrinat, "Highly Active NiMo/TiO_2-Al_2O_3 Catalysts: Influence of the Preparation and the Activation Conditions on the Catalytic Activity", Appl. Catal. A **328**, 99 (2007).

Hanafi, Z. M., M. A. Khilla and M. H. Askar, "The Thermal Decomposition of Ammonium Heptamolybdate", Thermochim. Acta **45**, 221-232 (1981).

Hein, F. J., "Heavy Oil and Oil (Tar) Sands in North America: An Overview & Summary of Contributions", Nat. Resources Res. **15**, 67-84 (2006).

Heinrich, G., "Petroleum Refining - 1 Crude Oil, Petroleum Products, Process Flowsheets", Institut Français Du Pétrole, (1995).

Heinrich, G. and S. Kasztelan, "Petroleum Refining - 3 Conversion Processes", Institut Français Du Pétrole, (2001).

Herron, E. H., "Heavy Oil: A Solution to Dwindling Domestic Oil Supplies", http://www.petroleumequities.com/HeavyOilReport.htm (2000).

Hill, C. G., "An Introduction to Chemical Engineering Kinetics and Reactor Design", John Wiley & Sons, Inc., New Jersey (1977).

INCO Special Products, "INCO High Surface Area Nickel Powders", http://www.incosp.com (2006).

International Petroleum Encyclopedia, "Worldwide Look at Reserves and Production", PennWell Publishing Co., (2000).

JADE, "JADE 6.5.12 XRD Pattern Processing", Materials Data Inc., Livermore, California (2003).

Kim, D. S., I. E. Wachs and K. Segawa, "Molecular Structures and Reactivity of Supported Molybdenum Oxide Catalysts", J. Catal. **149**, 268 (1994).

Komatsu, T. and T. Yashima, "Dispersion and Catalytic Activity of Molybdenum Supported of Y Zeolites", J. Mol. Catal. **40**, 83-92 (1986).

Kostorz, G., "Phase Transformations in Materials", WILEY-VCH, Zurich (2001).

Krawitz, A. D., "Introduction to Diffraction in Material Science and Engineering", John Wiley & Sons Inc., (2001).

Kuuskraa, V. A., E. C. Hammershaimb and M. Paque, "Exploration of Heavy Crude Oil and Natural Bitumen - Major Tar Sand and Heavy-Oil Deposits of the United States", American Association of Petroleum Geologists Studies in Geology, (1987).

Laine, N. R., F. J. Vastola and P. L. Walker, "The Importance of Active Surface Area in the Carbon-Oxygen Reaction", J. Phys. Chem. **67**, 2030-2034 (1963).

Laurent, E. and B. Delmon, "Influence of Water in the Deactivation of a Sulfided NiMo/[Gamma]-Al_2O_3 Catalyst During Hydrodeoxygenation", J. Catal. **146**, 281-291 (1994).

Lauritsen, J. V., M. V. Bollinger, E. J. Lægsgaard, K.W., J. K. Nørskov, B. S. Clausen, H. Topsøe and F. Besenbacher, "Atomic-Scale Insight into Structure and Morphology Changes of MoS_2 Nanoclusters in Hydrotreating Catalysts", J. Catal. **221**, 510 (2004).

Lauritsen, J. V., M. Nyberg, J. K. Norskov, B. S. Clausen, H. Topsoe, E. Laegsgaard and F. Besenbacher, "Hydrodesulfurization Reaction Pathways on MoS_2 Nanoclusters Revealed By Scanning Tunneling Microscopy", J. Catal. **224**, 94-106 (2005).

Li, Y., R. Wang and L. Chang, "Study of Reactions over Sulfide Catalysts in CO-CO_2-H_2-H_2O System", Catal. Today **51**, 25-38 (1999).

Lide, D. R., "CRC Handbook of Chemistry and Physics 84th Edition", CRC Press LLC, Boca Raton (2003).

Lisitsyn, A. S., A. V. Golovin, A. L. Chuvilin, V. L. Kuznetsov, A. V. Romanenko, A. F. Danilyuk and Y. I. Yermakov, "Thermal Decomposition of Metal Carbonyls on Oxide Supports Containing Surface Hydrides: A Route to Highly Dispersed Metal Catalysts with Unusual Properties", Appl. Catal. **55**, 235 (1989).

Lopez-Quintela, M. A., "Synthesis of Nanomaterials in Microemulsions: Formation Mechanisms and Growth Control", Curr. Opin. Coll. Inter. Sci. **8**, 137 (2003).

Lopez-Quintela, M. A., C. Tojo, M. C. Blanco, L. Garcia Rio and J. R. Leis, "Microemulsion Dynamics and Reactions in Microemulsions", Curr. Opin. Coll. Inter. Sci. **9**, 264 (2004).

Malvern Instruments, "Zetasizer Nano Series User Manual - MAN0317 Issue 1.0", Malvern Instruments Ltd., England (2003).

Marchionna, M., L. Massimo and F. Ancillotti, "Hydrotreating of Petroleum Residues with Dispersed Catalysts Derived from Thiomolybdates and Molybdenyl Acetylacetonate", Fuel Processing Technology **40**, 1994 (1994).

Materials Data Inc., "JADE XRD Pattern Processing", Version 6.5.12, Livermore, California (2003).

Meyers, R. A., "Handbook of Petroleum Refining Processes", McGraw-Hill, New York (2003).

Moll, N. G. and G. J. Quarderer, "Emulsion Catalyst for Hydrogenation Processes", United States Patent No. 4,136,013 to Dow Chemical Co. (1979).

Monteagudo, J. E. P., P. L. C. Lage and K. Rajagopal, "Towards a Polydisperse Molecular Thermodynamic Model for Asphaltene Precipitation in Live-Oil", Fluid Phase Equilib. **187-188**, 443-471 (2001).

Müller, A., T. P. Prasad and R. Menge, "Thermal Decomposition of $(NH_4)_2MoS_4$ and $(NH_4)_2WS_4$ Heat of Formation of $(NH_4)_2MoS_4$", Z. Anorg. Allg. Chem. **391**, 107-112 (1972).

Legislation L76, Directive 2003/17/EC of European Parliament and of the Council, Official J. Eur. Union **46**, 10-19 (2003).

Osseo-Asare, K., E. Boakye, M. Vittal and L. R. Radovic, "Novel Nanodispersed Coal Liquefaction Catalysts: Molecular Design Via Microemulsion-Based Synthesis", Master of Science Thesis, Pennsylvania State University, University Park, PA, (1995).

Oyama, S. T., "Preparation and Catalytic Properties of Transition Metal Carbides and Nitrides", Catal. Today **15**, 179 (1992).

Panariti, N., A. Del Bianco, G. Del Piero and M. Marchionna, "Petroleum Residue Upgrading with Dispersed Catalysts: Part 1. Catalysts Activity and Selectivity", Appl. Catal. A **204**, 203-213 (2000a).

Panariti, N., A. Del Bianco, G. Del Piero, M. Marchionna and P. Carniti, "Petroleum Residue Upgrading with Dispersed Catalysts: Part 2. Effect of Operating Conditions", Appl. Catal. A **204**, 215 (2000b).

Pelton, A. D. and W. T. Thompson, "Phase Diagrams", Prog. Solid State Chem. **10**, 119 (1975).

Pereira-Almao, P. R., "The Science and Technology of Catalysts - ENCH 619-56 Course Notes", University of Calgary, Calgary (2006).

Pereira, P., *Personal Communication*, University of Calgary, Calgary, Alberta (2007).

Pileni, M. P. and I. Lisiecki, "Nanometer Metallic Copper Particle Synthesis in Reverse Micelles", Colloids Surf. A **80**, 63 (1993).

Ren, R., Z. Wang, C. Guan and B. Shi, "Study on the Sulfurization of Molybdate Catalysts for Slurry-Bed Hydroprocessing of Residuum", Fuel Processing Technology **86**, 169-178 (2004).

Rostrup-Nielsen, J. R., "Fuels and Energy for the Future: The Role of Catalysis", Catal. Rev. **46**, 247-270 (2004).

Said, A. A. and S. A. Halawy, "Effects of Alkali Metal Ions on the Thermal Decomposition of Ammonium Heptamolybdate Tetrahydrate", J. Therm. Anal. **41**, 1075 (1994).

Scott, C., *Personal Communication*, University of Calgary, Calgary, Alberta (2007).

Skoog, D. A., F. J. Holler and T. A. Nieman, "Principles of Instrumental Analysis", Brooks/Cole - Thomson Learning, Crawfordsville, MD (1998).

Speight, J. G., "New Approaches to Hydroprocessing", Catal. Today **98**, 55-60 (2004).

Strausz, O. P. and E. M. Lown, "The Chemistry of Alberta Oil Sands, Bitumens and Heavy Oils", Alberta Energy Research Institute, Calgary (2003).

Sullivan, D. L. and J. G. Ekerdt, "Mechanisms of Thiophene Hydrodesulfurization on Model Molybdenum Catalysts", J. Catal. **178**, 226-233 (1988).

Suslick, K. S., T. Hyeon, M. Fang and A. A. Cichowlas, "Sonochemical Synthesis of Nanostructured Catalysts", Mater. Sci. Eng., A **204**, 186 (1995).

Thakur, D. S. and M. G. Thomas, "Catalyst Deactivation in Heavy Petroleum and Synthetic Crude Processing: A Review", Appl. Catal. **15**, 197-225 (1985).

Tian, K. P., A. R. Mohamed and S. Bhatia, "Catalytic Upgrading of Petroleum Residual Oil by Hydrotreating Catalysts: A Comparison Between Dispersed and Supported Catalysts", Fuel **77**, 1221-1227 (1998).

Topsoe, H., B. S. Clausen and F. E. Massoth, "Catalysis, Science and Technology", Springer-Verlag, Berlin (1996).

Topsøe, H., "The Role of Co-Mo-S Type Structures in Hydrotreating Catalysts", Appl. Catal. A **322**, 3 (2007).

Trujillo, G., *Unpublished Work*, University of Calgary, Calgary, Alberta (2008).

Vasquez, A., *Unpublished Work*, University of Calgary, Calgary, Alberta (2006).

Vasquez, A. and P. R. Pereira-Almao, "Ultradispersed Catalysts for Hydrotreating: Preparation Variable Effects and Fixed Bed Test Comparison with Conventional Catalysts", Proceedings, 19th Canadian Symposium on Catalysis, Saskatoon, SK, Canada (2006).

Vasquez, A., "Ultra Dispersed Catalysts for Hydroprocessing", Master of Science Thesis, University of Calgary, Calgary, (2007).

Vrinat, M. L., "The Kinetics of the Hydrodesulfurization Process - A Review", Appl. Catal. **6**, 137 (1983).

Wang, J., "Synthesis and Characterization of Submicron Molybdenum Catalyst Particles Obtained from Water/Oil Emulsions for Heavy Oil Upgrading", Master of Science Thesis, University of Calgary, Calgary, AB, Canada, (2004).

Wang, J., J. M. Hill and P. Pereira-Almao, "Controllable Synthesis in a Continuous Mode of Unsupported Molybdenum Catalysts with Micro/nano Size for Heavy Oil Upgrading", Proceedings, Canadian International Petroleum Conference, Calgary, AB, Canada (2004).

Weissman, J. G. and R. V. Kessler, "Downhold Heavy Crude Oil Hydroprocessing", Appl. Catal. A **140**, 1-16 (1996).

Wormuth, K., O. Lade, M. Lade and R. Schomacker, "Handbook of Applied Surface and Colloid Chemistry - Chapter 4 - Microemulsions", Wiley, Chichester; New York (2002).

Yoneyama, Y. and C. Song, "A New Method for Preparing Highly Active Unsupported Mo Sulfide. Catalytic Activity for Hydrogenolysis of 4-(1-Naphthylmethyl)bibenzyl", Catal. Today **50**, 19 (1999).

Yong, W. J., "The GC Study of the Thermal Decomposition of Ammonium Paramolybdate Tetrahydrate in a Hydrogen Atmosphere", Thermochim. Acta **158**, 183-186 (1990).

Yoshinaka, S. and K. Segawa, "Hydrodesulfurization of Dibenzothiophenes over Molybdenum Catalyst Supported on TiO_2-Al_2O_3", Catal. Today **45**, 293-298 (1988).

Zonnevylle, M. C. and R. Hoffmann, "Thiophene Hydrodesulphurization on MoS_2; Theoretical Aspects", Surf. Sci. **199**, 320-360 (1988).

Appendix A: Residence Time Calculations for CPU and SPRU

Ultra-Dispersed Catalyst Preparation Unit

The reactor used in the decomposition of the emulsion consisted of 9.5 mm (0.375 inch) diameter, 0.0889 mm (0.035 inch) wall thickness and 381 mm (15 inch) long stainless steel tubes.

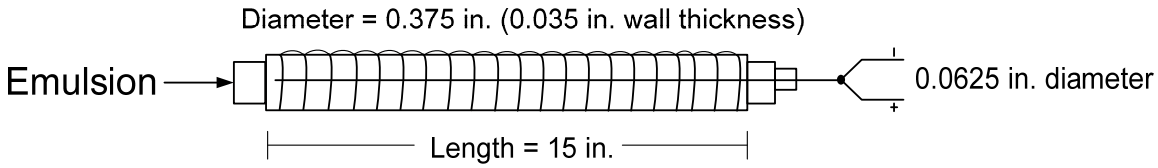

Cross-Sectional Area of Reactor = $\pi\left[\frac{0.375-2(0.035)}{2}\right]^2 = 0.0731\ \text{in}^2$

Cross-Sectional Area of Thermocouple = $\pi\left[\frac{0.0625}{2}\right]^2 = 0.0031\ \text{in}^2$

Available Cross-Sectional Area (Reactor – Thermocouple) x Reactor Length = Volume

$(0.0731-0.0031)\times 15 = 1.050\,\text{in}^3 = 17.20\ \text{cm}^3$

Emulsion flow rate = 250 cm^3/hour

Therefore, Residence Time = $\frac{17.20}{250}\times 60 = 4.13\,\text{min}$

Sand-Packed Reactivity Unit

The reactor consisted of two sections of stainless steel tubing, each 12.7 mm (0.5 inch) diameter, 0.0889 mm (0.035 inch) wall thickness and 140 mm (5.5 inch) long, connected by a stainless steel union tee yielding a total reactor volume of 27.3 cm^3. A porosity of 41.9 per cent was measured for the unconsolidated sand packs yielding a void volume of 11.4 cm^3. A stainless steel section of tubing 6.35 mm (0.25 inch) in diameter (with 0.0889 mm (0.035 inch) wall thickness) and 38.1 mm (1.5 inch) in length, coupled with a union tee, provided a decomposition zone prior to the catalyst entering the porous media.

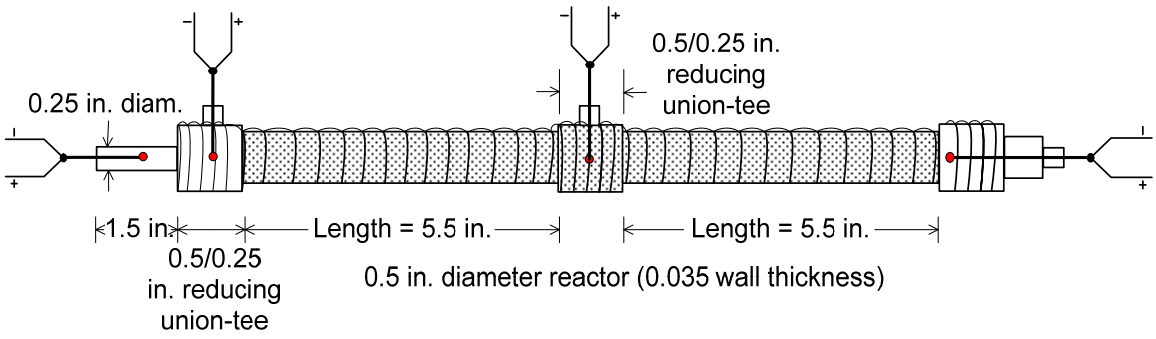

Stainless-Steel Tubing:

$$\text{Volume} = \pi\left[\frac{0.5 - 2(0.035)}{2}\right]^2 \times 5.5 = 0.7986 \text{ in}^3$$

2 sections of tubing = 2 (0.7986) = 1.597 in^3 = 26.17 cm^3

SS-810-3-8-4, Reducing Union Tee, 1/2 in. x 1/2 in. x 1/4 in. Tube OD:

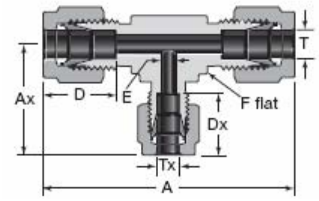

Reducing Union (Fractional)

Tube OD		Basic Ordering Number	Dimensions					
T	Tx		A	Ax	D	Dx	E	F
Dimensions, in.								
3/8	1/4	-600-3-6-4	2.40	1.14	0.66	0.60	0.19	5/8
1/2	1/4 3/8	-810-3-8-4 -810-3-8-6	2.84	1.25 1.31	0.90	0.60 0.66	0.19 0.28	13/16
5/8	3/8	-1010-3-10-6	3.06	1.42	0.96	0.66	0.28	1

$$\text{Volume} = \left[\pi(0.095)^2(2.84 - 1.80)\right] + \left[\pi(0.095)^2(1.345)\right] = 0.0295 + 0.0381$$

Volume = 0.0676 in^3 = 1.11 cm^3

Therefore, Empty Porous Media Reactor Volume = 26.17 cm^3 + 1.11 cm^3 = 27.3 cm^3

With Porous Media (@ 41.9% porosity), Available Volume in Reactor = 11.4 cm^3

Therefore, the residence time for the reactivity unit at the 2 flow rate conditions is:

11.4 cm^3 / 3 cm^3/hr = 3.8 hours ≈ 4 hours

11.4 cm^3 / 1 cm^3/hr = 11.4 hours ≈ 12 hours

Decomposition Zone = length of ¼ inch tubing + reducing union tee

¼ inch tubing cross-sectional area = $\pi\left[\frac{0.25-2(0.035)}{2}\right]^2 = 0.02545\ \text{in}^2$

1/16 inch thermocouple cross-sectional area = 0.00307 in^2 (from previous calculations)

Volume = ((0.02545 – 0.00307)(0.5)(1.5))+(0.02545(0.5)(1.5)) = 0.0359 in^3 = 0.59 cm^3

because thermocouple only enters half-way down the tube. (length of tubing = 1.5 inches)

Void Volume for Reducing Union Tee = 1.11 cm^3 (from previous calculations)

Therefore, Total volume for decomposition zone = 0.59 cm^3 + 1.11 cm^3 = 1.70 cm^3

Appendix B: Precursor Solution Calculation

All sample calculations are based on catalyst synthesis emulsion preparation parameters using the CPU. This procedure was also applied for SPRU emulsion preparation.

All CPU emulsions were prepared in 177.7 gram batches with the following composition: 150 grams of base oil, 16.8 grams of water (corresponding to 10% w/o by wt.), 1.87 grams of AHM salt (corresponding to 10% salt-in-water and 6770 ppm Mo in oil) and 9 grams of SPAN 80 surfactant (approximately 5% of emulsion by wt.).

In order to achieve a 10% w/o emulsion using 150 grams of base oil, the amount of water required was determined as follows:

$$\frac{W}{W+O} = \frac{W}{W+150} = 0.10 \Rightarrow W = 16.8\,\text{grams}$$

The necessary AHM salt addition to achieve a 10% salt-in-water concentration was determined as follows:

$$\frac{AHM}{AHM+W} = \frac{AHM}{AHM+16.8} = 0.10 \Rightarrow AHM = 1.87\,\text{grams}$$

The concentration of molybdenum metal in the product stream, given that AHM is 54.3% Mo, was determined as follows:

$$\frac{AHM}{O}(Mo\%)(ppm) = \frac{1.87}{150(0.87)}(0.543)(10^6) \Rightarrow [Mo] = 7820\,\text{ppm}$$

assuming the density of the base oil remains 0.87 grams per cubic centimetre at the outlet of the unit

Appendix C: Mass Balance for *Pelletized* Catalyst Reactivity

In order to determine the conversion and selectivity for the reaction of toluene on the pelletized catalysts, the mass balance for each reactivity test was calculated. An example of the mass balance calculation is presented for Mass Balance 4 (400^{o}C/673 K) for Catalyst B, synthesized from run-28 (325^{o}C/598 K decomposition).

Catalyst B (synthesized @ 325^{o}C / 598 K) – Mass Balance 4

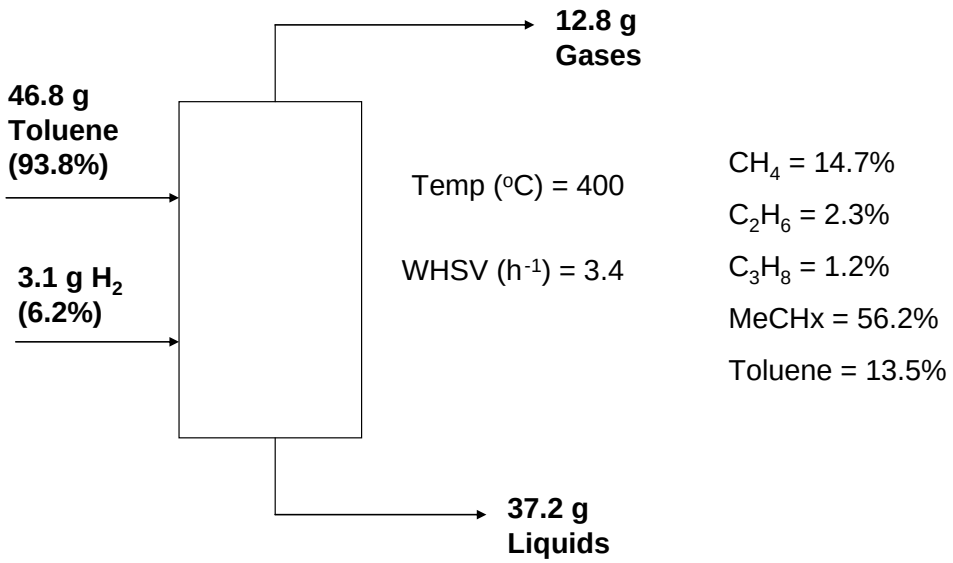

The above illustration shows a simplified block diagram of the (*Pelletized)* Catalyst Reactivity Unit. The inlet streams of the unit include the feed (i.e. toluene) and hydrogen gas. The outlet streams include 'gases' which contains light hydrocarbons and un-reacted hydrogen and 'liquids' which contains the heavier condensed hydrocarbons. The gases and the liquids are quantified by a GC-FID and a GC-MS respectively.

The following page presents the spreadsheet used to tabulate the calculations required to achieve the combined composition of the products (gases + liquids) and determine the additional hydrogen gas required to complete the balance.

CATALYST B (from CPU Run-28, synthesized at 325°C) Mass Balance 4 (400°C)

		Carbon (g)	C (g/mol)	H_2 (g)	**Add. H_2 (g)**
Feed (g)	46.82	42.7	84	4.14	
MW feed (g/mol)	92.14				
Products					
Gases (g)	12.76	10.5	32	2.21	
MW gases (g/mol)	39.32				
Liquids (g)	37.15	32.1	83	5.01	**3.09**
MW liquids (g/mol)	95.53				

flow rate (µl/min) =	16
flow rate (ml/hr) =	0.96
s.g. of toluene (g/ml) =	0.87
flow rate (g/hr) =	0.8352
mass of catalyst (g) =	0.246
Space velocity (h^{-1}) =	3.40

COMPOUND	MW	No. of carbons	G wt.(%)	G Units	y_i	N^o C	L Wt.(%)	L units	x_i	N^o C	Prod %
Methane	16	1	23.25	1.453	0.571	0.571	0.000	0.000	0.000	0.000	14.60
Ethane	30	2	6.78	0.226	0.089	0.178	0.002	0.000	0.000	0.000	2.28
Propane	44	3	5.01	0.114	0.045	0.134	0.028	0.001	0.001	0.002	1.19
Iso-Butane	58	4	2.46	0.042	0.017	0.067	0.068	0.001	0.001	0.004	0.51
n-Butane	58	4	3.64	0.063	0.025	0.099	0.166	0.003	0.003	0.011	0.83
Iso-pentane	72	5	4.85	0.067	0.027	0.133	0.730	0.010	0.010	0.048	1.40
2 Methyl 1 Butene	70	5	2.04	0.029	0.011	0.057	0.000	0.000	0.000	0.000	0.29
n-Pentane	72	5	0.00	0.000	0.000	0.000	0.445	0.006	0.006	0.030	0.44
Cyclopentadiene	66	5	0.00	0.000	0.000	0.000	0.003	0.000	0.000	0.000	0.00
Cyclopentane	70	5	0.53	0.008	0.003	0.015	0.231	0.003	0.003	0.016	0.31
2 Methylpentane	86	6	2.18	0.025	0.010	0.060	1.135	0.013	0.013	0.076	1.19
3 Methylpentane	86	6	1.45	0.017	0.007	0.040	0.861	0.010	0.010	0.057	0.88
2 Ethyl 1 Butene / n-hexane	84	6	0.61	0.007	0.003	0.017	0.445	0.005	0.005	0.030	0.45
t-3-Methyl-2-pentene	84	6	0.00	0.000	0.000	0.000	0.002	0.000	0.000	0.000	0.00
Methylcyclopentane	84	6	0.93	0.011	0.004	0.026	0.775	0.009	0.009	0.053	0.77
2,4 Dimethylpentane	100	7	0.00	0.000	0.000	0.000	0.099	0.001	0.001	0.007	0.07
Benzene	78	6	0.00	0.000	0.000	0.000	0.102	0.001	0.001	0.007	0.09
1 Methyl - 1 - Cyclopentene	82	6	0.00	0.000	0.000	0.000	0.006	0.000	0.000	0.000	0.01
Cyclohexane	84	6	2.29	0.027	0.011	0.064	2.521	0.030	0.029	0.172	2.41
2 Methylhexane	100	7	0.48	0.005	0.002	0.013	0.926	0.009	0.009	0.062	0.71
1,1 Dimethylcyclopentane	98	7	0.00	0.000	0.000	0.000	0.013	0.000	0.000	0.001	0.01
3 Ethylpentane	100	7	0.73	0.007	0.003	0.020	1.213	0.012	0.012	0.081	0.94
c 1,3 Dimethylcyclopentane	98	7	0.00	0.000	0.000	0.000	0.229	0.002	0.002	0.016	0.17
Iso-Octane	114	8	0.00	0.000	0.000	0.000	0.245	0.002	0.002	0.016	0.15
Cycloheptane	98	7	0.00	0.000	0.000	0.000	0.193	0.002	0.002	0.013	0.14
n-Heptane	100	7	0.00	0.000	0.000	0.000	0.189	0.002	0.002	0.013	0.13
Methylcyclohexane	98	7	35.82	0.366	0.144	1.006	72.479	0.740	0.706	4.945	56.27
Ethylcyclopentane	98	7	0.00	0.000	0.000	0.000	0.052	0.001	0.001	0.004	0.04
Toluene	92	7	6.94	0.075	0.030	0.208	16.468	0.179	0.171	1.197	13.49
c 4 Methyl 2 Heptene	112	8	0.00	0.000	0.000	0.000	0.022	0.000	0.000	0.002	0.01
2 Methylheptane	114	8	0.00	0.000	0.000	0.000	0.002	0.000	0.000	0.000	0.00
3 Methylheptane	114	8	0.00	0.000	0.000	0.000	0.162	0.001	0.001	0.011	0.10
3 Ethylhexane	114	8	0.00	0.000	0.000	0.000	0.072	0.001	0.001	0.005	0.05
c 1,3 ethylmethylcyclopentane	112	8	0.00	0.000	0.000	0.000	0.007	0.000	0.000	0.000	0.00
2,4 Dimethylheptane	128	9	0.00	0.000	0.000	0.000	0.011	0.000	0.000	0.001	0.01
Ethylcyclohexane	112	8	0.00	0.000	0.000	0.000	0.044	0.000	0.000	0.003	0.03
Ethylbenzene	106	8	0.00	0.000	0.000	0.000	0.007	0.000	0.000	0.000	0.00
m-Xylene	106	8	0.00	0.000	0.000	0.000	0.032	0.000	0.000	0.002	0.02
o-Xylene	106	8	0.00	0.000	0.000	0.000	0.011	0.000	0.000	0.001	0.01
Nonane	128	9	0.00	0.000	0.000	0.000	0.002	0.000	0.000	0.000	0.00
3,3 Dimethyloctane	142	10	0.00	0.000	0.000	0.000	0.002	0.000	0.000	0.000	0.00
Naphthalene	128	10	0.00	0.000	0.000	0.000	0.003	0.000	0.000	0.000	0.00
			100.00	2.54	1.00	2.71	100.00	1.05	1.00	6.887	100.00
			MW (gas)	**39.32**			**MW (liq)**	**95.53**			

Appendix D: Brine Preparation for SPRU Runs

Brine Preparation Calculations for McMurray Formation water (Athabasca):

Lake, W. and Rogers, W., "Acute lethality of mine depressurization water on trout-perch and rainbow trout", Prepared for Alberta Oil SandsEnvironmental Research Program by Alberta Environment, AOSERP Report23, 1979

- This 2-volume reference can be found at the U of C library, Call number CA6/AO 20/79R23

Component	Molar Mass (g/mol)	Conc. (mg/L)	Conc. (g/L)	Conc. (mol/L)
Na	22.99	**5623**	5.623	0.24458
Ca	40.08	**72**	0.072	0.00180
Mg	24.31	**134**	0.134	0.00551
K	39.10	**45**	0.045	0.00115
CO_3	60.01	**27**	0.027	0.00045
HCO_3	61.02	**3150**	3.15	0.05162
SO_4	96.06	**10**	0.01	0.00010
Cl	35.45	**7615**	7.615	0.21481
Fe	55.85	**1.5**	0.0015	0.00003
TDS		15561		
pH (units)		7.5		

Cations	Salt	Required (mol/L)	Cl Remaining (mol/L)
Mg^{2+}	$MgCl_2 \cdot 6\ H_2O$	0.005512	0.20379
Ca^{2+}	$CaCl_2 \cdot 2\ H_2O$	0.001796	0.20019
Fe^{3+}	$FeCl_3 \cdot 6\ H_2O$	0.000027	0.20011
K^+	KCl	0.001151	0.19896

Anions	Salt	Required (mol/L)	Na Remaining (mol/L)
HCO_3^-	$NaHCO_3$	0.051622	0.19296
SO_4^{2-}	Na_2SO_4	0.000104	0.19275
CO_3^{2-}	Na_2CO_3	0.000450	0.19185

Na^+ remaining =	0.191854	mol/L
Cl^- remaining =	0.198961	mol/L
NaCl used =	0.191854104	mol/L

Compounds	Molar Mass (g/mol)	Conc. (mol/L)	Conc. (g/L)	Conc. (g/10L)
$MgCl_2 \cdot 6\ H_2O$	203.3	0.005512	1.121	11.21
$CaCl_2 \cdot 2\ H_2O$	147.01	0.001796	0.264	2.64
$FeCl_3 \cdot 6\ H_2O$	270.3	0.000027	0.007	0.07
KCl	74.55	0.001151	0.086	0.86
$NaHCO_3$	84.01	0.051622	4.337	43.37
Na_2SO_4	142.04	0.000104	0.015	0.15
Na_2CO_3	105.99	0.000450	0.048	0.48
NaCl	58.44	0.191854	11.212	112.12

Appendix E: Gas Chromatography of SPRU Product Gases

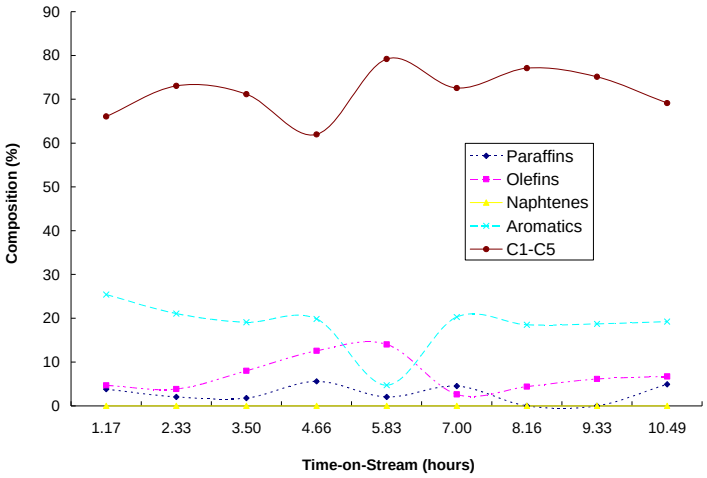

PM-6 (573 K, 4 hour) – Mo Run

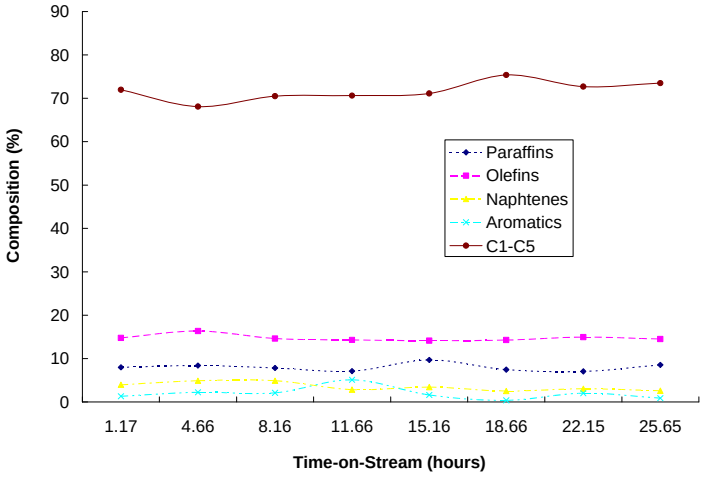

PM-8 (573 K, 12 hour) – Blank Run

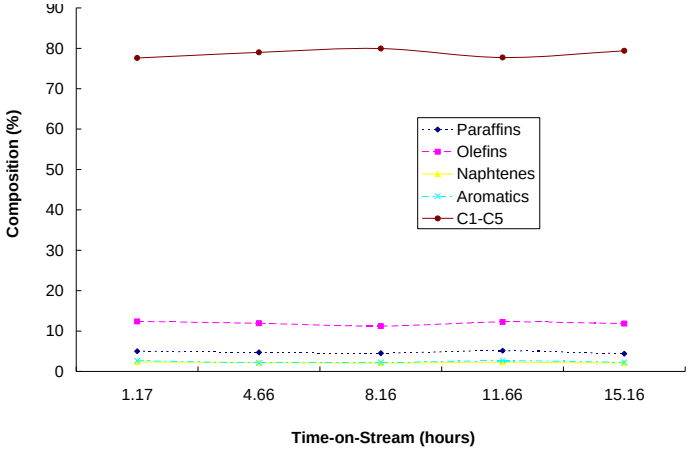

PM-8 (573 K,12 hour) – Mo Run

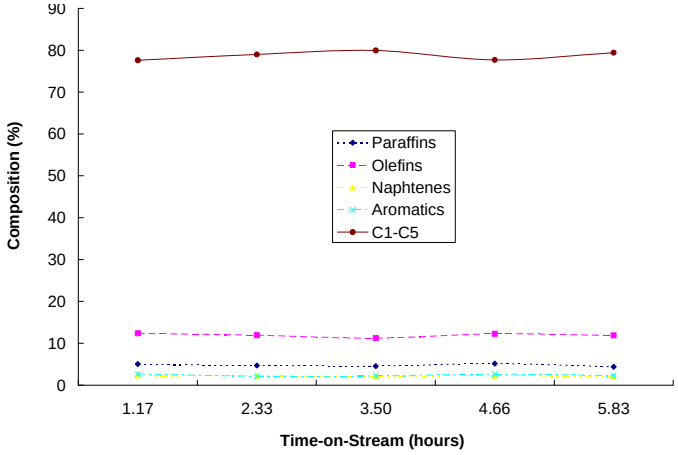

PM-9 (633 K, 4 hour) – Blank Run

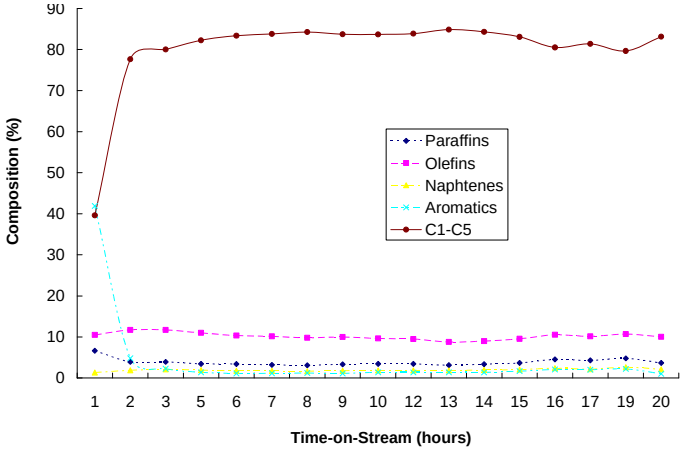

PM-9 (633 K, 4 hour) – Mo Run